GEOLOGY, PETROLOGY AND GEOCHEMISTRY OF TRAVELER RHYOLITE

AND KATAHDIN PLUTON (NORTHCENTRAL MAINE)

by

RUDOLPH HON

M.Sc., Charles University (Czechoslovakia)

(1964)

SUBMITTED IN PARTIAL FULFILLMENT
OF THE REQUIREMENTS FOR THE
DEGREE OF DOCTOR OF
PHILOSOPHY

at the

MASSACHUSETTS INSTITUTE OF TECHNOLOGY

January, 1976

Signature of Author ....
Department of Earth and Planetary Sciences

Certified by ....
Thesis Supervisor

Accepted by ....
Chairman, Departmental
Committee on Graduate Students

GEOLOGY, PETROLOGY AND GEOCHEMISTRY OF TRAVELER RHYOLITE

AND KATAHDIN PLUTON (NORTHCENTRAL MAINE)

BY

RUDOLPH HON

SUBMITTED TO THE DEPARTMENT OF EARTH AND PLANETARY SCIENCES

IN PARTIAL FULFILLMENT OF THE REQUIREMENTS FOR THE DEGREE OF

DOCTOR OF PHILOSOPHY

ABSTRACT

The Traveler Rhyolite-Katahdin Pluton Igneous Complex of
of the Lower Devonian age in Northcentral Maine consists of
two penecontemporaneous but genetically independent magmatic
episodes. The earlier, voluminous episode includes the Tra-
veler Rhyolite and the Katahdin Granite, whereas the slight-
ly younger episode is comprised of minor intrusions of Horse-
race Quartz Diorite, Harrington Lake Porphyry and Debsconeag
Granodiorite. Electron microprobe analyses of mineral assem-
blages, as well as major element geochemistry, provide data
that show the earlier episode being derived by partial melt-
ing of graphite bearing sediments at a depth af 25-30 km
and at a temperature of $810^{\circ}C$. The pre-eruption temperature
and $P(H_2O)$ for the Traveler Rhyolite is estimated at $800^{\circ}C$
and 1100 bars respectively. Similar estimates for Katahdin
Granite yield $710^{\circ}C$ and 1200 bars. Both units were buffered
at oxygen fugacities slightly below the QFM buffer
($10^{-15.00}$ for rhyolites; and $10^{-17.25}$ for granites) as a
consequence of the presence of graphite in the parental
sediments. The younger episode, as evidenced by the trend
on an AFM diagram, crystallized under oxidizing conditions.

Trace element abundances are consistent with the deri-
vation of the earlier episode from the Appalachian eugeo-
synclinal sediments. In particular, the unusually high Sc
abundances (25-35 ppm) in the acidic rocks preclude a deri-
vation by extensive fractional crystallization of a basaltic
magma. Variations of trace element abundances in the Traveler
Rhyolite and Katahdin Granite are best explained if the gra-
nites represent fractionated rhyolitic magma after removal

ABSTRACT (continued)

of 25% crystals of alkali feldspar (35 wt%),plagioclase
(25 wt%), quartz (31 wt%), biotite (8 wt%), and magnetite
(1 wt%). Aplitic magmas require approximately 80-90%
crystal removal of the same mineral proportions as granites.
The calculated mean partition csefficients required by this
model for Co, Rb, Hf, Sr, and Eu are 3.18, 0.49, 2.42, 2.08,
and 2.41. The mean partition coefficient for Hf is largely
due to a removal of accessory zircon. The similar values of
partition coefficients for Eu and Sr are consistent with the
estimated very low oxygen fugacities. The trace element data
further show that the Horserace Quartz Diorite and Harring-
ton Lake Porphyry are genetically independent from the
earlier episode and that the Debsconeag Granodiorite is a
result of mixing of 40% Traveler Rhyolite magma and 60%
Harrington Lake Porphyry. Higher abundances of heavy rare
earth elements (Gd-Lu) and Hf in aplites, relative to gra-
nites, suggest that zircon ceased to crystallize during the
late stages of differentitation due to the gradual loss of
zirconium via an exsolving vapor phase.

Thesis Supervisor: F.A. Frey

Title: Associate Professor of Geochemistry

OBJECTIVE AND STUDY PLAN

The goal of this study is to gain an understanding of the tectonic significance of the two igneous belts in north-central Maine, the Piscataquis Volcanic Belt and the Greenville Plutonic Belt. As a first step in achieving this goal, this study is focused on the origin, evolution, and mode of emplacement of the Traveler Rhyolite - Katahdin Granite Igneous Complex.

Noting the geological proximity of the Traveler Rhyolite and Katahdin Granite, Rankin (1968) tentatively suggested their origin to be from the same parental magma. In order to test this hypothesis, a detailed geological, petrological and geochemical study of the Traveler Rhyolite and Katahdin Granite is hereby undertaken. Furthermore this study can provide additional insights into the geological processes that lead to the formation of a volcano-plutonic association.

This work is divided into three parts. The first part is devoted to the geology, mineralogy and major element geochemistry of the Traveler Rhyolite, emphasizing the equilibria among mineral phases as a tool to estimate intensive parameters. In the second part, a similar approach is used to study plutonic rocks of the Katahdin Pluton. The third section studies the trace element geochemistry of the Traveler Rhyolite - Katahdin Pluton Igneous Complex.

TABLE OF CONTENTS

TABLE OF CONTENTS (continued)

LIST OF FIGURES

LIST OF FIGURES (continued)

LIST OF TABLES

ACKNOWLEDGMENT

I.   INTRODUCTION

A linear distribution of Lower Devonian extrusive acidic rocks in northwestern and northcentral Maine, and another subparallel belt of intrusive granitic and gabbroic bodies to the southeast (Fig. 2) has led some geologists to interpret these linear features, in terms of plate tectonic models, as an island arc structure (D. W. Rankin, 1968), or as a plate suture (G. M. Boone, 1974), resulting from a closure of Iapetus Ocean between the Avalon Prong and the North American continent (McKerrow, Ziegler, 1972; Dewey, Kidd, 1974). Both belts, the extrusive Piscataquis Volcanic Belt of Rankin (1968) and the intrusive Greenville Plutonic Belt (after the town of Greenville, situated approximately in the center of the belt--this study), are about 10 to 50 km wide and about 160 to 200 km long. They are approximately 25 km apart at their southwestern extension and converge slightly to the northeast where Traveler Rhyolite is intruded by granites of the Katahdin Pluton (D. W. Rankin, 1968). These granites are in turn intruded by a few stocks of Debsconeag Granodiorite and by a stock of Horserace Diorite (A. Griscom-in preparation). The close spatial association and good exposures of extrusive and intrusive rocks, as well as their well defined intrusive contacts, make this volcano-plutonic complex most suitable for detailed geological, petrological, and geochemical studies.

Fig. 1. Index Map With Metamorphic Zones in Maine.

Legend: TR – Traveler Rhyolite
        KP – Katahdin Pluton
        1a – Subchlorite Zone
         1 – Chlorite Zone
         2 – Biotite Zone
         3 – Garnet Zone
         4 – Staurolite Zone
         5 – Sillimanite Zone
         6 – Sillimanite & Orthoclase Zone

Note: Metamorphic zones in the extreme
      SW Maine are omitted.

13
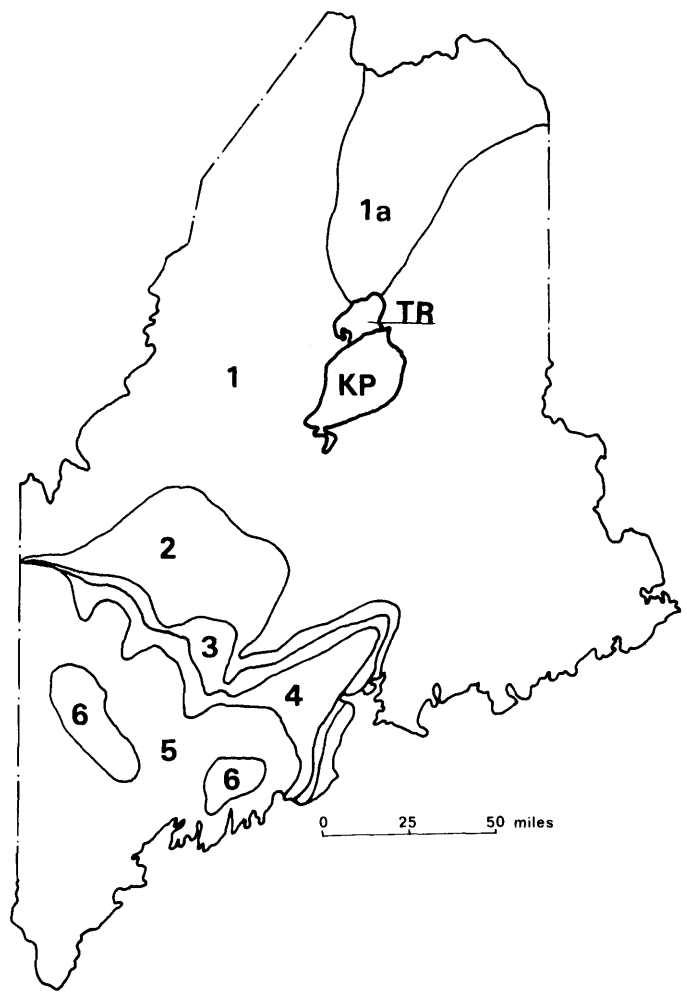
**INDEX MAP AND
METAMORPHIC ZONES
(GEOLOGIC MAP OF MAINE, 1967)**

Fig. 2. Generalized Geological Map of Western Maine.
          Legend: 1 - Rhyolitic Volcanics of Piscataquis
                      Volcanic Belt
                  2 - Mafic Plutonics of Greenville
                      Plutonic Belt
                  3 - Silicic Plutonics of Greenville
                      Plutonic Belt
                  4 - Silurian and Older Rock Formations
                  5 - Other Granitoids (Not Part of Greenville
                      Plutonic Belt)
                  6 - Devonian Rock Formations

■	1
▨	2
▧	3
▢	4
▢	5
▢	6

MOOSE RIVER SYNCLINORIUM

TRAVELER MTN SYNCLINORIUM

ROACH RIVER SYNCLINORIUM

0   10   20   30   40   50   100 KM
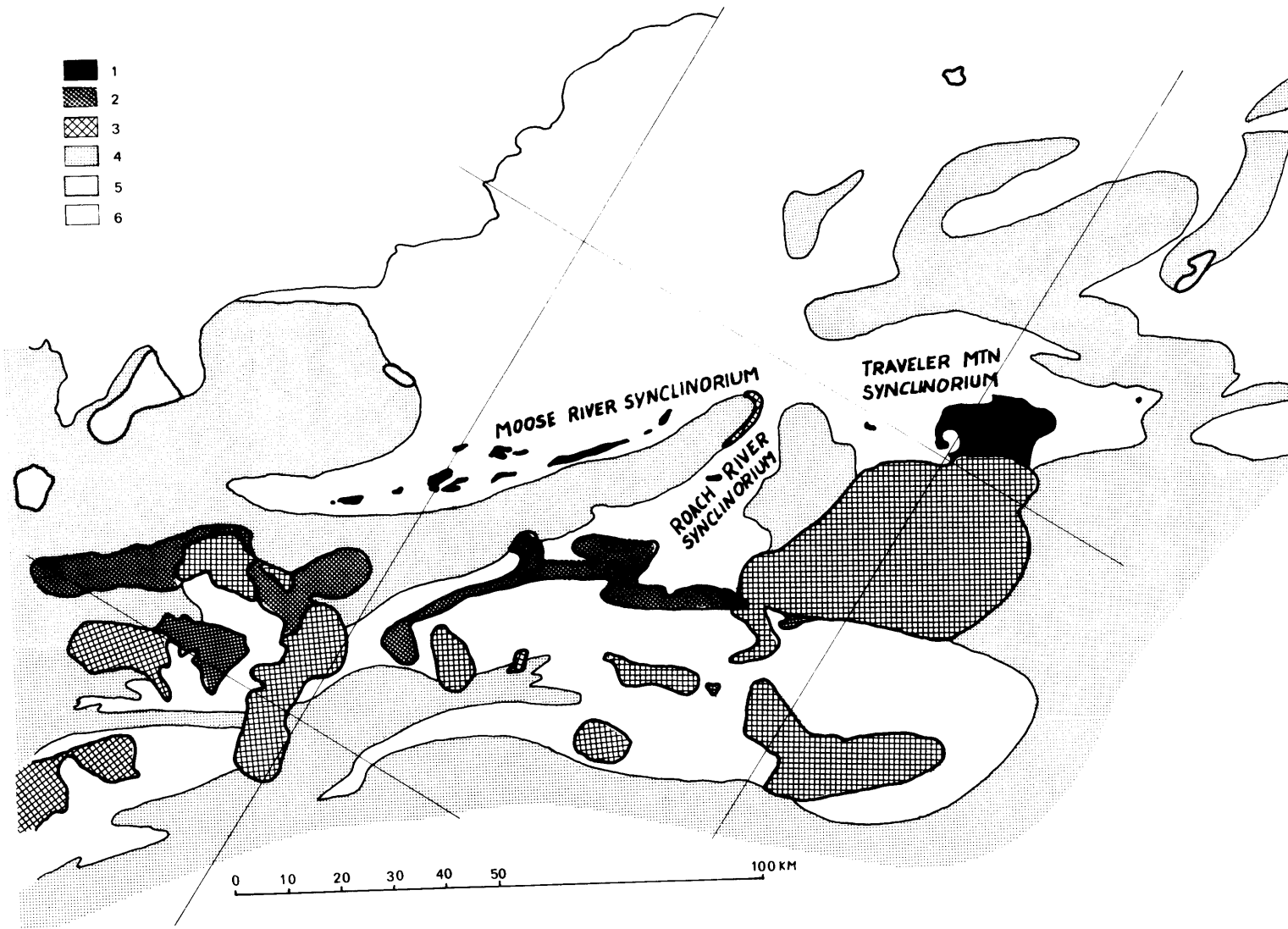
GENERALIZED GEOLOGIC MAP OF WESTERN MAINE

Fifty-five major element analyses and fifty-two trace element abundance data for 18 elements (9REE, Sc, Co, Rb, Cs, Hf, Ta, Th, U, Sr) were determined by electron microprobe, XRF and instrumental neutron activation techniques. The samples include the Traveler Rhyolite (11), Kineo Rhyolite (1), Katahdin Granite (22), aplites and pegmatites (9), Horserace Diorite (3), Debsconeag Granodiorite (2), Harrington Lake Granite Porphyry (2), mafic dike rock (1), Granite of the Moxie Pluton (1), Lexington Granite (1), Echo Pond Granite (1), and Pierce Pond Gabbro (3) (See Fig. 3). Additional microprobe data were obtained on coexisting minerals in two very fresh samples of Traveler Rhyolite (biotite, olivine, clinopyroxene, plagioclase, groundmass, opaques, and "chlorite") and on four samples of Katahdin Granite (alkali feldspar, plagioclase, opaques, biotite and, in one case, also olivine). Biotite and opaque minerals were also analyzed by microprobe in four other samples of Katahdin Granite.

These data, as well as the geologic setting and the rock petrography, are discussed with the objective of understanding the relationships within the intrusive and volcanic belts.

II. GEOLOGY, MINERALOGY, AND PETROLOGY OF TRAVELER RHYOLITE

A. General Statement

The Traveler Rhyolite is a large, almost rectang-

Fig. 3.   Location of Igneous Bodies Included in This Study.

Legend: Light Stipple - Granites
        Medium Stipple - Rhyolites
        Heavy Stipple - Mafic Plutonics

Traveler Rhyolite

Kineo Rhyolite

Katahdin Pluton

Pierce Pond Pluton

Moxie Pluton

CANADA

CANADA
VERMONT

N.H.

MAINE

O
Newport

Lexington Batholith

Echo Pond Pluton

Bangor
O

O
Berlin

Augusta
O

N

0   50   100   150
                                      km
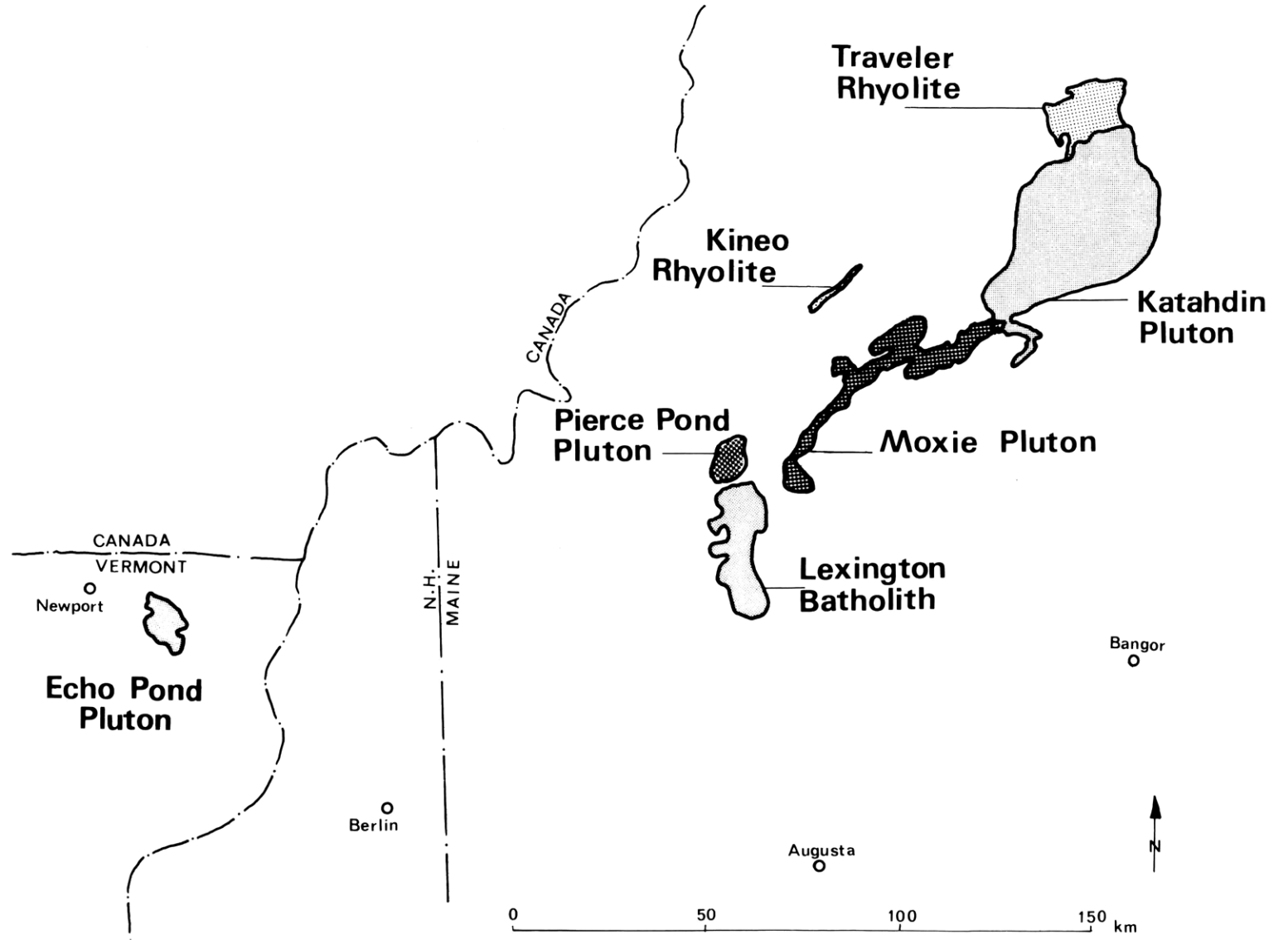
ular (20 X 12 km, 215 km^2), tectonically sunken block of topographically prominent Lower Devonian volcanic rocks, occurring on the northern side of the Katahdin Pluton (Rankin, 1968). The estimated present day stratigraphic thickness of the volcanic sequence is approximately 3.5 km.

On a regional scale, the Traveler Rhyolite, and a few outlying rhyolitic and granophyric occurrences between Snowshoe Mountain and Soubunge Mountain (all considered to be part of the same magmatic sequence), are situated within a broader synclinorial structure on strike with the Roach River and Moose River synclinoria to the southwest (Boucot, 1969) (Fig. 2). All three regional depressions are doubly plunging synclinoria with weakly metamorphosed (chlorite zone) axial Lower Devonian sedimentary strata, containing large masses of Lower Devonian acidic volcanic rocks of identical stratigraphic correlation (Table 1).

From fossil records of the respective underlying and overlying sedimentary formations, the best stratigraphic age for the Traveler Rhyolite is Middle to Upper Lower Devonian: Oriskany to Schoharile (Boucot, 1969; Andrews, Kasper, 1970).

The Traveler Rhyolite unconformably overlies the Matagamon Sandstone (type locality at Horserace Mountain) and is in turn overlain with angular unconformity by con- tinental deposits of the Trout Valley Formation within and along the northern edge of the block (Table 1). The con- tact with the granites of the Katahdin Pluton clearly show

			Moose River	Roach River	Traveler Mtn.
Middle Devonian					Trout Valley Formation
Lower	Upper	Schoharie	Tomhegan Sandstone		
		Esopus	Kineo Rhyolite	Spencer Rhyolite	Traveler Rhyolite
Devonian	Middle	Oriskany	Tarratine Sandstone / Seboomook Argillite	Tarratine Sandstone / Seboomook Argillite	Matagamon Sandstone / Seboomook Argillite
		Upper Helderberg			

Stratigraphic correlation of Traveler Rhyolite with Spencer and Kineo Rhyolites in Roach River and Moose River Synclinoria. Modified from Boucot (1969); Rankin (1965, 1968); Andrews, Kasper (1970).

Table 1

the granite intruding the rhyolites: at several places,
numerous aplogranitic, apophysical injections of the Katah-
din Granite are observed to intrude for a short distance
into the rhyolites. This contact is also marked by a narrow,
50-100 m wide, hornfelsitic zone of recrystallized meta-
rhyolites which retained the original porphyritic texture,
but the groundmass consists of a fine-grained mosaic of
newly formed feldspars, quartz, biotite, and hornblende. A
system of steep faults, believed to be partly the result of
cauldron subsidence, terminates the volcanics on their
western and northern sides.

From the character of the lower contact of Traveler
Rhyolite, Rankin (1968) deduced that the early volcanics
were deposited into a shallow marine environment which
changed rapidly into a land area. The dominant volcanic
type throughout the volcanic sequence is an ignimbritic
welded ash flow tuff, with varying degrees of compaction
and variable phenocrystic contents. Based on the latter,
the volcanics were subdivided by Rankin (1961, 1968) into
the basal Pogy Member and the overlying Black Cat Member
(Table 2).

    B.   Geology of the Traveler Rhyolite

        1. Pogy Member

The basal Pogy Member, named after type ex-
posures on North Pogy Mountain, occurs as a unit about 1000
m thick, between underlying Matagamon Sandstone and overly-
ing Black Cat Member. A number of features indicate that

Fig. 4. Geologic Map of Traveler Rhyolite and Sample
         Locations. Geology Modified After Rankin (1968).

         Legend: 1 – Black Cat Member of Traveler Rhyolite
                 2 – Pogy Member of Traveler Rhyolite
                 3 – Trout Valley Formation
                 4 – Matagamon Sandstone
         Sample Locations: Diamonds – Samples Analyzed
                           Circles – Samples Not Analyzed

TROUT BROOK MTN ▲

HORSE MTN ▲

lower

Fowler Ponds

◇ TR 10
◇ TR 8
◇ TR 3

BURNT MTN ▲

lower

◇ 219   ◇ 220

South Branch Ponds

upper

middle

little

○ 218

BLACK CAT MTN ▲

◇ 217

NORTH
TRAVELER MTN ▲

216 ◆

LORD MTN ▲

215 ◆

214 ◆

TRAVELER MTN ▲

CENTER
▲ MTN

NORTH POGY MTN ▲

46   ○◇

51 ○○
    50

SOUTH
TRAVELER MTN ▲

Wassataquoik Lake

N

0   1
⊢───┴───┤ k m

☐ 1
▦ 2
▨ 3
■ 4
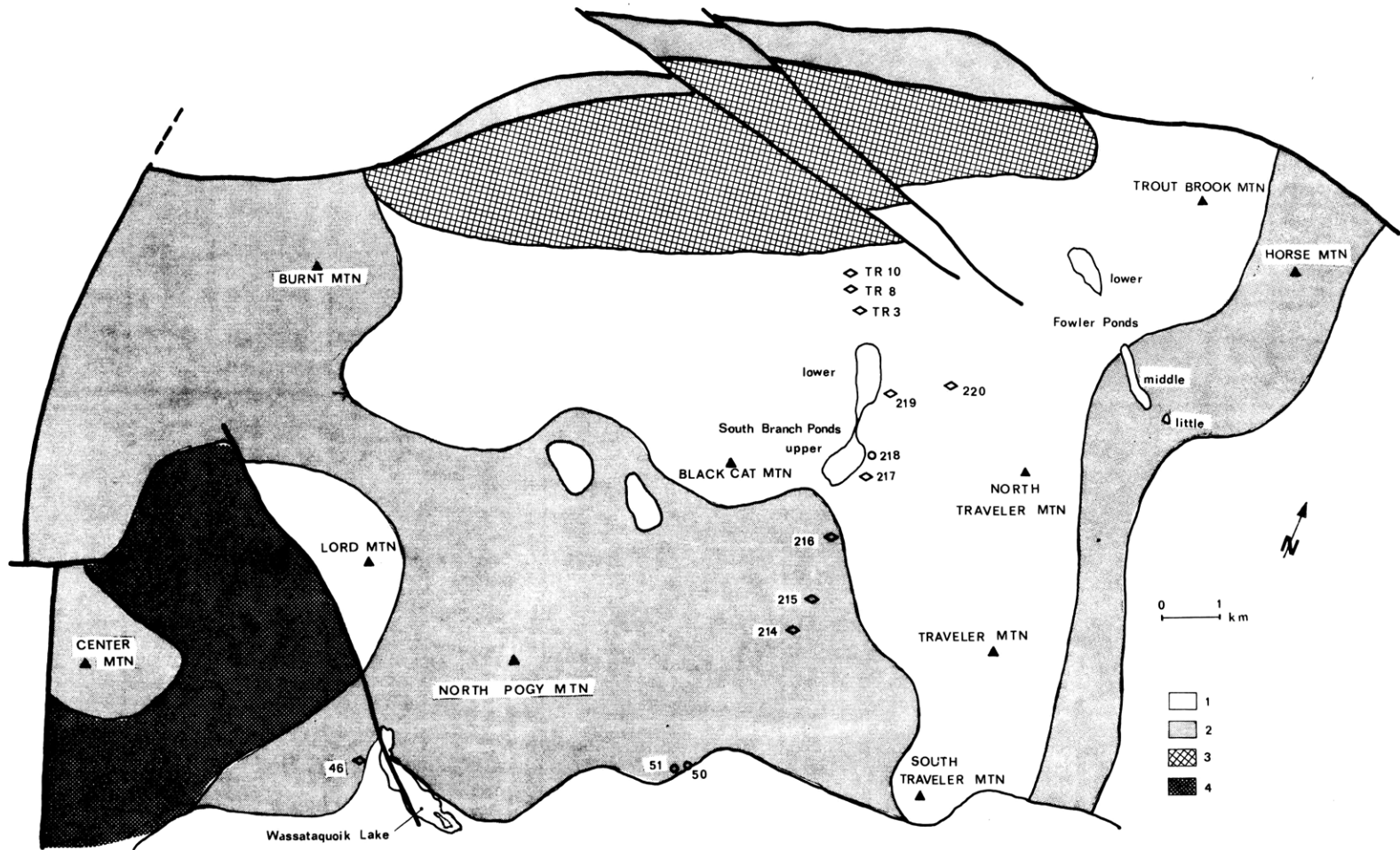
the early volcanic deposits were emplaced on unconsolidated
sediments and in a shallow marine environment (tuffaceous
character of the sediments directly below the contact,
scouring, clastic dikes, etc.--Rankin, 1968). The contact
with the upper Black Cat Member is gradational, marked by:
(1) quartz, the major phenocrystic component of the Pogy
unit, becomes rare or absent; (2) mafic silicates are more
abundant and less altered in the Black Cat unit; and (3) the
total amount of phenocrysts is lower in the Black Cat unit.
The prominent rock types are welded ash flow tuffs, deposit-
ed as loosely packed, ignimbritic pyroclastics, which were
subsequently compacted while still retaining their own heat
and "welded" into a banded solid rock.

The welded tuff in fresh hand-speciments is a dark,
almost black, flint-like, dense rock with conchoidal frac-
ture surfaces and large, glassy phenocrysts of quartz and
plagioclase up to 3 mm in size. Upon hydrothermal altera-
tion, the rock is gradually bluish, greyish, greenish and
light greenish-grey, with plagioclase phenocrysts becoming
opaque-white or greenish-white. Banding, produced by
numerous subparallel flattened shards and lithic fragments,
is not commonly visible in fresh hand-specimens; however,
it is strongly enhanced on whitish, weathered surfaces by
a selective erosion of the softer groundmass. Frequently,
crude columnar jointing is well developed.

2. Black Cat Member

The upper Black Cat Member, named after type exposures on Black Cat Mountain, has a stratigraphic thickness of about 2.5 km. It is composed mainly of well compacted, welded ash flow tuffs with a compaction ratio of up to 1:20. The ash flow sheets have well developed planar features and columnar jointing. Compared to the Pogy Member, it has less extensive deuteric alteration, a lower phenocryst content, and a much lower abundance of quartz phenocrysts (Table 2).

C. Mineralogy of the Traveler Rhyolite

The lower Pogy unit contains between 10 and 25% phenocrysts, typically about 15%, made up of 60% plagioclase, 30% quartz, 8% mafic silicates (clinopyroxene, biotite), and 2% opaques, plus accessory zircon, monazite(?), apatite, and occasionally alkali feldspar, garnet and hornblende (Table 2). The Black Cat Member has on average a smaller proportion of phenocrysts (10%), ranging from about 5 to 15%, and a significantly different proportion of phenocrysts: 75% plagioclase, 20% mafic silicates, 4% opaques plus accessory zircon, apatite, monazite(?), 0 to 5% quartz, no alkali feldspar, no garnet and frequently fayalitic olivine. These mineral differences, particularly the virtual absence of quartz in the Black Cat Member, are fundamental and serve as the criteria for distinguishing these two units (Rankin, 1968). Noticeable differences also include the

Table 2

UNIT	POGY MEMBER	BLACK CAT MEMBER
Stratigraphic Position	Lower	Upper
Estimated Thickness	1000 m	2500 m
Average Content Of Phenocrysts	15%	10%
Percentage Range Of Phenocrysts	10-25%	5-15%
Extent Of Alteration	Extensive	Moderate
Aggregation Of Phenocrysts	Single Crystals	Common Mineral Aggregates

Modal Composition Of Phenocrysts:

Plagioclase	60	75
Quartz	30	±
Alkali Feldspar	±	-
Clinopyroxene & Biotite	8	20
Hornblende	±	±
Garnet	±	-
Olivine	-	+
Opaques	2	4
Microphenocrysts Of Apatite, Zircon, Monazite	+	+

freshness of phenocrysts and their mode of aggregation.
Rocks within the Pogy unit display phenocrysts freely sus-
pended in the groundmass, whereas the phenocrysts in the
Black Cat unit frequently form mineral aggregates. The
phenocrysts of the Pogy Member show a more advanced degree
of alteration. The mafics are commonly fully altered and
the plagioclase is often completely obliterated by secondary
minerals. Occasionally, the mafic phenocrysts of the Black
Cat unit are also altered, but more frequently they are fresh
or have at least unaltered remnants in their centers.
Plagioclase is usually fresh.

Two rhyolitic samples from the Black Cat unit (Sample
#217 taken near the contact with the Pogy unit, and Sample
#219 taken from the interior of the Black Cat member) were
selected for a detailed electron microprobe study. All the
samples collected along the Pogy Notch (N-S) profile, how-
ever, were examined optically. The sample localities are
given on Fig. 4.

Plagioclase:

Plagioclase forms up to 4 mm large, thick tabular
euhedral or subhedral phenocrysts. They are typically
oscillatory zoned, with continuous or stepwise normal zoning
in each oscillatory section. Occasionally, one of the inner
oscillatory sections is resorped or corroded. Plagioclase
composition in Sample #219 ranges from An54 Ab44 Or2 to
An33 Ab63 Or4, and in Sample #217 from An53 Ab45 Or2 to
An31 Ab65 Or4 (Fig. 5). Optical examination indicates a

similar compositional range for all samples. There is a slightly lower anorthite content (by 2 to 5 mol.% An) in plagioclases from the Pogy unit. When mildly altered, plagioclase is either sericitized or saussuritized, or in a more advanced alteration stage, it is completely replaced by a mixture of secondary minerals: sericite, calcite, kaolinite, epidote group, and chlorite, with calcite being the dominant phase. Many plagioclase phenocrysts contain accessory apatite or, less commonly, zircon and opaques. Polysynthetic albite twinning is pronounced; Carlsbad twinning is frequent.

Alkali Feldspar:

No alkali feldspar has been observed in any of the samples examined in this study, but Rankin (1968) reported its infrequent trace occurrence in a few samples of the Pogy Member. In one sample, where he reports the presence of alkali feldspar in large amounts, the alkali feldspar is slightly perthitic, low sanidine, with an estimated composition of Or67. Alkali feldspars have never been found in the Black Cat unit.

Quartz:

Quartz is present in significant amounts in the Pogy unit only. Euhedral, subhedral or fragmental quartz phenocrysts have an hexagonal outline (high quartz); they are up to 2 mm large and contain frequent, open or closed, embayments of groundmass. Quartz also contains numerous fluid

Fig. 5.   Plagioclase and Alkali Feldspar Compositions
          Determined by Electron Microprobe Analysis.
          Plotted on Molecular An-Ab-Or Diagram.

          Legend: TRBC – Traveler Rhyolite: Black Cat Member
                  KGD – Katahdin Granite: Doubletop Facies
                  KGCT – Katahdin Granite: Cathedral Facies
                  HQD – Horserace Quartz Diorite

PLAGIOGLASE

• 219 TRBC
○ 217 TRBC

COEXISTING FELDSPARS

△ 150 KGD
▲ 121 KGCT- Phenocrysts
□ 74 KGD
■ 29 KGD

⬡ 235 HQD

◇ 121 KGCT- Groundmass

● 74 KGD - Perthite Lamellae

AN

AB

OR

30
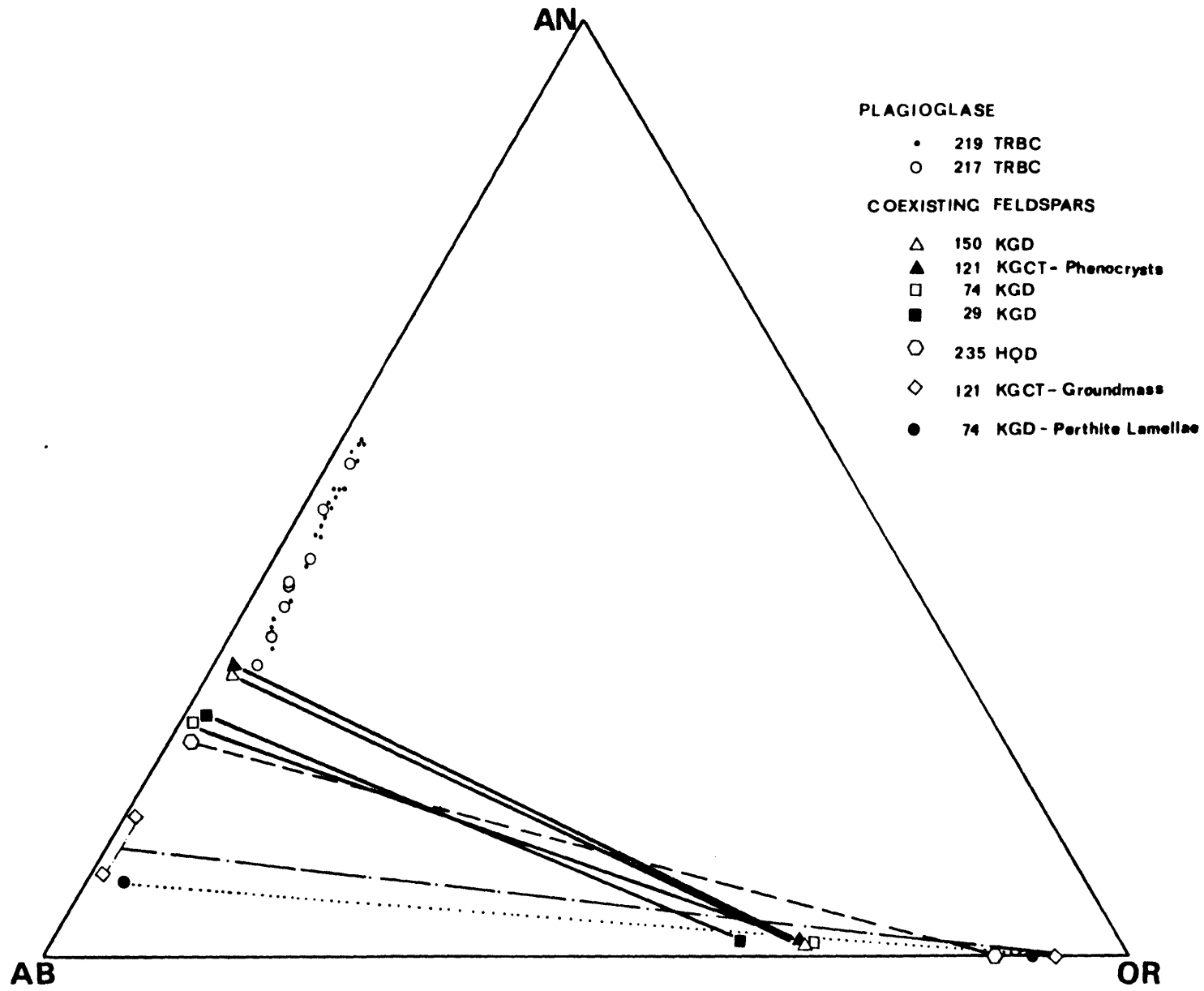
inclusions (in tens of microns or less) and occasionally
small inclusions of apatite and opaques.

The volcanics of the Black Cat Member contain quartz
only occasionally and only in trace amounts. There is,
however, no proof that the quartz in the Black Cat samples
is of a primary magmatic nature. Most of the quartz is
believed to be of a secondary origin; that is, it crystal-
lized into open voids upon cooling of the stil hot layers
of tuffaceous deposits.

Clinopyroxene:

Clinopyroxene was positively identified only in samples
from the Black Cat Member. Its presence in the Pogy Member
is implied on the basis of abundant pseudomorphs now filled
by chlorite, calcite, epidote minerals, opaques, and possib-
ly prehnite. Short prismatic, up to 2 mm large, euhedral or
subhedral crystals of clinopyroxene are frequently twinned
with infrequent inclusions of accessory apatite, zircon,
monazite(?), and opaques. Microprobe data on clinopyroxene
from Samples #217 and #219 show a tight clustering of indi-
vidual analyses around Wo39 En20 Fs21--ferroaugite (Fig. 6).
These phenocrysts are very homogeneous except for the cores
which show slight enrichment in the Tschermark's molecule.
Based on identical optical properties, it is concluded that
the composition of clinopyroxene was essentially constant
throughout the Black Cat Member and possibly throughout the
entire section of the Traveler Rhyolite.

Fig. 6. Chemical Compositions of Coexisting Olivine And
         Clinopyroxene in Black Cat Member of Traveler
         Rhyolite: Sample # 219. Compositions Determined
         by Electron Microprobe Analysis. Olivine Compo-
         sitions Are Plotted on Molecular Forsterite-
         Fayalite-Tefroite Diagram And Clinopyroxene
         Compositions Are Plotted on Wollastonite-Ensta-
         tite-Ferrosilite Molecular Diagram. Heavy Con-
         toured Lines And Tie-Lines Are For Coexisting
         Olivines, Orthopyroxenes And Clinopyroxenes in
         Tertiary Acid Glasses as Determined by
         Carmichael (1960).

CaSiO₃ : $CaSiO_3$

Mn₂SiO₄ : Mn_2SiO_4

- • CPX
- x OLIVINE
- ○ CPX ⎫
- □ OPX ⎬ Carmichael (1960)
- △ OLIVINE ⎭

MgSiO₃ : $MgSiO_3$

Mg₂SiO₄ : Mg_2SiO_4

FeSiO₃ : $FeSiO_3$

Fe₂SiO₄ : Fe_2SiO_4
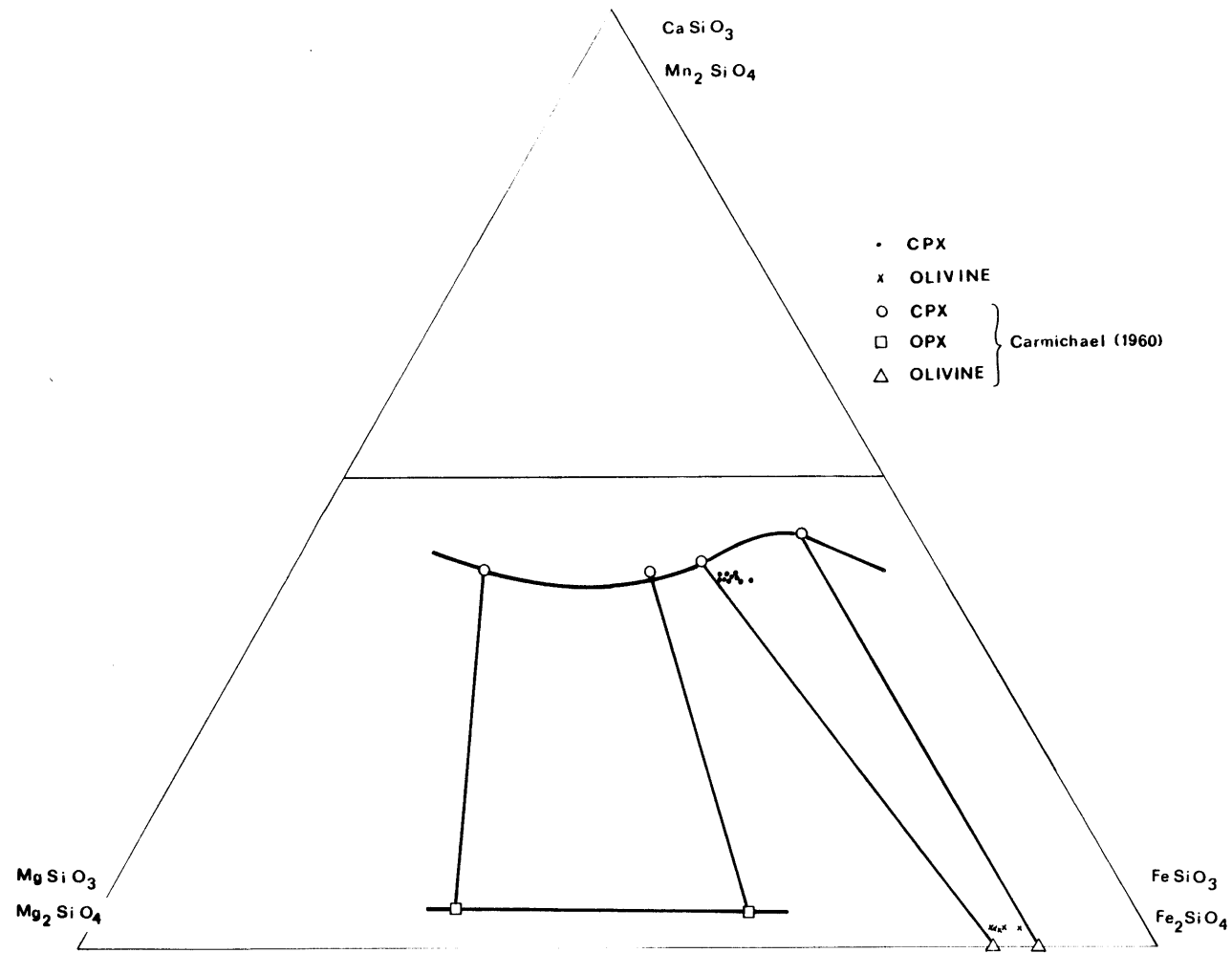
<u>Olivine</u>:

Fayalitic olivine (Fo14 Fa84 Tf2), representing about
10% of phenocrysts, was found in only one fresh sample
(Sample #219) from the Black Cat unit (Fig. 6). Here, the
olivine is unaltered and forms equidimensional subhedral,
fractured grains (up to 1.5 mm in size), with frequently
attached or enclosed opaques. Microprobe data of the
opaques show that they are mostly magnetites and only rarely
ilmenites. The textural relationships within the fayalite-
opaque aggregation suggest that at least some of the magnet-
ite may be the product of oxidation of fayalites (QFM
reaction).

Since it is difficult to relate the chlorite-epidote-
calcite-opaque pseudomorphs to their original minerals, it
is probable that the fayalitic olivine was originally far
more widespread, not only within the Black Cat Member, but
possibly even within some parts of the Pogy Member. This
conclusion is supported by the occurrence of fayalitic
olivine in the Katahdin Granite, which is, as will be shown
later, comagmatic with the rhyolites.

<u>Biotite</u>:

Next to clinopyroxene, biotite is the most frequently
preserved mafic mineral commonly found in both the Pogy and
the Black Cat Members. Biotite forms up to 1 mm in diameter,
euhedral to subhedral, flaky phenocrysts, which contain
abundant inclusions of apatite and zircon. The intense

pleochroism of biotite from straw-yellow to dark-reddish brown is in accordance with the microprobe-determined, chemical composition: Fe/(total octahedral ions) = 0.52 and 4.05 wt.% TiO_2. Upon alteration, biotite is replaced by chlorite with numerous sagenitic needles.

Chlorite(?):

A number of conspicuous grains in Sample #219 display pronounced, hornblende-like, pleochroism, from yellow-tan to deep green. Upon detailed microscope examination, this mineral shows parallel extinction, one direction of excellent cleavage, birds-eye texture typical of sheet silicates, uniaxial or nearly uniaxial negative character, and a moderate birefrigence.

Up to 1.5 mm large, thick tabular, subhedral grains, representing about 5% of phenocrysts, are alteration-free and the overall appearance suggests a primary origin. The microprobe-determined chemical composition shows very low oxide total (87.5%) and the absence of alkali metals, alkali earth, and titanium. The cation proportions are best matched by the general formula for chlorites:

$$(Mg_{1.63}Mn_{0.12}Ca_{0.08}Fe_{8.39}Al_{1.69})$$

$$(Al_{1.51}Si_{6.59}O_{20})(OH)_{16}$$
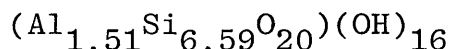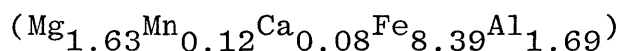
In the chlorite quadrilaterial (Fig. 7), this composition lies near the extreme limit of naturally occurring chlorites; therefore, it is believed that this mineral belongs to the

Fig. 7.. Plot of Electron Microprobe Determined Composition
of Primary Chlorite(?) Phenocrysts in Sample #219
From the Black Cat Member of Traveler Rhyolite.
Chlorite Quadrilateral After Deer, Hovie, Zussman,
1963.

37

Fe/(Fe+Mg)

Fe in octahedral site

LIMIT OF NATURAL CHLORITES

$Mg_8 Al_4 (Al_4 Si_4 O_{20}(OH)_{16}$

$Mg_{12} Si_{12} O_{20} (OH)_{16}$
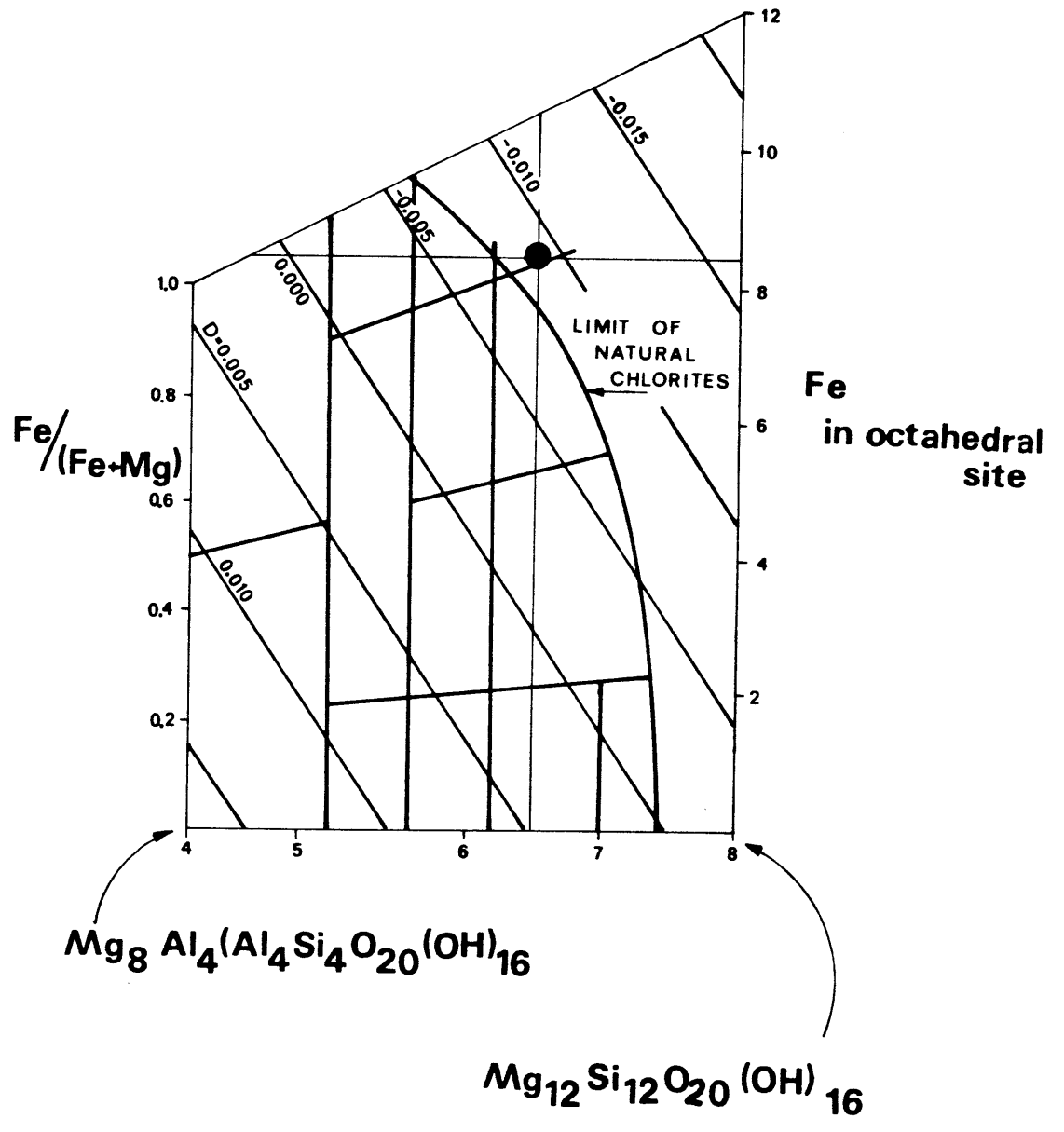
chlorite group, the dominant end-member being the iron
analogue of pennin (brunswigite).

Other Mafic Silicates:

Garnet is a rare, medium-size, euhedral, equidimension-
al mineral not observed in any of the samples studied here,
but reported by Rankin (1968) as an occasional accessory.
Also reported by Rankin (1968) is the rare occurrence of
hornblende.

Iron-Titanium Oxides:

In all the fresh samples studied, the titanomagnetites
and ilmenites are ubiquitous microphenocrysts. The micro-
phenocrysts, usually 0.05-0.1 mm in size, constitute approx-
imately 2% and 4% of the total phenocryst content within
the Pogy and Black Cat units, respectively. In Sample #219
(Black Cat Member) ilmenites are frequently associated with
clinopyroxene and plagioclase, whereas titanomagnetites are
always attached to fayalites. Microprobe analyses of co-
existing titanomagnetites and ilmenites from Sample #219
were recalculated according to the method described by
Carmichael (1967): the ulvospinel content (mole percent of
the titanomagnetites) ranges from 44.3% to 54.2% (average
50.4%). The ilmenites contain between 2.8% and 4.6% of
Fe_2O_3 in solid solution (average 4.0%). The average ilmenite-
titanomagnetite tie-line is shown on Fig. 8. The analysis
of Co, Ni, V and Zn was attempted, but none of these elements
were found. Low oxide totals of titanomagnetites are at-
tributed to deuteric oxidation.

Fig. 8. Chemical Compositions of Coexisting Ilmenite And
         Magnetite in Black Cat Member of Traveler Rhyolite:
         Sample # 219. Compositions Determined by Electron
         Microprobe Analysis Are Plotted on Molecular TiO_2 –
         FeO – Fe_2O_3 Diagram.

         Legend: 1 – Magnetite s.s. of Sample # 219
                 2 – Ilmenite of Sample # 219
                 3 – Range And Limits of Naturally Occurring
                     Coexisting Fe-Ti Oxides And Their
                     Tie-lines (Carmichael, 1967)
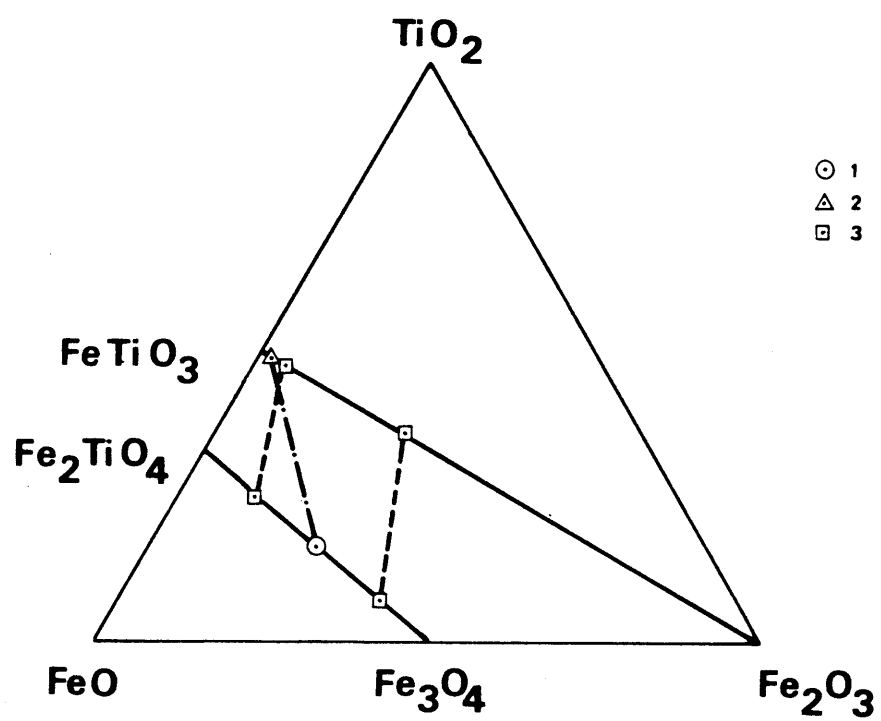
D. Petrology of the Traveler Rhyolite

1. Estimates of Temperature, Oxygen Fugacity,
and Water Fugacity

A preliminary optical examination of 11 samples
showed that only one specimen, Sample #219, was fresh enough
to ensure accurate estimates of intensive parameters from co-
existing mineral phases. The essentially identical mineral-
ogy of other samples, even if not as fresh, warrants a cau-
tious but reasonable extrapolation to the entire volcanic
sequence, or, at least, to a major part of it.

Oxygen Fugacity Estimates

Estimated values of oxygen fugacity and temp-
erature from ilmenite-magnetite pairs have resulted in
considerably uncertainties, largely due to a compositional
variation of the magnetite solid solution (Mt45 Usp55 –
Mt55 Usp45) and due to a decreased sensitivity of the
ilmenite-hematite solid solution in the range of low oxygen
fugacities. Since both opaques coexist with fayalitic
olivine, the temperature and $f(O_2)$ can be estimated, instead,
from an oxidation reaction of fayalitic olivine, as deter-
mined by Wones and Gilbert (1969):
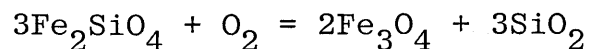
$$3Fe_2SiO_4 + O_2 = 2Fe_3O_4 + 3SiO_2$$

Fayalite + Oxygen = Magnetite + Quartz

$$\text{Log } f(O_2) = -25738/T(^OK) + 9.00 + 2 \log a(Mt) + 3 \log a(Q) - 3 \log a(Fa)$$

Fig. 9. Plot of Log $f(O_2)$ - T(^{O}C) for Coexisting Ilmenite s.s.
And Magnetite s.s. in Black Cat Member of Traveler
Rhyolite: Sample # 219.(Buddington, Lindsley,1964).
Compositions Determined by Electron Microprobe
Analysis. Lines Designated as QFM-1, QFM-2, QFM-3 Are
Quartz + Magnetite + Fayalite Univariant Lines Calcu-
lated For a(Q)=0.95, a(Fa)=0.72, a(Mt)=0.45; 0.50;
0.55, Resp. Equilibrium Constant For QFM Reaction
From Wones, Gilbert, 1969.

	T °C	log f (O_2)
1	788	-15.42
2	810	-15.00
3	837	-14.51
OX	803	-15.22
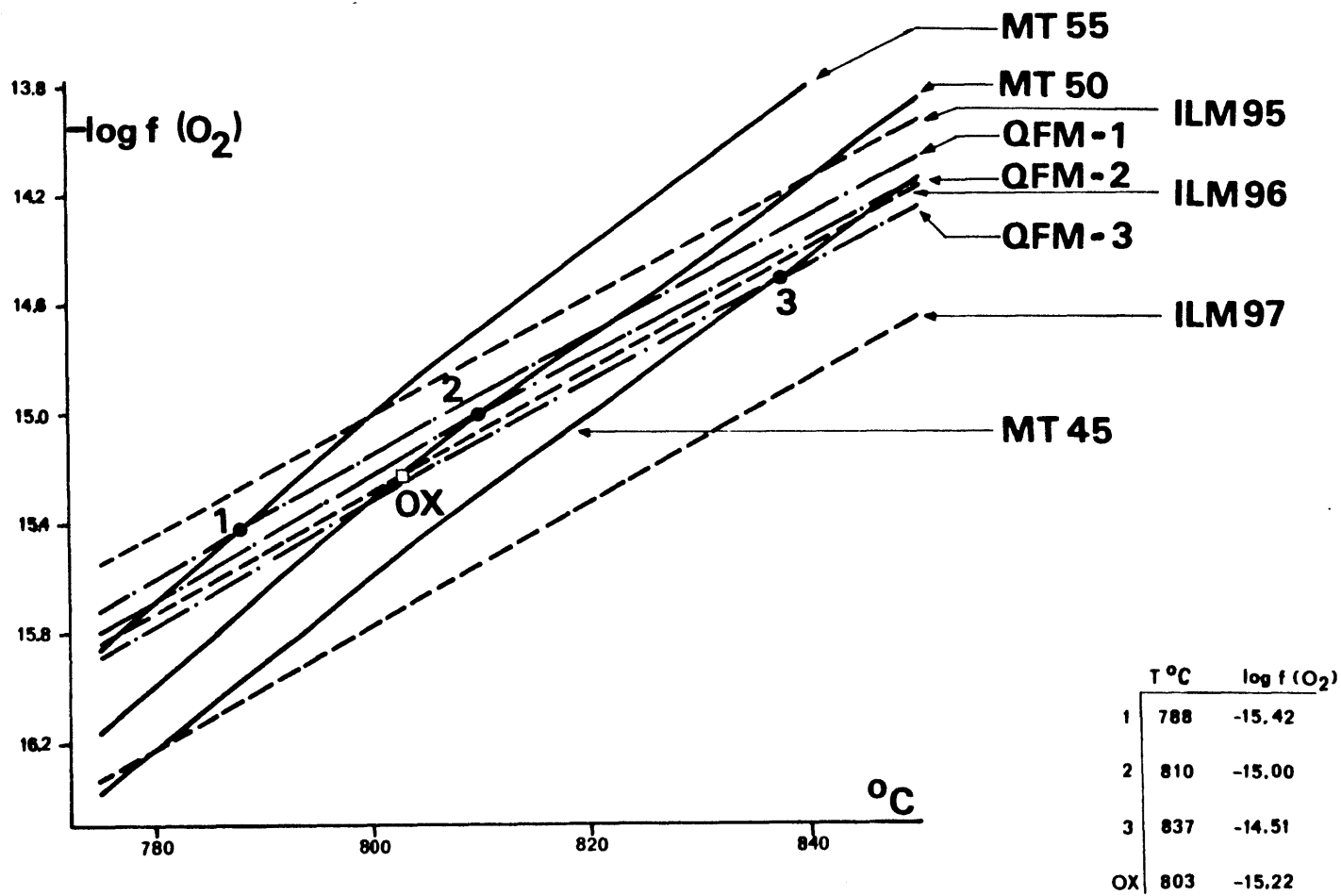
Assuming ideal solution models for magnetite and olivine solid solutions, and assuming the activity of quartz to be about 0.95, the oxygen fugacity can be readily expressed in terms of temperature. The activity of quartz, equal to 0.95, is based on equilibrium constant for reaction SiO_2 (glass) and quartz (Nicholls, 1972). The quartz is assumed to be a stable phase at temperatures 50 degrees lower than the liquidus. Three curves, relating temperature and $f(O_2)$, were calculated for a compositional range determined by microprobe analysis: olivine x(Fa) = 0.85 and X(Mt) = 0.45; 0.50; 0.55. These curves, including relevant curves for coexisting ilmenite-magnetite pairs from Buddington, Lindsley (1964), are shown in Fig. 9.

$$a(Fa) = (x(Fe))^2 = 0.72$$

$$a(Mt) = x(Mt) = 0.45; \ 0.50; \ 0.55$$

The intersection of the calculated QFM curve, with the corresponding curve for magnetite solid solution, indicates the temperature and $f(O_2)$ at which olivine, magnetite, and ilmenite are in equilibrium. The intercepts are (Fig. 9):

	x(Mt)	x(Hm)	T $^{\circ}$C	Log $f(O_2)$
1.	0.55	0.045	787	-15.42
2.	0.50	0.043	810	-15.00
3.	0.45	0.039	837	-14.51
Fe-Ti Oxides:	0.50	0.040	803	-15.22

The estimates based on the coexisting titanomagnetite and ilmenite pair are given for comparison.

Note that the equilibrium ilmenite composition should lie between Ilm96.1 Hm3.9 and Ilm95.5 Hm4.5, which agrees well with the compositions determined via microprobe (Ilm96 Hm4). The uncertainty due to the estimated activity of quartz is very small and can for all practical purposes be ignored. However, there is a possibility that the magnetite solid solution is not in equilibrium with ilmenite and, in such a case, these temperature estimates would represent minimum values.

Temperature Estimates:

Kudo, Weill (1970), Roeder, Emslie (1970), and Roeder (1974) give empirical sets of equations which enable temperature estimates to be made based on equilibrium of plagioclase or olivine with their respective groundmasses. The rim of plagioclase phenocrysts (Sample #219) has a composition of An34.5 and coexists with a groundmass of normalized molar proportions equal to:

$$x \ (SiO_2) = 0.7890, \ x(Al_2O_3) = 0.1485, \ x(CaO) = 0.0120$$
$$and$$
$$x \ (Na_2O) = 0.0505.$$

Temperature estimates calculated for several assumed values of $P(H_2O)$ yield the following results (Kudo, Weill, 1970):

P(H_2O) (Kb)	T $^{\circ}$C
Dry	927
0.5	877
1.0	805
1.5	709
1.8	605

The equation coefficients for 1.5 Kb and 1.8 Kb were obtained by interpolation. The equation at pressures above 1.8 Kb becomes unsolvable; this pressure places a minimum limit on temperature and a maximum limit on P(H_2O).

The olivine-groundmass equilibrium equation gives the following set of temperature estimates:

	Roeder, Emslie (1970)	Roeder (1974)	Avg.
MgO distribution	795°C	758°C	776°C
FeO distribution	685°C	661°C	673°C

The temperature estimates, based on FeO distribution, are clearly too low. This can be partly attributed to the large scatter of data on which the equation is based, especially since the experiments were done at temperatures above 1150°C. The above calculations assume the total absence of Fe^{+3} in the melt; if Fe^{+3} were present, the temperature estimates would yield even lower values.

Water Fugacity Estimates:

A semi-quantitative method for estimating the pre-eruption water pressure for the Black Cat rhyolite is provided by the plagioclase geothermometer of Kudo, Weill (1970). The thermometer allows calculations of equilibration temperatures between plagioclase and groundmass for several assumed water pressures (dry, 0.5, 1.0, and 5 Kb). By interpolation, it can be solved for other values of water pressures to obtain an agreement with the temperature calculated from coexisting iron-titanium oxides and/or from coexisting olivine and groundmass. Such an agreement is obtained at water pressures in the range of 1050 to 1200 bars.

A direct calculation of $P(H_2O)$ utilizes the stability of biotite, as expressed by the following reaction:

(1) $2KFe_3AlSi_3O_{10}(OH)_2 + 3SiO_2 = 2KAlSi_3O_8 + 3Fe_2SiO_4 + 2H_2O$
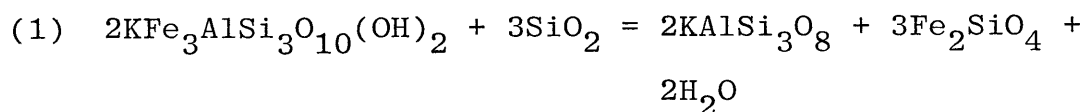
Annite + Quartz = Sanidine + Fayalite + Water

An oxidation-dehydration reaction suggested earlier by Wones, Eugster (1965) and Wones (1972) is expressed as follows:

(2) $KFe_3AlSi_3O_{10}(OH_2) + \frac{1}{2}O_2 = KAlSi_3O_8 + Fe_3O_4 + H_2O$
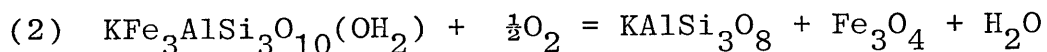
Annite + Oxygen = Sanidine + Magnetite + Water

The equation based on the above reaction requires as input data from the ilmenite-magnetite oxygen barometer-thermo-meter. Since there is a considerable compositional uncertainty associated with this pair, particularly in the composition of magnetite, reaction (1) is, therefore, preferred.

The equilibrium constant for the annite-fayalite reaction is readily obtained by arithmetical manipulation of the equilibrium constants of the annite oxidation-dehydration reaction (2) and the QFM buffer reaction (3):

(3) $3Fe_2SiO_4 + O_2 = 2Fe_3O_4 + 3SiO_2$
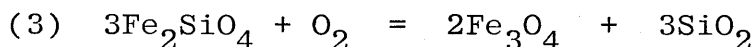
Fayalite + Oxygen = Magnetite + Quartz

When expressed as functions of $f(O_2)$ and $f(H_2O)$, the equilibrium constants are:

ad(2) $\log f(H_2O) = \dfrac{7409}{T} + 4.25$ Wones (1972)

ad(3) $\log f(O_2) = \dfrac{-25738}{T} + 9.00$ Wones, Gilbert (1969)

ad(1) $\log f(H_2O) = \dfrac{-5460}{T} + 8.75 + 3\log x \ (Ann) + \dfrac{3}{2} \log a(Q) - \log a(San) - \dfrac{3}{2} \log a(Fa)$

The annite mole fraction taken from microprobe analysis as Fe*/(sum octahedral ions) would be equal to x(Ann) = 0.52. Wones, Eugster (1965) have shown that x(Ann) at QFM buffer is actually 5 mol.% lower than the Fe*/(sum octahedral ions) value. (Note: Fe* is total atomic iron).

After applying this correction, x(Ann) is 0.47. Assuming ideal solution model for olivines, the a(Fa) taken as x^2(Fa) is equal to 0.72, and the activity of quartz is assumed to be 0.95 (see discussion on Oxygen Fugacity). The activity of sanidine is estimated from x(Or) in plagioclase, i.e., x(Or) = 0.046. According to Seck (1972), the Or level of saturated plagioclase at a temperature of 800°C and 1 Kb pressure is x(Or) = 0.063. On the assumption that the Or component in plagioclase obeys Henry's law, the sanidine activity in the TRBC magma is equal to a fractional value (0.046/0.063) of a(Or) in the plagioclase-alkali feldspar pair. From the coexisting alkali feldspar and the numerical model of Waldbaum and Thompson (1969), the calculated a(Or) for the olivine-biotite reaction is equal to 0.55.

Table 3 tabulates f(H_2O)'s calculated for several assumed values of sanidine and quartz activities. For reasons that biotite may contain an appreciable amount of fluorine, the f(H_2O)'s represent maximum values.

As shown on the diagram in Fig. 10, all temperature and P(H_2O) estimates, including the estimates derived from the fayalite-annite reaction (a(Q) = 0.93, a(San) = 0.55), are graphically illustrated. P(H_2O)'s were obtained from f(H_2O)'s, using the tables of Burnham et. al. (1973). Since the olivine-biotite pair indicates maximum P(H_2O)'s, the best temperature and P(H_2O) estimate is 800°C and 1100 bars.

Table 3

a(Q)	a(San)	Temperature °C
		760	780	800	820	840
0.90	0.45	936	1180	1474	1826	2245
	0.50	843	1062	1326	1643	2020
	0.55	766	965	1206	1494	1837
	0.60	702	885	1105	1369	1684
	0.65	648	817	1020	1264	1554
0.95	0.45	1015	1279	1518	1980	2435
	0.50	914	1151	1438	1782	2191
	0.55	831	1047	1307	1620	1992
	0.60	761	959	1199	1485	1826
	0.65	703	886	1106	1371	1685
1.00	0.45	1097	1382	1726	2138	2629
	0.50	987	1243	1553	1925	2366
	0.55	897	1130	1412	1750	2151
	0.60	822	1036	1294	1604	1972
	0.65	759	956	1195	1480	1820

Water fugacities calculated from equation (3):

a(Fa) = 0.72, x(Ann) = 0.47.

Fig. 10. Plot of Various Geothermometers And Geobarometers
          For the Black Cat Member of Traveler Rhyolite:
          Sample # 219. See Text For More Details on Calcu-
          lations And Selected Reactions.

Various Geothermometers And Geobarometers Obtain From Mineral

Assemblages of Sample # 219 of Black Cat Member, Traveler Rhyolite.

P (H₂O)

Kb

P (H$_2$O)

Kb

- - - - PL- Groundmass

- · - · - Granitic minima

━━━━ OL- Groundmass

━━━━ OL- BI

············ ILM-MT

— · · — OL- MT-(ILM)

T °C
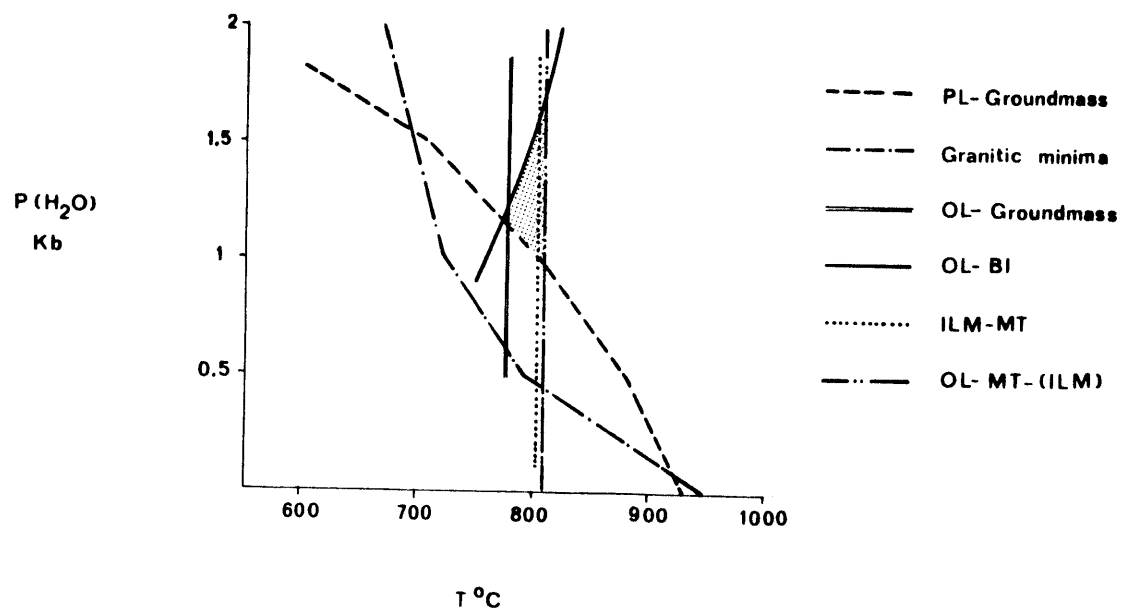
2. Major Element Geochemistry and Origin of the Traveler Magma

The equilibrium composition of granitic melts coexisting with one or two feldspars and quarts has been shown by several investigators to be sensitive to changing water pressure, temperature, total pressure, and other volatile components. Experimental studies presenting data on these equilibria are listed below:

(1) Tuttle, Bowen (1958), and Luth, Jahns, Tuttle (1964) studied the water saturated portion of Q-AB-OR-H_2O systems at pressures up to 10 Kb $P(H_2O)$;

(2) v. Platten (1965), James, Hamilton (1969), Winkler, Lindemann (1972) and Winkler, Ghose (1973) investigated similar systems but included an AN component;

(3) Luth (1969), Whitney (1972), and Steiner, Jahns, Luth (1975) studied the effect of water undersaturation in the granitic system;

(4) Goranson 1931), Burnham, Jahns (1962), Burnham (1967), Brown (1970), and Cann (1970) determined water solubility and the role of water during partial melting in granitic systems;

(5) Wyllie, Tuttle (1961, 1964), v. Platten (1965), and Glyuk, Anfilogov (1973) presented data on water saturated granitic systems containing halogens (HF, HCl) as additional volatile components.

Fig. 11 illustrates pertinent experimental data within the
Q-OR-AB-AN tetrahedron. The lower part of the diagram shows
projections of the alkali feldspar-plagioclase-quartz melt
cotectics onto the front AN-AB-OR plane, whereas the center
part is a projection on the Q-OR-AB base.

This combined diagram allows a reconstruction in space
of each of the cotectic curves within the tetrahedron. The
important characteristic of each cotectic line is a nearly
constant AN content, decreasing sharply as it approaches its
corresponding minimum melting point in the Q-OR-AB plane.
The Ab/Or ratio of the cotectic "elbows" is a very sensitive
function of $P(H_2O)$. The ratio increases with increasing
$P(H_2O)$. This effect is counteracted by even a very small
concentration of halogens (v. Platten, 1965). There are
also indications of the possibility of a quarternary minim-
um near the vicinity of the cotectic "elbow". Strongly
differentiated granitic melts, e.g., aplitic dikes, still
contain significant amounts of CaO. Noble et. al. (1970)
documented a quarternary minimum in natural, slightly
paralkaline melts. Any set of granitic melts that clusters
near one of these "elbows" can be considered as being in
equilibrium with two feldspars and quartz at $P(H_2O)$ indicated
by the particular cotectic line.

Thirteen fresh samples of whole rocks and groundmass
from the Traveler and Kineo Rhyolites were analyzed for
major elements by electron microprobe. The techniques

55

Fig. 11. Experimentally Determined Crystal-Liquid Equilibria
Within Q-Or-Ab-An Tetrahedron For P(H$_2$O) Up to 4 Kb.

Legend: 1 - Shift And Range of Change of Q-Or-Ab
Eutectics With Increasing Water Under-
saturation at P(T)= 4 Kb (Steiner and
Others, 1975)

2 - Two Feldspar, Quartz And Melt 4 Kb P(H$_2$O)
Cotectic;   (From Winkler And Lindeman,
1972, And From Luth and Others, 1964)

3 - Data Points And Quaternary Cotectic For
P(H$_2$O)= 2 Kb (v.Platten, 1965; Winkler
And Lindeman, 1972; Tuttle And Bowen,
1958)

4 - Data Points And Quaternary Cotectic For
P(H$_2$O)= 1 Kb (James and Hamilton,1969)

5 - Data Points For P(H$_2$O)= 2 Kb With 0.05 M
Added HCl (v.Platten, 1956)

6 - Q-Or-Ab Ternary Minima And Eutectics For
P(H$_2$O)= 0.5; 1; 2; 3; 4; 5; 10 Kb.(Tuttle
And Bowen, 1958; Luth And Others, 1964)

Q

AN
Q
AB   OR

1 ·····················△
2 ─ ─ ─
3 ─··─··─ ○
4 ─·─·─ ●
5 ··········· □
6 ⊢──⊣ ⊢──

OR

AB

5.
1
3 2
4
5

10

AN

708°
730°
745°

675°
685°
695°
705°
700° 780°
665° 680°
745° 690°
730°
655° 670° 725° 660° 990°

AN

AB

OR
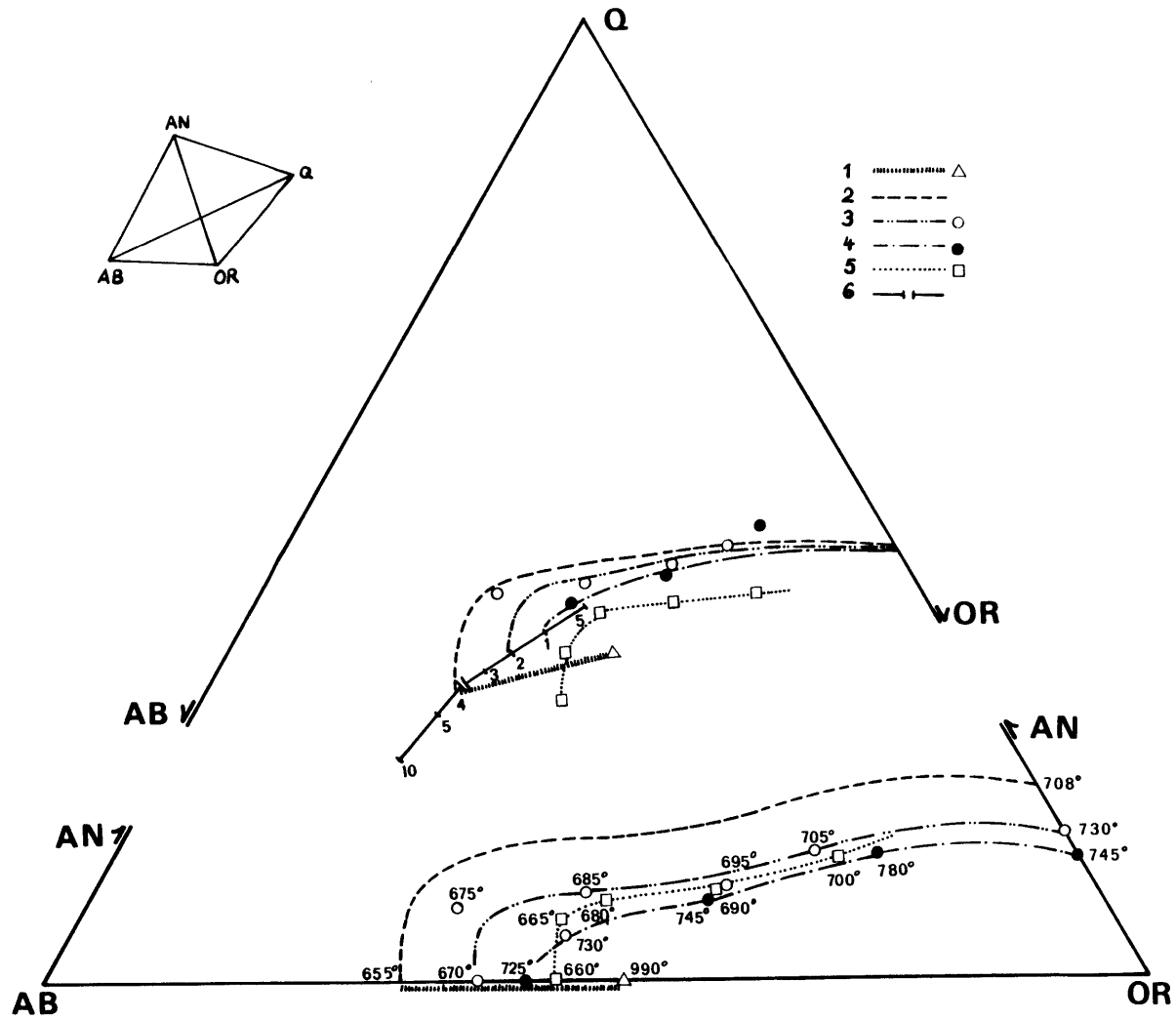
used employed a defocused beam (groundmass) and analysis of fluxed glasses (whole rock); included are also three analyses from Rankin's Ph.D. thesis and one from Smith (1933). The analyses given in Smith's (1930) and Boucot's (1969) works were excluded on the grounds of high Fe_2O_3 or H_2O^+ contents. The plots of normative (wt.%-CIPW) Q-AB-OR and OR-AB-AN ratios are illustrated in Fig. 12.

The whole rock data cluster near two lines defined by Black Cat and Pogy samples. These lines can be interpreted as halogen-bearing cotectics at 4 Kb and 3.5 Kb $P(H_2O)$, respectively. The presence of halogens in the Traveler magma is consistent with the occurrence of fluorite in the groundmass of the Traveler rhyolites.

From water solubility data of Burnham and Jahns (1962), the water content in granitic magma at $P(H_2O) = 1100$ bars is 4.4 wt.%, which represents the average solubility for temperatures between 750 and $850^{O}C$. However, if the anhydrous phenocrysts are included as part of the molten magma, the whole rock water content is somewhat lower (3.9 wt. %). Assuming that there was no significant change of water content after the magma was formed, and that the original magma temperature was slightly higher (e.g., $810^{O}C$), Fig. 13 then demonstrates that the maximum total pressure at which an undersaturated granitic magma, with 3.9 wt.% of H_2O at $810^{O}C$ can still form, is approximately 8 Kb.

It is evident that the Traveler magma was formed by partial fusion at a depth of 25-30 km and at a temperature

Table 4. Major Element Geochemistry. Samples Arranged in Ascending Numeric Order and Alphabetically.

Sample Symbol :	4	8	13	21	29	41	43	46	64	69	74
Rock Unit :	HLP	HLP	DGD	Mafic Dike	KGD	KGD	KGW	TRP	KGS	KGCH	KGD
SiO_2	70.60	70.85	72.42	55.88	72.90	75.89	74.38	74.18	75.65	75.18	76.36
TiO_2	0.35	0.36	0.33	0.71	0.26	0.23	0.30	0.26	0.23	0.23	0.21
Al_2O_3	15.78	16.13	14.70	14.29	13.21	12.54	12.76	13.12	12.64	12.86	12.07
FeO	2.40	2.30	2.43	7.05	2.48	2.01	2.32	2.28	2.32	2.41	1.53
MnO	0.02	0.07	0.05	0.16	0.03	0.09	0.02	0.07	0.13	0.04	0.03
MgO	1.03	0.95	0.72	9.97	0.24	0.14	0.26	0.18	0.13	0.11	0.08
CaO	2.55	1.81	2.06	6.69	1.35	0.50	0.43	1.15	0.86	1.15	0.63
Na_2O	4.66	5.83	3.91	2.59	3.60	4.27	3.90	3.48	3.37	3.01	3.18
K_2O	2.35	1.68	3.90	1.48	4.64	4.20	5.05	4.83	4.79	4.77	4.94
P_2O_5	0.09	0.17	0.02	0.41	0.07	0.07	0.23	0.11	0.02	0.03	0.14
Total	99.83	100.17	100.54	99.23	98.78	99.96	99.65	99.66	100.14	99.79	99.17
Loss on Ignition	1.81	1.71	0.52	5.44	0.60	0.35	0.38	0.68	0.64	0.69	0.49
CIPW Norm:											
Or	13.89	9.93	23.05	8.75	27.42	24.82	29.84	28.54	28.31	28.19	29.19
Ab	39.43	49.33	33.09	21.92	30.46	36.13	33.00	29.45	28.52	25.47	26.91
An	12.07	7.88	10.09	23.00	6.18	1.90	0.65	4.99	4.14	5.51	2.22
Q	25.99	23.98	27.49	3.23	29.25	32.36	29.97	31.26	33.86	34.99	36.73
C	1.15	1.83	0.35	--	--	0.27	0.64	0.34	0.40	0.73	0.68
Di	--	--	--	6.10	0.05	--	--	--	--	--	--
Wo	--	--	--	3.15	0.03	--	--	--	--	--	--
En	--	--	--	1.99	0.00	--	--	--	--	--	--
Fs	--	--	--	0.97	0.02	--	--	--	--	--	--
Hy	6.43	6.13	5.80	33.95	4.75	3.83	4.45	4.34	4.45	4.39	2.72
En	2.57	2.37	1.79	22.84	0.59	0.35	0.65	0.45	0.32	0.27	0.20
Fs	3.87	3.76	4.01	11.11	4.16	3.48	3.80	3.89	4.12	4.12	2.52
Ap	0.21	0.40	0.05	0.95	0.16	0.21	0.53	0.26	0.05	0.07	0.33
Il	0.66	0.68	0.63	1.35	0.49	0.44	0.57	0.49	0.44	0.44	0.40

Table 4. Major Element Geochemistry (cont.).

Sample Symbol :	81	115	121	127A	134-1	134-2	134-3	134-4	134-5	134-6	134-7
Rock Unit :	KGD	KGD	KGCT	HQD	KGD	KGD	AP3	PEG3	PEG3	AP3	AP3
SiO_2	73.92	73.99	74.08	62.67	74.91	75.14	76.89	75.90	76.42	77.32	77.35
TiO_2	0.20	0.29	0.25	0.67	0.26	0.27	0.04	0.05	0.08	0.06	0.08
Al_2O_3	13.43	13.09	13.44	15.69	13.06	13.29	13.17	13.06	13.19	12.23	12.21
FeO	3.07	2.28	2.02	4.30	2.57	2.56	0.63	0.56	0.56	0.99	0.90
MnO	0.05	0.07	0.06	0.08	0.02	0.04	0.00	0.02	0.03	0.03	0.03
MgO	0.26	0.20	0.28	4.60	0.24	0.20	0.05	0.08	0.12	0.09	0.08
CaO	1.29	1.07	1.36	4.55	1.08	0.84	0.40	0.28	0.28	0.53	0.60
Na_2O	4.82	3.37	3.48	4.25	3.38	3.80	4.21	3.52	3.22	3.85	3.90
K_2O	3.29	4.79	4.49	2.57	4.70	4.50	5.04	6.51	6.96	4.75	4.88
P_2O_5	0.20	0.13	0.02	0.28	0.02	0.04	0.02	0.03	0.05	0.00	0.00
Total	100.53	99.28	99.48	99.66	100.24	100.68	100.45	100.01	100.91	99.85	100.03
Loss on Ignition	1.39	0.92	0.53	1.14	0.50	0.62	0.24	0.43	0.33	0.82	0.40
CIPW Norm:											
Or	19.44	28.31	26.53	15.19	27.78	26.59	29.79	38.47	41.13	28.07	28.84
Ab	40.79	28.52	29.45	35.96	28.60	32.16	35.62	29.79	27.25	32.58	33.00
An	5.11	4.47	6.62	16.15	5.23	3.91	1.86	0.61	0.98	2.06	1.40
Q	28.24	32.08	31.82	10.12	32.67	31.85	31.74	29.55	30.00	34.79	34.20
C	0.07	0.72	0.43	--	0.50	0.74	0.11	--	--	--	--
Di	--	--	--	3.76	--	--	--	0.51	0.07	0.50	1.38
Wo	--	--	--	1.93	--	--	--	0.24	0.04	0.24	0.66
En	--	--	--	1.14	--	--	--	0.04	0.01	0.03	0.08
Fs	--	--	--	0.69	--	--	--	0.22	0.03	0.23	0.64
Hy	6.05	4.34	4.11	16.56	4.92	4.83	1.22	0.92	1.21	1.74	1.05
En	0.65	0.50	0.70	10.32	0.60	0.50	0.12	0.15	0.29	0.19	0.12
Fs	5.40	3.84	3.41	6.25	4.33	4.33	1.09	0.76	0.92	1.54	0.93
Ap	0.46	0.30	0.05	0.65	0.05	0.09	0.05	0.07	0.12	0.00	0.00
Il	0.38	0.55	0.47	1.27	0.49	0.51	0.08	0.09	0.15	0.11	0.15

Table 4. Major Element Geochemistry (cont.).

Sample Symbol	134-8	145	150	166	188	190F	190W	198	209	214	215
Rock Unit	AP3	AP2	KGD	DGD	AP4	KGD	KGD	KGCT	KGD	TRP	TRP
SiO_2	78.25	76.79	74.67	73.00	77.31	75.20	75.05	72.86	74.34	73.47	75.78
TiO_2	0.09	0.11	0.19	0.36	0.08	0.14	0.27	0.34	0.26	0.36	0.30
Al_2O_3	12.19	12.28	12.86	13.82	13.11	13.60	13.09	13.80	13.30	13.09	12.50
FeO	0.93	1.06	2.38	2.68	0.99	1.41	2.47	2.95	2.55	2.60	2.43
MnO	0.03	0.03	0.07	0.02	0.04	0.08	0.09	0.05	0.05	0.02	0.01
MgO	0.10	0.04	0.19	0.54	0.08	0.35	0.24	0.27	0.16	0.19	0.23
CaO	0.59	0.31	1.08	2.34	0.46	1.38	0.79	1.43	1.23	1.71	1.45
Na_2O	3.71	3.65	3.30	3.70	4.21	4.21	3.65	3.32	3.26	2.79	1.85
K_2O	4.73	4.80	4.55	3.38	4.90	3.86	4.55	4.42	4.62	5.04	4.73
P_2O_5	0.01	0.00	0.08	0.13	0.00	0.13	0.14	0.04	0.14	0.00	0.00
Total	100.63	99.07	99.37	99.97	101.18	100.36	100.34	99.48	99.91	99.27	99.28
Loss on Ignition	0.40	0.47	0.48	0.68	0.44	0.40	0.77	0.75	0.79	2.22	2.07

CIPW Norm:

	134-8	145	150	166	188	190F	190W	198	209	214	215
Or	27.95	28.37	26.89	19.98	28.96	22.81	26.89	26.12	27.30	29.79	27.95
Ab	31.39	30.89	27.92	31.31	35.62	35.62	30.89	28.09	27.59	23.61	15.65
An	2.64	1.54	4.84	10.77	2.28	6.01	3.01	6.84	5.20	8.31	7.19
Q	36.49	35.63	33.78	31.10	32.16	31.68	32.81	31.02	33.23	32.12	41.65
C	--	0.52	0.73	0.13	0.04	0.30	1.06	1.05	1.03	--	1.70
Di	0.19	--	--	--	--	--	--	--	--	0.15	--
Wo	0.09	--	--	--	--	--	--	--	--	0.07	--
En	0.01	--	--	--	--	--	--	--	--	0.01	--
Fs	0.09	--	--	--	--	--	--	--	--	0.07	--
Hy	1.76	1.92	4.66	5.71	1.96	3.38	4.85	5.62	4.74	4.61	4.56
En	0.24	0.10	0.47	1.34	0.20	0.87	0.60	0.67	0.40	0.47	0.57
Fs	1.53	1.82	4.19	4.36	1.76	2.51	4.26	4.95	4.35	4.15	3.99
Ap	0.02	0.00	0.19	0.30	0.00	0.30	0.33	0.09	0.33	0.00	0.00
Il	0.17	0.21	0.36	0.68	0.15	0.27	0.51	0.65	0.49	0.68	0.57

Table 4. Major Element Geochemistry (cont.).

Sample Symbol :	216	217	219	220	235	238	240	244	247	6291	KM1
Rock Unit :	TRP	TRBC	TRBC	TRBC	HQD	HQD	KGD	Moxie Granite	Kineo Rhyol.	Echo Pond Gr.	KGS
SiO_2	69.58	71.48	71.06	73.00	62.46	63.71	76.61	74.03	73.79	72.09	74.28
TiO_2	0.56	0.40	0.50	0.39	0.63	0.55	0.50	0.27	0.27	0.40	0.21
Al_2O_3	13.95	13.20	13.65	13.27	16.42	16.43	12.55	12.88	13.37	12.77	13.00
FeO	5.33	4.34	4.13	3.93	4.35	4.05	1.40	2.43	2.45	3.99	2.97
MnO	0.07	0.08	0.04	0.04	0.10	0.00	0.02	0.05	0.06	0.09	0.04
MgO	0.52	0.30	0.36	0.20	3.62	3.48	0.12	0.21	0.21	0.29	0.13
CaO	2.13	1.94	2.04	1.44	4.92	4.61	0.50	1.06	1.18	1.86	0.86
Na_2O	3.68	2.99	3.02	3.11	4.47	4.47	3.22	3.38	3.74	3.24	3.50
K_2O	3.93	4.74	4.58	4.31	1.99	2.03	5.11	4.71	5.00	4.36	5.02
P_2O_5	0.21	0.06	0.09	0.09	0.20	0.24	0.08	0.12	0.18	0.28	0.00
Total	99.96	99.53	99.47	99.78	99.16	99.57	100.11	99.14	100.25	99.37	100.01
Loss on Ignition	1.22	0.57	0.42	1.13	0.83	0.79	0.58	0.41	0.48	0.52	0.48

CIPW Norm:

Or	23.23	28.01	27.07	25.47	11.76	12.00	30.20	27.83	29.55	25.77	29.67
Ab	31.14	25.30	25.55	26.32	37.82	37.82	27.25	28.60	31.65	27.42	29.62
An	9.21	8.60	9.54	6.56	18.86	18.77	1.96	4.48	4.69	7.42	4.27
Q	24.28	28.24	28.19	32.25	11.13	13.12	36.48	32.22	28.66	29.81	30.31
C	0.27	--	0.23	1.08	--	--	1.00	0.58	0.09	0.00	0.25
Di	--	0.56	--	--	3.49	2.09	--	--	--	--	--
Wo	--	0.27	--	--	1.78	1.06	--	--	--	--	--
En	--	0.03	--	--	0.96	0.58	--	--	--	--	--
Fs	--	0.27	--	--	0.76	0.44	--	--	--	--	--
Hy	10.29	7.91	7.73	7.15	14.43	14.17	2.08	4.63	4.69	7.56	5.51
En	1.29	0.72	0.90	0.50	8.06	8.08	0.30	0.52	0.52	0.72	0.32
Fs	8.99	7.19	6.83	6.65	6.38	6.09	1.78	4.11	4.16	6.83	5.18
Ap	0.49	0.14	0.21	0.21	0.46	0.56	0.19	0.28	0.42	0.65	0.00
Il	1.06	0.76	0.95	0.74	1.20	1.04	0.95	0.51	0.51	0.76	0.40

Table 4. Major Element Geochemistry (cont.).

Sample Symbol :	KM2	KM6	KM6	KM8	KM9	NNP2	TR3	TR8	TR10	217GR(*)	219GR(*)
Rock Unit :	KGCT	KGS	AP1	KGS	KGCH	Lexington Granite	TRBC	TRBC	TRBC	TRBC	TRBC
SiO_2	72.58	74.40	77.87	74.26	74.63	73.67	72.94	72.79	73.57	77.46	76.37
TiO_2	0.35	0.24	0.09	0.24	0.28	0.17	0.35	0.42	0.43	0.02	0.13
Al_2O_3	14.24	12.37	12.68	13.09	13.08	14.59	13.15	13.30	13.35	12.36	12.19
FeO	3.03	2.68	1.33	2.63	2.80	1.37	3.57	4.56	3.86	0.54	1.49
MnO	0.05	0.06	0.03	0.04	0.04	0.05	0.05	0.06	0.06	0.03	0.00
MgO	0.31	0.15	0.08	0.13	0.16	0.37	0.32	0.38	0.15	0.01	0.12
CaO	1.24	0.96	0.26	0.91	1.08	0.93	1.53	0.67	1.47	0.64	1.08
Na_2O	3.83	3.18	3.48	3.55	3.36	2.91	3.31	3.74	3.13	2.58	2.52
K_2O	4.39	4.95	4.64	4.97	4.47	5.10	4.49	4.25	4.04	6.69	5.63
P_2O_5	0.15	0.12	0.00	0.06	0.02	0.25	0.08	0.08	0.07	0.00	0.00
Total	100.17	99.11	100.46	99.88	99.91	99.41	99.79	100.25	100.13	100.34	99.53
Loss on Ignition	0.81	0.64	0.60	0.65	0.38	0.80	1.10	1.78	2.14	--	--
CIPW Norm:											
Or	25.94	29.25	27.42	29.37	26.37	30.14	26.53	25.12	23.88	39.54	33.27
Ab	32.41	26.91	29.45	30.04	28.43	24.62	28.01	31.65	26.49	21.83	21.32
An	5.18	3.99	1.29	4.13	5.23	3.00	7.07	2.81	6.84	2.39	5.32
Q	28.49	32.90	38.12	30.56	33.35	34.32	30.20	29.44	33.77	35.18	36.53
C	1.29	0.32	1.46	0.36	0.81	3.18	0.25	1.52	1.32	--	--
Di	--	--	--	--	--	--	--	--	--	0.70	0.03
Wo	--	--	--	--	--	--	--	--	--	0.33	0.01
En	--	--	--	--	--	--	--	--	--	0.01	0.00
Fs	--	--	--	--	--	--	--	--	--	0.36	0.01
Hy	5.85	5.01	2.55	4.83	5.15	3.25	6.87	8.74	6.86	0.67	2.80
En	0.77	0.37	0.20	0.32	0.40	0.92	0.80	0.95	0.37	0.02	0.30
Fs	5.08	4.64	2.35	4.51	4.75	2.33	6.07	7.79	6.49	0.65	2.51
Ap	0.35	0.28	0.00	0.14	0.05	0.58	0.19	0.19	0.16	0.00	0.00
Il	0.66	0.46	0.17	0.46	0.53	0.32	0.66	0.80	0.82	0.04	0.25

(*) Data for the groundmass ONLY.

Fig. 12. Q-Or-Ab-An Normative (CIPW) Plot of Chemically
          Analyzed Samples of Traveler Rhyolite.

          Legend: Traveler Rhyolite: Black Cat Member
                    1 - This Study
                    2 - Rankin, 1961
                    3 - Composition of Coexisting Groundmass
                    Traveler Rhyolite: Pogy Member
                    4 - This Study--Fresh Samples
                    5 - This Study--Hydrothermally Altered
                    6 - This Study--Specimen With Abundant
                        Plagioclase Crystals (Xenocrysts ?)
                    7 - Rankin, 1961
                    Kineo Rhyolite
                    8 - This Study
                    9 - Smith, 1935

TRAVELER RHYOLITE :
BLACK CAT MEMBER-TRBC

○ 1
⊙ 2
△ 3

POGY MEMBER-TRP

● 4
■ 5
□ 6
⬣ 7

KINEO VOLCANICS

◇ 8
◆ 9
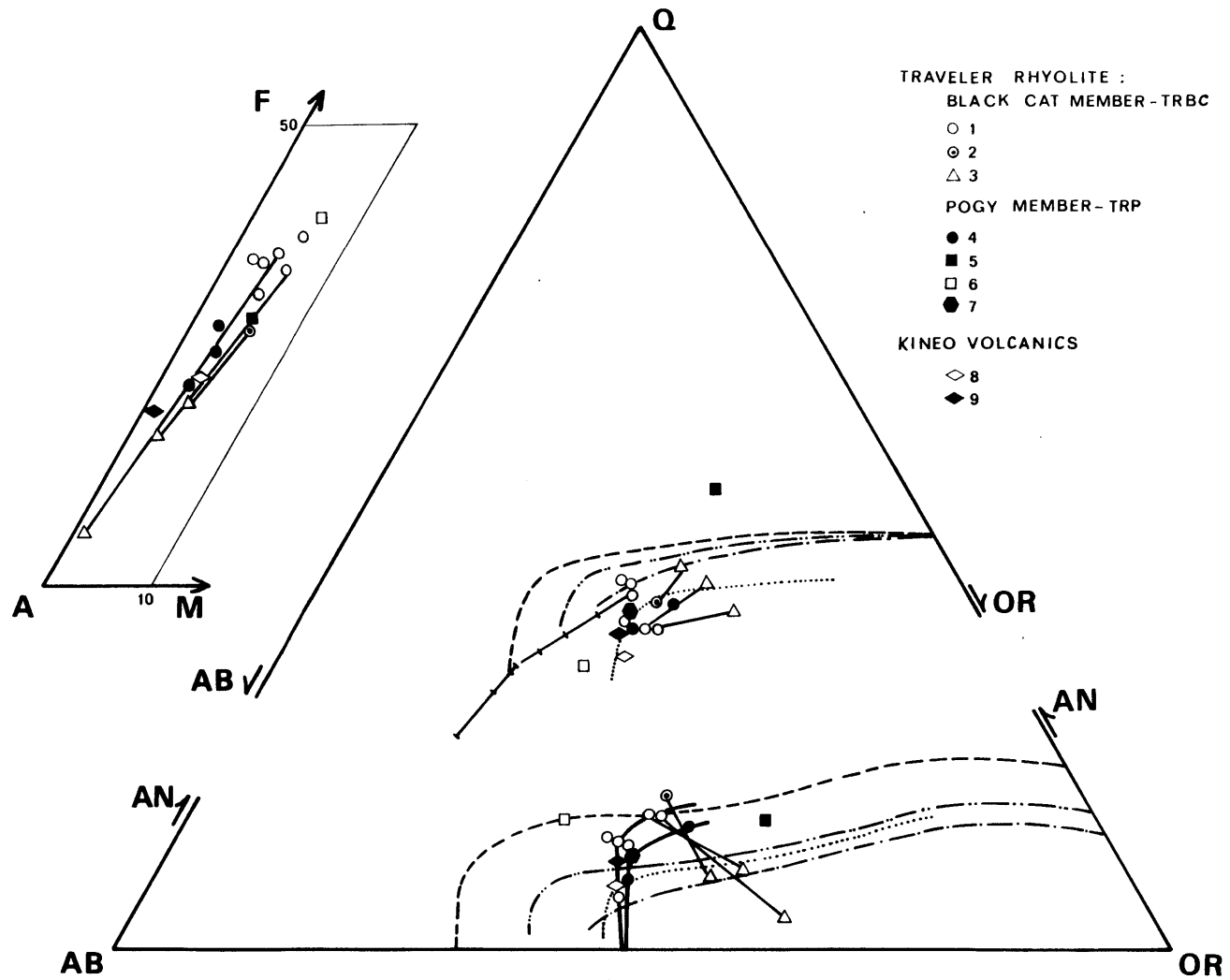
Fig. 13. Minimum Melting Temperatures for Granitic Liquids
For Various P(T) in Kb, $P(H_2O)$ in Kb, And T in $^\circ$C.
Corresponding Water Content of The Granitic Melts
in Wt% H_2O. Open Circle And Dashed Lines Are For
Sample # 219 From Traveler Rhyolite. See Text For
Further Discussion. (Based on Data of Burnham And
Jahns, 1962; and Steiner And Others, 1975. Muscovite
Plus Quartz Reaction is After Althaus And Others,
1970).
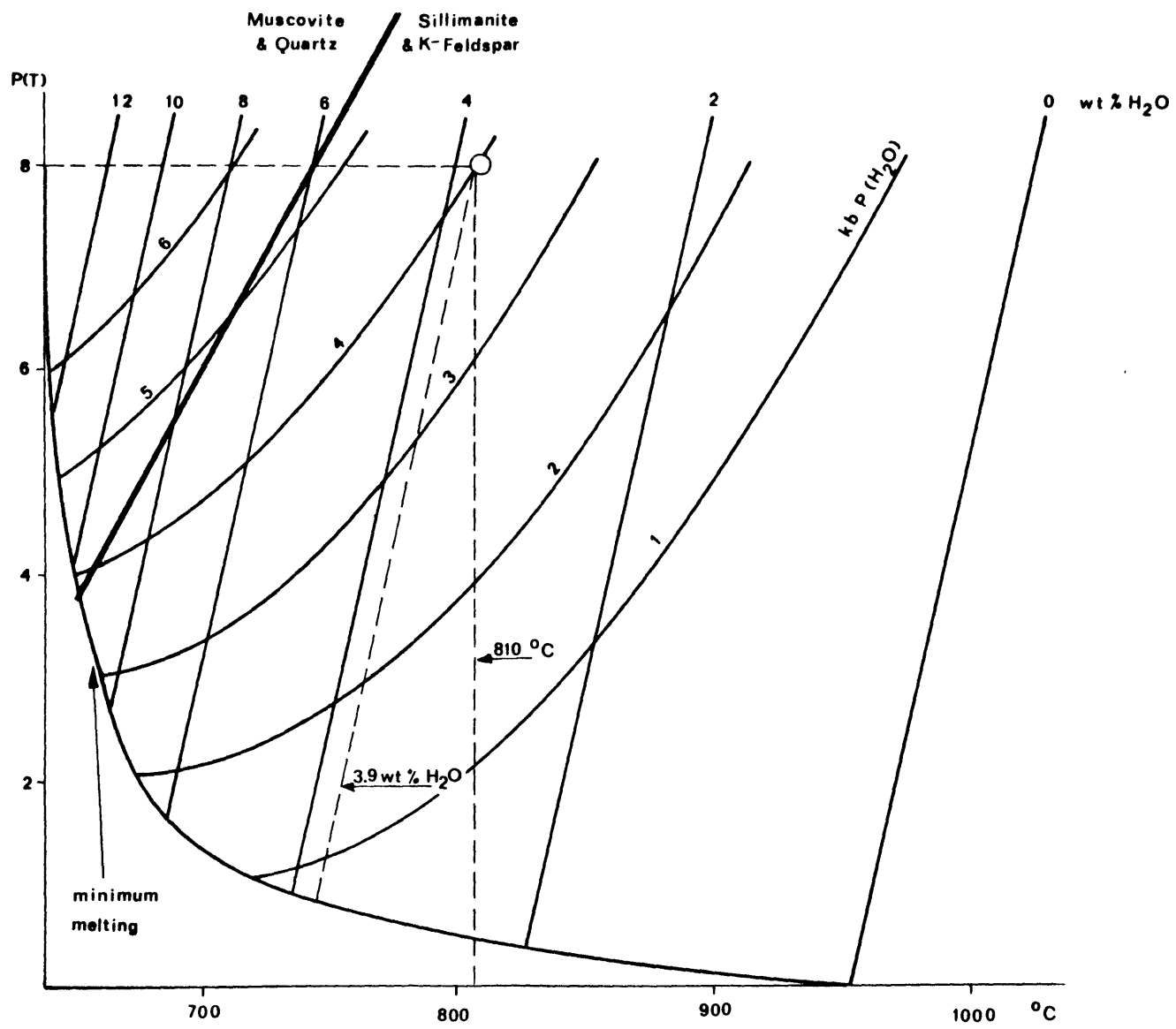
of 800-820°C. The melting process was apparently initiated by a breakdown of micas. On Fig. 13 the muscovite-quartz reaction occurs at temperatures about 60°C lower than the temperature indicated for the formation of the Traveler magma. Either muscovite was not present (only biotite mica) or the stability of muscovite was increased by the presence of fluoromuscovite in the solid solution. The oxygen fugacity was presumably maintained through an equilibrium with graphite between the QFM and MW buffers (French, 1966). The estimated partial pressure of H_2O (Fig. 13) was 4 Kb and the composition of the melt was controlled by an equilibrium with quartz, alkali feldspar, and plagioclase. Partial pressure of H_2O is also implied by projections of the Black Cat Member analyses near a 4 Kb $P(H_2O)$ cotectic (Fig. 12). Since the geometry of the cotectics is essentially independent of the confining pressure, the 4 Kb $P(H_2O)$ estimate from Fig. 12 provides additional support in favor of the above model.

Forces resulting from a gravitational instability forced the newly formed magma to move upward. At a shallower depth of approximately 3 km, the magma reached a stagnation point during which time the $P(H_2O)$ became equal to lithostatic pressure. At occasional intervals, violent eruptions transported the rhyolitic melt to the earth's surface where a sudden release of confining pressure brought about the formation of dense and thick ash flows. These ignimbritic deposits were, while still hot, compressed and

compacted under their own lithostatic pressure and were "welded" into a dense rock known as welded ash flow tuffs (Smith, 1960).

At the time of eruption, the magma of the Pogy Member was undoubtedly colder and possibly slightly more fraction- ated, presumably because it had to migrate through a colder overlying sedimentary section which was already "preheated" during the ascent of the later Black Cat magma.

Thornton's differentiation index and an AFM diagram show that the whole rock Pogy samples are more fractionated than the Black Cat samples, and that they are in line with the groundmass of the Black Cat Rhyolite. A higher per- centage of phenocrysts, ubiquitous quartz, and the occasion- al presence of alkali feldspar in the Pogy unit, are all consistent with the above model.

The homogeneous major element composition and relative- ly constant petrology throughout the Traveler Rhyolite imply a steady state of a continuous melting process and concur- rent continuous removal of the magma as the only possible mechanism that was able to generate such large quantities of chemically very homogeneous magma. This magma, which at its origin was in equilibrium with two feldspars and quartz, was most likely formed by a partial melting of eugeosynclinal sedimentary rocks from which the magma was separated by filter-pressing mechanism.

The fraction of partial fusion can be indirectly estimated from the typical content of micas in metamorphosed sediments. Since micas and TRBC magma have about the same water content, e.g., 4 wt.%, the maximum partial melt fraction should therefore be equivalent to the fraction of micas in parental rocks, typically between 20 and 40%. This estimate is in accord with the experimental results of Brown (1970).

III. GEOLOGY, MINERALOGY, AND PETROLOGY OF THE
     KATAHDIN PLUTON

A. Katahdin Pluton

The Katahdin Pluton (KP) marks the northeastern limit of a linear belt of plutonic rocks, extending across north-central and northwestern Maine. With an exposed area of 1330 square kilometers it ranks among the most prominent intrusive bodies of the Northern Appalachians.

The pluton is a shallow, composite, predominantly granitic body, with a pear-like shape, having a longer axis in the NE-SW direction, which parallels the prevalent tectonic trend (Preliminary Geologic Map of Maine, 1967). The name of the pluton is borrowed from the highest mountain in Maine--Mount Katahdin (1580 m), which is situated approximately in the center of the intrusion (Jackson, 1838; Hitchcock, 1861; Griscom, in prep.).

Topographically, the pluton consists of two unequal areas of strikingly contrasting morphologies with approximate divisions running along the West Branch Penobscot River and following a line between Katahdin Lake and Togue Pond. The northern, mountainous part is formed by an elevated plateau, gently dipping northward and sharply edged by steep ridges along the southern side and by deep valleys and glacial cirques in the remaining part of the plateau (Caldwell, 1969). The plateau, with a mean slope of 6.2%, extends from Thoreau's Springs (1380 m) in the south and near the summit of Mount

Katahdin to the 8.8 km distant Russell Mountain (840 m) in
the north (Fig. 15). This inclination is caused by a later
differential regional uplift in northwestern Maine and it is
not intrinsic to the pluton. The gradient of this regional
uplift, as estimated from the metamorphic isograds (progres-
sively deeper toward the southwest), is identical with the
earlier stated mean slope of the plateau.

In contrast, the much larger, southern area of the
pluton is a hilly lowland covered mostly by thick, glacial
deposits with elevations generally less than 450 m. The
area investigated in this study is principally restricted to
the northern mountainous part, where excellent outcrops are
abundant.

As suggested by several lines of evidence to be dis-
cussed, the pluton is a slightly flattened, funnel-shape
intrusion, not yet fully unroofed along the northern border
(Fig. 14). The contact on the northwestern side of the
Harrington Lake quadrangle dips under the pluton. This
observation is evident from the exposures near the power
house in Ripogenus Gorge and by the inward inflection of the
contacts into the valleys north of Harrington Lake. On the
northeast side, the continuation into the pluton of strong
magnetic anomalies associated with Ordovician volcanics
suggests the presence of these volcanics at a shallow depth
beneath the granites (A. Griscom, 1964). The lack of a
negative gravity anomaly near the pluton margin implies that
the granitic rocks near the contacts cannot extend to greater

72

Fig. 14. Geologic Map of Katahdin Pluton and Stock of
          Harrington Lake Porphyry.

          (Note: For Geologic Map of Traveler Rhyolite
               see Fig. 4.)

          Legend: HLP   - Harrington Lake Porphyry
                  DGD   - Debsconeag Granodiorite
                  HQD   - Horserace Quartz Diorite
                  KGW   - Katahdin Granite: Wassataqoik Facies
                  KGD   - Katahdin Granite: Doubletop Facies
                  KGCH - Katahdin Granite: Chimney Facies
                  KGS   - Katahdin Granite: Summit Facies
                  KGSB - Katahdin Granite: South Brother Facies

HLP
DGD
HQD
KGW
KGD
KGCH
KGS
KGSB

0   10   20
km

GEOLOGIC MAP OF KATAHDIN PLUTON
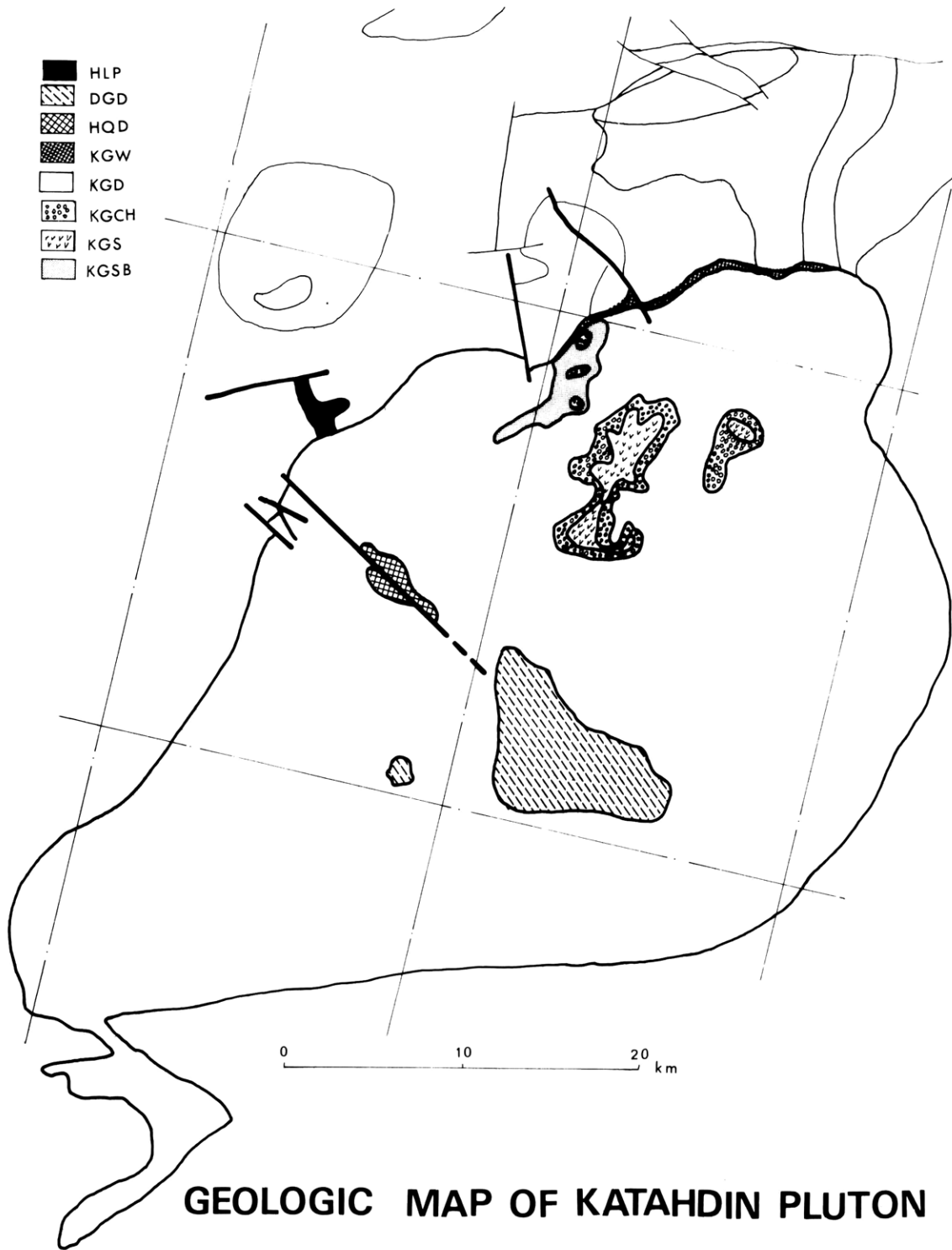
Fig. 15.   Localities of Chemically Analyzed Samples from
           Katahdin Pluton and from Harrington Lake Porphyry.
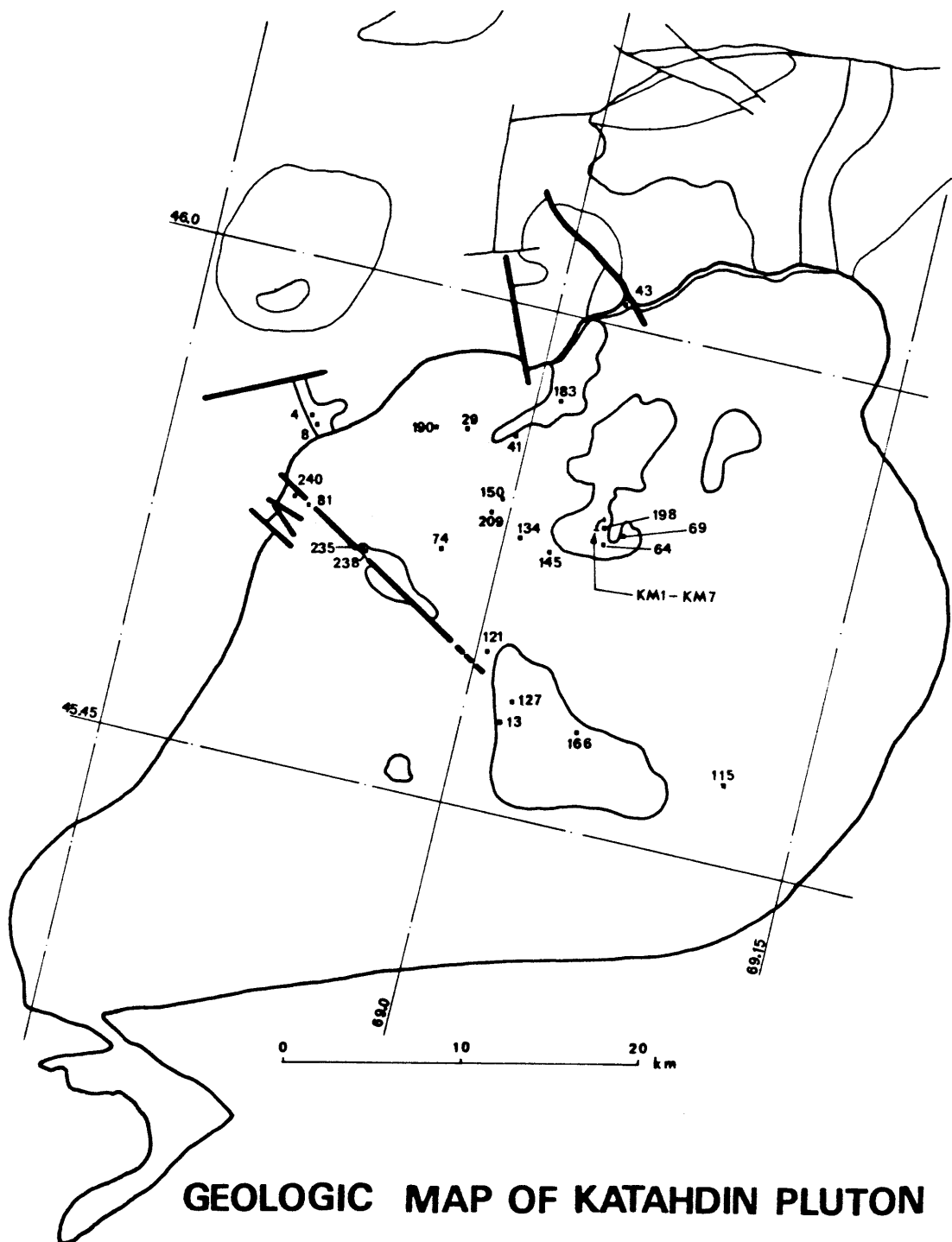
GEOLOGIC MAP OF KATAHDIN PLUTON

depths (M. Kane, 1974). Another indication of the funnel-shape of the pluton stems from the outline of the pluton. The structurally deeper southern part is conspicuously narrower than the shallower northern part. The contacts with the Traveler Rhyolite volcanics on the northern side undoubtedly dip under the volcanics.

The character of the contacts implies a rather permissive intrusion of granitic magma. The contacts are generally sharp, with only a few incidental blocks of country rock enclosed in the granite, crosscut by short, thin apophyses typically 20 cm wide and up to 10 m long. However, where the country rocks are ductile (pre-Silurian metamorphosed, sedimentary and igneous rocks), the intrusion takes on a more pervasive character. These contacts are formed by a brecciated zone, up to 100 m wide, of closely packed inclusions of country rock cemented by granitic matrix. The proportion of granitic matrix lessens with the distance from the pluton. The relatively narrow (approximately 100 m wide) metamorphic aureole of the pluton consists almost exclusively of biotite hornfels.

About 95% of the KP area is underlain by one of the six textural types (facies) of the Katahdin Granite. All the facies are massive, medium-to-fine grained biotite granites of identical mineralogy. Except for the porphyritic dikes, the facies have mutually gradational contacts and possess definite spatial positions within the pluton, undoubtedly as a response to local differences in cooling rates.

Fig. 16.   Generalized N-S Cross-section through Traveler
           Rhyolite - Katahdin Pluton Complex.

           Legend: 1 - Seboomook Formation
                   2 - Traveler Rhyolite
                   3 - Katahdin Granite: Chimney Facies
                   4 - Katahdin Granite: Summit Facies
                   5 - Trout Valley Formation
                   6 - Katahdin Granite: Wassataqoik Facies
                   7 - Matagamon Sandstone
                   8 - Katahdin Granite: Doubletop Facies
                   9 - Debsconeag Granodiorite
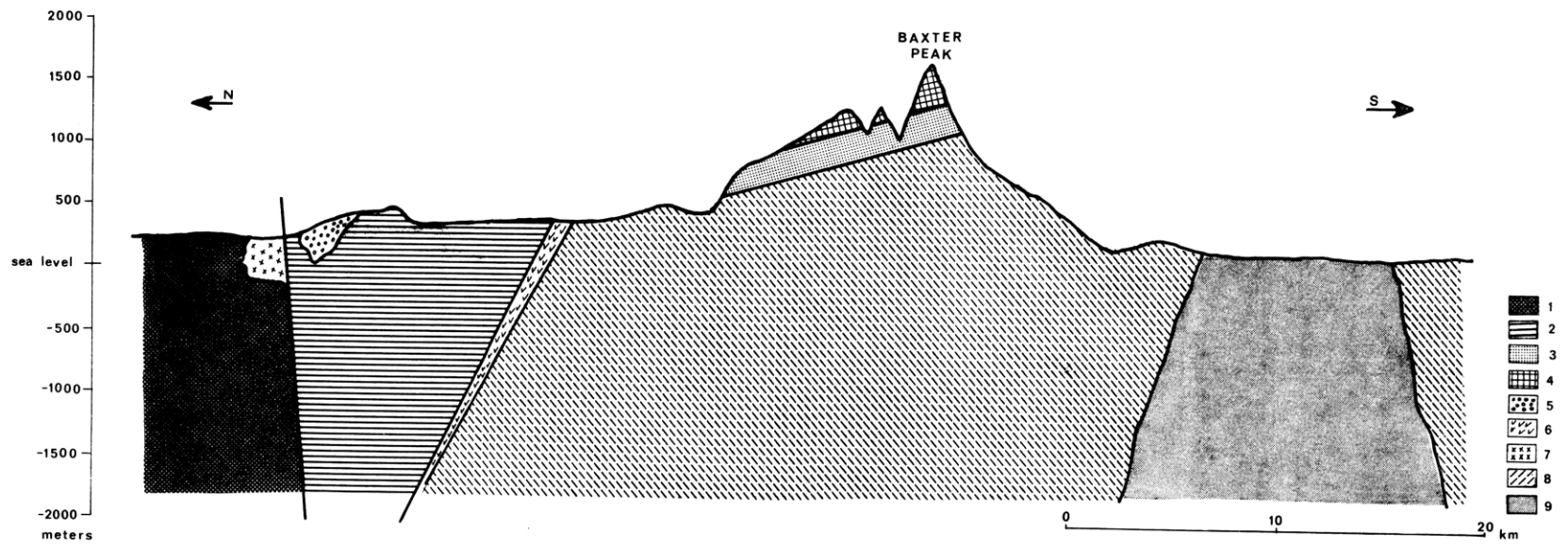
GENERALIZED GEOLOGIC CROSS-SECTION
TRAVELER RHYOLITE-KATAHDIN GRANITE

The composite character of the Katahdin Pluton results
from the presence of two younger rocks of medium grained,
amphibole-bearing, biotitic Debsconeag Granodiorite and by a
stock of the youngest intrusion--the Horserace Quartz Dio-
rite (Fig. 14). The Harrington Lake porphyry, still another
igneous body nearly colinear with the Debsconeag and Horse-
race intrusion, is outside of the NW limit of the Katahdin
Pluton south of Harrington Lake. It seems almost certain
that the location of these small, younger intrusions results
from tectonic control by the Chesuncook Lake-West Branch
Penobscot River fault system, which shows evidence of activity
during the ascent of the Horserace intrusion.

B. Katahdin Granite

1. Geology

The rocks of the Katahdin Granite (KG) are massive,
structureless, mineralogically and chemically homogeneous
granites, underlying over 95% of the Katahdin Pluton (KP).
This description purposely omits any reference to the rock
textures solely to emphasize, that all textural types of the
KG have crystallized from the same original magma. Six tex-
tural types of KG are identified below:

Table 5A. Textural Facies of Katahdin Granite.

Katahdin Granite Facies	Characteristic Texture	Occurrence Within The Pluton
1. Doubletop	Granitic	Core of the Pluton
2. Chimney	Granophyric	
3. Summit	Granophyric With Miarolitic Cavities	Outer Zone Near The Roof Of The Pluton
4. South Brother	Subporphyritic With Rapakivi Overgrowths	
5. Wassataqoik	Aplogranitic	
6. Cathedral	Porphyritic With Aplitic Groundmass	Porphyritic Dikes

An idealized distribution of these facies is schematically illustrated in Fig. 17. The predominant Doubletop facies forms the core of the pluton, whereas the other non-dike facies are found near the actual and presumed upper contacts. Excluding the porphyritic dikes of the Cathedral facies, all other contacts within the pluton are of a gradational nature, having a width of up to several hundred meters.

Toward higher elevations, the first appearance of a granophyric texture in the center of the pluton marks the transition point from the Doubletop to the Chimney facies. With increasing elevations, the granophyric texture becomes even more prominent. The first appearance of filled, miarolitic cavities indicates the transition from Chimney facies to Summit facies. At the highest structural levels, the filled miarolitic cavities change into open cavities. Identified minerals contained in the miarolitic cavities are: epidote, tourmaline, and, infrequently, fluorite.

Toward the side contacts, the vertical cross-section is markedly different from the analogous cross-section in the center of the pluton. The landslide exposures on the western face of South Brother Mountain show a transitional change from Doubletop into South Brother facies by the gradual increase of fine-grained groundmass. Near the contact with Traveler Rhyolite, the Wassataquoik facies of KG is aplogranitic with abundant "nests" containing black to dark-blue tourmaline. The Summit, Chimney, Wassataquoik, and South Brother form an 'outer shell' around the Doubletop facies

core of the Katahdin Pluton. The stratigraphic thickness
of this 'outer shell' varies from zero to a minimum of 450 m
in the center of the pluton, which may be best explained by
differential cooling rates. The 'outer shell' granites, when
compared with the Doubletop facies, are often more hydro-
thermally altered, less texturally uniform, and more resistant
to erosion. The extensive hydrothermal alteration of the
'outer shell' correlates with the joint pattern. The common,
vertical sheeting observed at the highest elevations may have
provided pathways for the escaping pneumatolytic and hydro-
thermal solutions of the late magmatic stages. The frequency
of hydrothermal and pneumatolytic alterations is inversely
proportional to the frequency of pegmatitic dikes. The
pegmatitic dikes are absent at the highest elevations but
become more frequent toward the core of the pluton. At inter-
mediate levels, the pegmatites are restricted to thin linings
along selected fractures. At intermediate and lower eleva-
tions, the pegmatites and aplites occasionally form layered
dikes of either single or multiple intrusions. Aplitic dikes
occur throughout the pluton and their frequency seems to be
independent of elevation. The 'outer shell' facies have
structural features suggesting a complex and dynamic crystal-
lization environment. For example, biotite is concentrated
into schlieren, but most often it is merely lineated. Also,
north of Mt. Katahdin (Baxter Peak), near the headwalls around
North and Great Basins, there are rare, sharp internal con-
tacts with chilled margins. However, the rocks are identical

83

Fig. 17. Idealized Distribution of Textural Facies of
         Katahdin Granite Within the Katahdin Pluton.

         Legend: KGS - Katahdin Granite: Summit Facies
                 KGCH- Katahdin Granite: Chimney Facies
                 KGW - Katahdin Granite: Wassataqoik Facies
                 KGSB- Katahdin Granite: South Brother Facies
                 KGD - Katahdin Granite: Doubletop Facies
                 KGCT- Katahdin Granite: Cathedral Facies
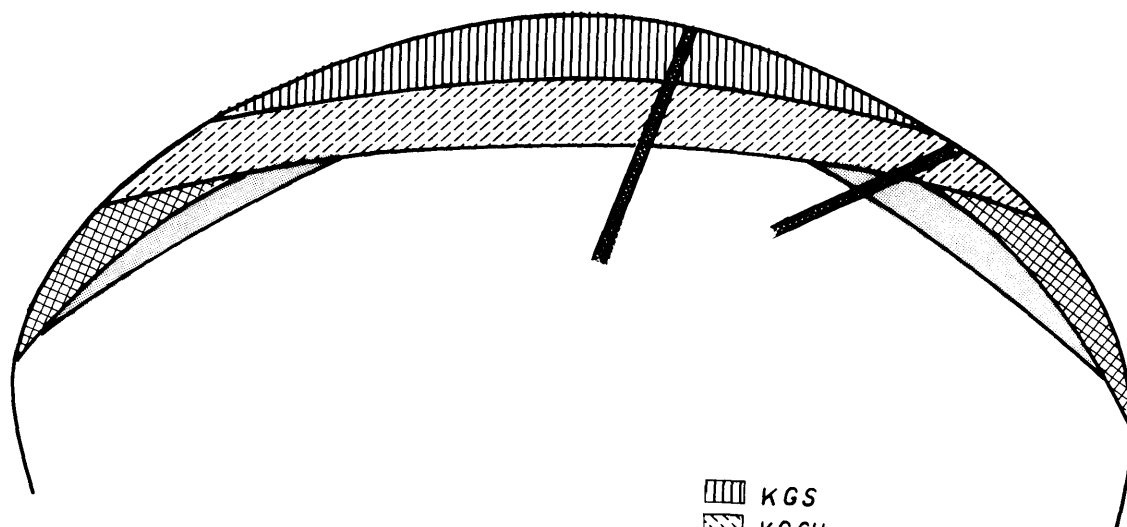
KGS
KGCH
KGW
KGSB
KGD
KGCT

85

in appearance only half a meter on either side of the contacts.

The erosional resistance of the 'outer shell' granites provides an explanation for the contrasting morphology of the pluton. The areas underlain by the Doubletop facies are often deeply weathered (up to 10 m) into decayed and crumbling granites, as evidenced in the lower parts of landslides on the south side of Mt. OJI and the west side of South Brother Mtn. In contrast, the Summit facies is extremely resistant to weathering and erosion and provides an effective shield against erosion. Wherever this shield eroded away, the granite of Doubletop facies was in turn eroded relatively quickly because of its poor resistance. This explains the existence of steep ridges around the exposures of the Summit facies and the topographic lows in the remaining part of the pluton. Except for two occurrences, mafic dikes are conspicuously absent throughout the pluton. One sub-horizontal dike, about 0.75 m thick, crops out along the mid-elevation of the entire eastern side of Doubletop Mtn. The second dike, as reported by Rankin (personal communication) occurs near the Chimneys underneath Pamola in the South Basin.

2. Mineralogy

The principal minerals of all six facies of the Katahdin Granite are (in decreasing abundance): alkali feldspar, quartz, plagioclase, biotite, opaques, and minor or

trace occurrences of amphibole, fayalite, tourmaline, epi-
dote and fluorite. Accessories are apatite, zircon, alla-
nite, and possibly monazite. The noted absence of primary
magmatic muscovite and sphene places an upper limit for
$P(H_2O)$ at 3.7 Kb and an upper limit for $f(O_2)$ at approxima-
tely the nickel-nickel oxide buffer curve (Czamanske and
Wones, 1973). As muscovite occurs only extremely rarely in
the pegmatitic dikes and pegmatitic linings of joints, the
water pressure may have been as low as 1 Kb if the tempera-
ture is assumed to be 550° to 600° (Althaus, et. al., 1970;
Kerrick, 1972).

A scanning electron microscope study of feldspars
from the Chimney facies (Sprunt, 1973) revealed an extensive
abundance of submicroscopic open cavities, frequently show-
ing a negative crystallographic outline. In this same study,
albite from Amelia pegmatites had an identical texture.
These 'holes', thought to represent trapped vapor bubbles,
suggest a water-saturated, magmatic environment.

Alkali feldspar:

In equigranular granites, the perthitic alkali feld-
spar is generally subhedral to anhedral, and occurs as eu-
hedral phenocrysts in the Summit and Cathedral facies. The
average grain size is about 3 mm with a maximum grain size
of 5 mm. The composition of four perthitic alkali feldspars
was determined by microprobe analysis of fluxed glasses to
ensure exact bulk composition (Or70 Ab28.5 An1.5); one sample

was slightly more albitic (see Fig. 5). The above composi-
tions fall within the range Or66-Or75, as determined by the
sanidization and x-ray techniques used by A. Griscom (in
prep.). The composition of the perthite host and the ex-
solved albite lamellae from Sample #74 yield Or90 Ab10 and
Or40 Ab88 An8, respectively. The bulk composition of this
alkali feldspar, as determined from fused glasses, can be
reconstituted by mixing 86% of the host and 24% of the
lamellae, which is in accord with the microscopic estimate.

The structural states of alkali feldspars in unhomo-
genized samples (A. Griscom - in prep.) vary from orthoclase
to maximum microcline, with intermediate microcline being
the most frequent state. A. Griscom identified orthoclase
in samples from near the contacts and maximum microcline in
a sample from the Summit facies. However, there is no
systematic correlation between structural state or composi-
tion of the alkali feldspar and sample location (notably its
elevation).

In the Doubletop facies, the ubiquitous Carlsbad twin-
ning is occasionally combined with fine microcline grid twin-
ning. In the Summit facies, alkali feldspar, as well as
plagioclase phenocrysts, are surrounded by a fan-like,
graphic matrix of very fine intergrowth of alkali feldspar
and quartz. The crystal size of the intergrowth increases
toward the miarolitic cavities. The alkali feldspar pheno-
crysts of South Brother and Cathedral facies often show
rapakivi overgrowth of albite or sodic oligoclase. The

average composition of alkali feldspars in the groundmass
of the Cathedral facies is Or94 Ab6. In some fresh samples,
alkali feldspar is slightly sericitized and in the red-
colored, hydrothermally altered samples, alkali feldspar is
densely clouded and impregnated by submicroscopic hematite
specks.

Quartz:

Equidimensional quartz is usually anhedral and com-
monly agglomerated into groups of several grains of an
average grain size of 1.5 mm. The quartz contains numerous
fluid inclusions and sometimes inclusions of accessories or
opaques. Porphyritic quartz of the Summit and Cathedral
facies is euhedral with occasional embayments.

Plagioglase:

The thick, tubular grains of plagioclase are sub-
hedral in the equigranular facies of KG, or euhedral as
phenocrysts in the porphyritic facies; the average grain
size is about 2 mm. Albite polysynthetic twinning is com-
mon and is often combined with less frequent Carlsbad
twinning. Compositional zoning is normal and continuous;
sudden steppings are rare. The plagioclase composition,
determined by electron microproble, varies from An34 to An4
with an average of An25 to An30. The calcic cores of the
interior of Katahdin Pluton are commonly saussuritized and
sericitized while the more acidic rims remain clear. This
deuteric re-equilibration is believed to have caused a
partial resetting of the feldspar geothermometer (about 60°C

in sample #74 located near the center of the Katahdin Pluton).
These plagioclases also contain approximately half of the
'normal' K_2O content: approximately 0.25 wt.% instead of the
usual 0.50 wt.%.

Groundmass plagioclase in the Cathedral facies has an
anomalous composition (An0 to An15). The presence of sodic
plagioclase and Or-rich alkali felspar, in combination with
the aplitic texture, suggests that the intruding magma was
supercooled and that the groundmass feldspars crystallized
by devitrification from the glass-like matrix at much lower
temperatures.

Biotite:

Biotite constitutes approximately 6% of all samples.
It is frequently partially chloritized and it occurs as sub-
hedral tablets up to 2.5 mm large and 1 mm wide; its size
decreases slightly toward the contacts. Intense pleochro-
ism, deep brown to straw yellow in color is further accentuat-
ed within the halos mantling common zircon inclusions. The
composition of biotite throughout the KG is almost constant,
except for noticeable differences in the rapidly cooled or
quenched Summit and Cathedral facies, as well as in the
aplites. Biotites of the Summit facies are lower in Fe and
Ti and higher in Mn; Cathedral facies shows lower Fe content,
whereas aplitic biotite is enriched in Fe and is poorer in
Ti.

Olivine:

A single grain of equidimensional and subhedral
olivine was identified in Sample #29 of Doubletop facies.
From microprobe analysis, the composition corresponds to
mangano-ferrous fayalite: Fo2.0 Fa90.5 Tf7.5. Although
the grain is almost entirely enclosed in plagioclase, it
is believed that during crystallization, the olivine was in
equilibrium with magnetite and quartz. This indicates that
the granitic magma crystallized under oxygen fugacites near
the QFM buffer. Identical mineralogical and chemical com-
position of Sample #29 with other Doubletop samples suggests
that fayalite may be more widespread though it is rarely
found in thin sections.

Amphibole:

Two rare amphibole occurrences are reported from
outcrops along the West Branch Penobscot River (A. Griscom-
in preparation).

Tourmaline, Epidote, and Fluorite:

Tourmaline, epidote, and fluorite are mainly found in
the Summit facies. Tourmaline, which is a deep-blue variety
of indicolite, is present in both matrix and in miarolitic
cavities; epidote occurs in cavities and along microcracks,
and fluorite mainly along microcracks. Tourmaline and flu-
orite are seldom observed in the Doubletop facies, where
epidote and clinozoisite are common alteration products.
Tourmalines of the Wassataquoik facies are noted not only

for their presence within the rock matrix but mainly for their conspicuous tourmaline nests and linings along the joints.

Opaques:

Optical examination and microprobe study revealed that ilmenites are essentially absent and, when present, they occur only as cores of magnetite grains. Magnetite is always oxidized, displaying common exsolution textures which inhibit the use of the magnetite-ilmenite geothermometer and the geobarometer. The pre-exsolution composition was estimated by two different averaging techniques, both yielding identical results: Mt75 Usp25. The first method averaged 10 to 15 random microprobe point analyses, and the second method utilized a defocused electron beam with a diameter equivalent to the approximate width of the magnetite grains (50 to 60 microns).

3. Facies of the Katahdin Granite

a. Doubletop Facies

The Doubletop facies is a medium grained biotite granite. The type exposures are on the lower east side of Doubletop Mtn. Recent landslides in that region unearthed excellent bedrock ledges. The granite is a massive, structureless rock with a typical granitic, hypidiomorphic granular texture. The color in fresh specimens is bluish-gray turning into whitish-gray, pinkish or red near the joints, faults, and/or pegmatitic and aplitic dikes. The

Fig. 18. Plot of Normative (CIPW) Q-OR-AB-AN Components
for Doubletop Facies of Katahdin Granite.

Upper Diagram: Projections onto Q-AB-OR Plane.

Lower Diagram: Projections onto AN-AB-OR Plane.

Legend: 1 - Fresh Samples - No Alteration Observed
        2 - Sample Next to Aplitic Dike (#134-2)
        3 - Hydrothermaly Altered Granite (#240)
        4 - Slightly Weathered Granite (#41 & #190W)
        5 - Mylonitized Granite (#81)
        6 - From Griscom (in prep.)

Note: Cotectic Lines, Minima and Eutectic Points
      are From Fig. 11.
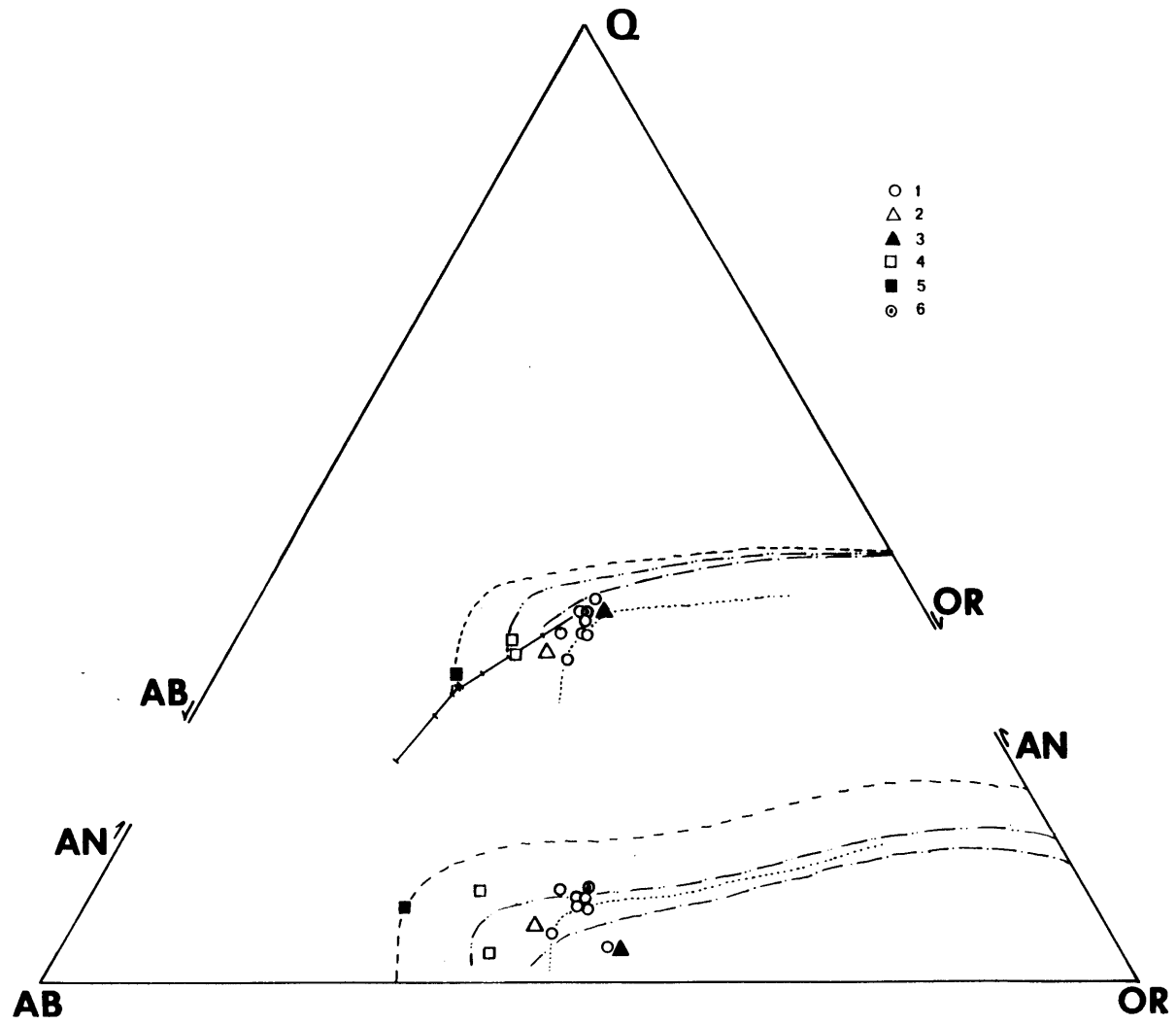
mineral components are perthitic alkali feldspar (34%),
plagioclase (26%), quartz (34%), biotite (6%); the remain-
ing components are accessory apatite, zircon, allanite,
tourmaline, and opaques. Representative modal analyses are
given in Table 5B, and all available modal analyses from
Griscom and Rankin (Griscom-in prep.; Rankin, 1961) are
plotted on Fig. 22. Rare minerals, which include fayalitic
olivine and amphibole, are found in only a few of the
specimens; sphene and magmatic muscovite were never observed.

Twelve selected samples from the northern section of
the pluton were analyzed chemically. The AN-OR-AB and
Q-OR-AB normative compositions (including one chemical
analysis of A. Griscom (in preparation) are given on Fig. 18.
The comparison of these diagrams with experimentally deter-
mined cotectic lines is complicated by the presence of
biotite (which contributes to the OR component), and by the
rock's "chemical memory". Nevertheless, an inspection of
this diagram places an upper limit of 2 Kb $P(H_2O)$ for the
granites of this facies.

b. Chimney Facies

The Chimney facies is sandwiched between the
Doubletop facies on the bottom and the Summit facies on the
top. This facies differs from the Doubletop facies by the
presence of granophyric texture, and from the Summit facies
by the absence of miarolitic cavities. The contact between
the Doubletop and Chimney facies dips toward the north.

Table 5B

Modal Analysis of Doubletop Facies of

Katahdin Granite.

Sample #	29	41	74	115	150	190	209	134-1	Avg.
Alk.Feldspar	34.4	31.4	38.5	35.7	33.5	29.7	33.8	34.0	33.9
Plagioclase	26.6	28.1	20.4	24.2	24.1	32.4	26.2	24.5	25.8
Quartz	20.9	34.7	36.2	33.1	35.5	32.8	32.7	34.3	33.8
Biotite	6.8	5.4	4.5	6.7	6.5	4.8	6.9	6.9	6.1
Others	0.3	0.4	0.4	0.3	0.4	0.3	0.4	0.3	0.4
Average An	22	18	17	28	26	22	26	23	

Fig. 19A. Plot of Normative (CIPW) Q-OR-AB-AN Components
For Other Than Doubletop Facies of Katahdin
Granite.

Upper Diagram: Projections onto Q-AB-OR Plane.

Lower Diagram: Projections onto AN-AB-OR Plane.

Legend: KGS - Katahdin Granite: Summit Facies
        APl - Aplite (Sample #KM-7)
        KGCH- Katahdin Granite: Chimney Facies
        KGW - Katahdin Granite: Wassataqoik Facies
        KGCT- Katahdin Granite: Cathedral Facies

Note: Cotectic Lines, Minima and Eutectic Points
      are From Fig. 11.
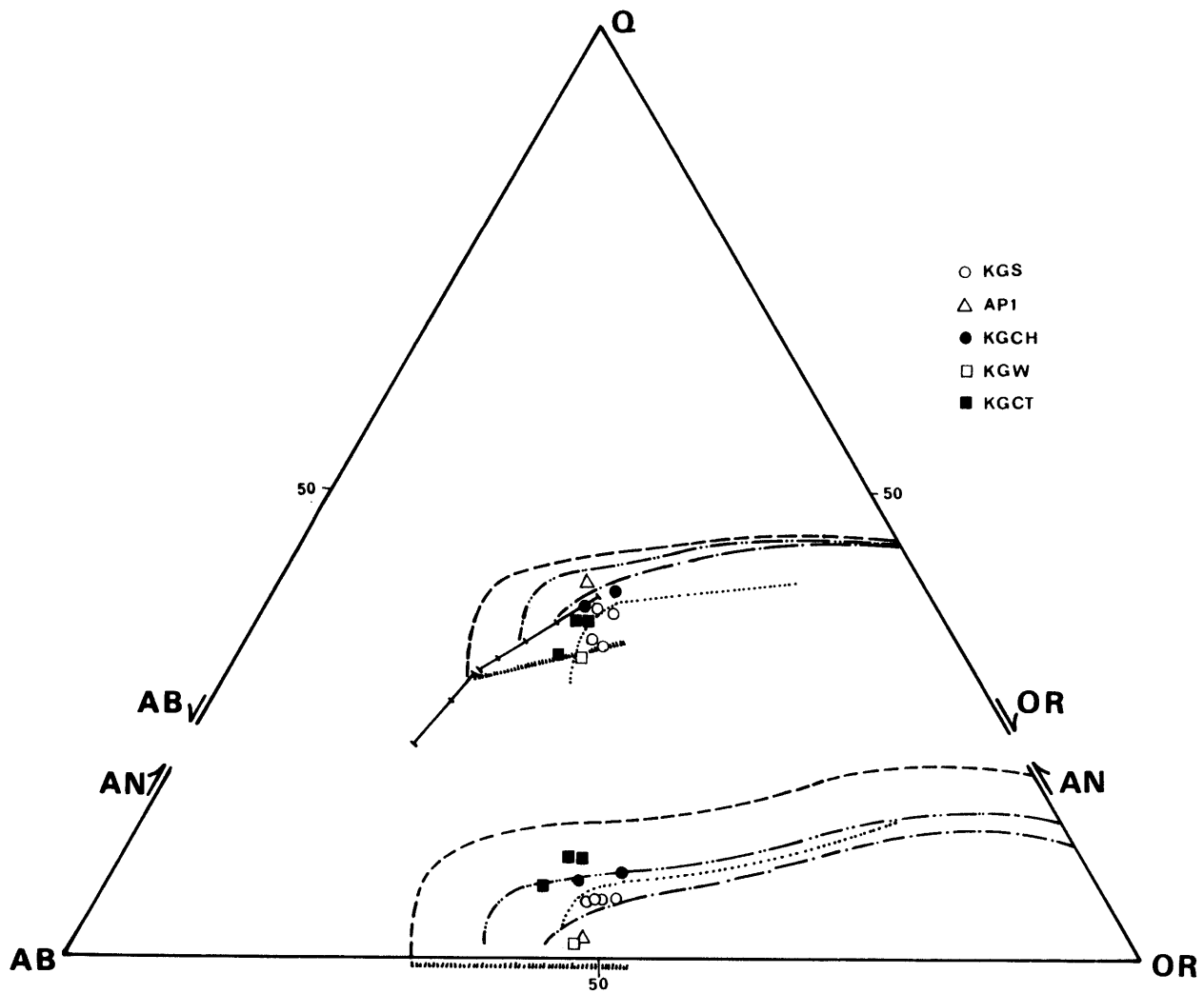
Fig. 19B. Plot of Normative (CIPW) Q-OR-AB-AN Components
for Aplites and Pegmatites from Katahdin Pluton.

Upper Diagram: Projections onto Q-AB-AN Plane.

Lower Diagram: Projections onto AN-AB-OR Plane.

Note: Cotectic Lines, Minima and Eutectic Points
are From Fig. 11.

Q

● Aplites
○ Pegmatites

AB

OR

AN

AN

AB

OR
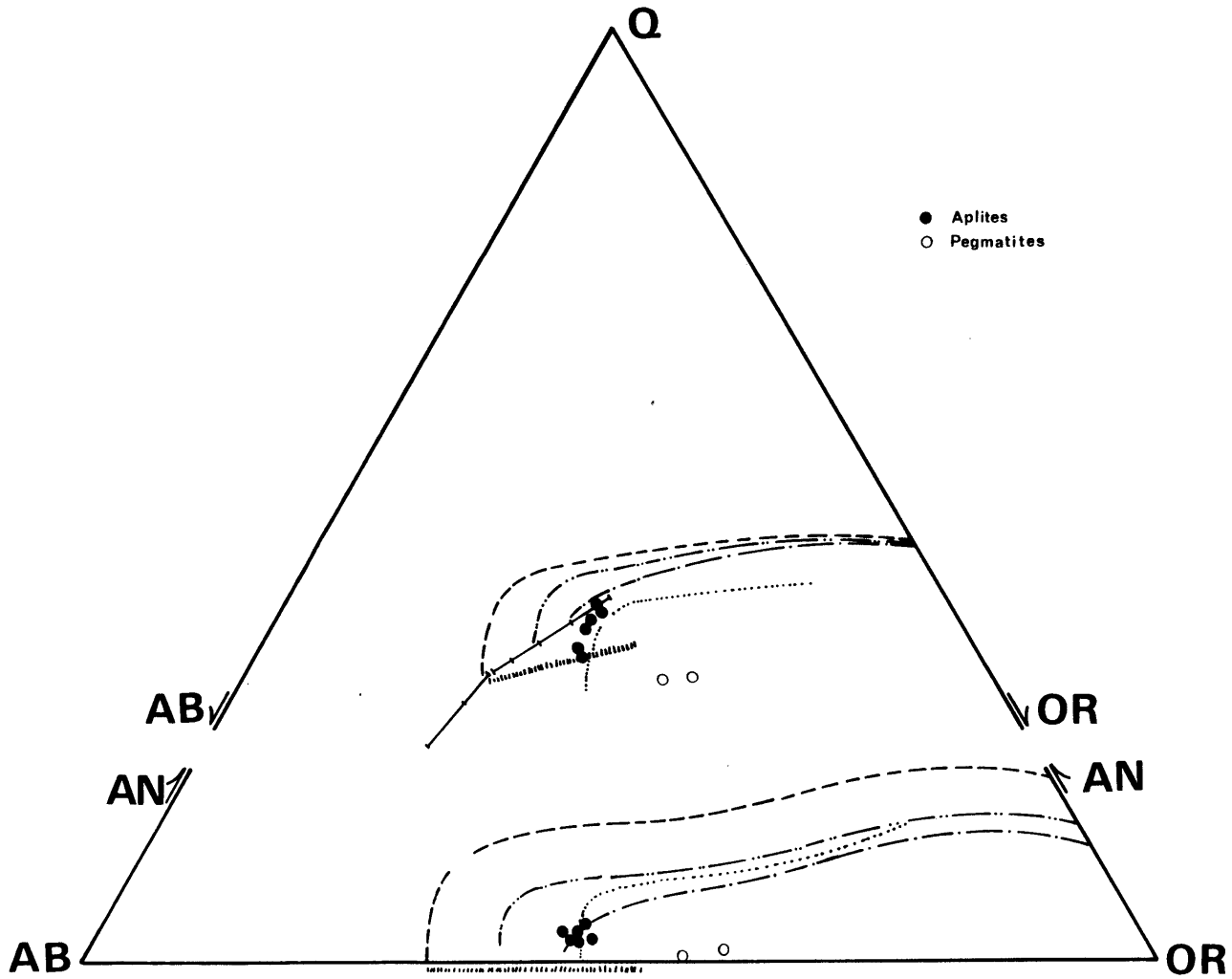
Fig. 20. Plot of Normative (CIPW) Q-OR-AB-AN Components
for All Chemicaly Analyzed Samples From the
Entire Traveler Rhyolite - Katahdin Granite
Magmatic Complex.

Upper Diagram: Projections onto Q-AB-OR Plane.

Lower Diagram: Projections onto AN-AB-OR Plane.

Legend: TRBC - Traveler Rhyolite: Black Cat Member
        TRP   - Traveler Rhyolite: Pogy Member
        KGD   - Katahdin Granite: Doubletop Facies
        KGCH - Katahdin Granite: Chimney Facies
        KGS   - Katahdin Granite: Summit Facies
        KGCT - Katahdin Granite: Cathedral Facies

Note: Cotectic Lines, Minima and Eutectic Points
      are From Fig. 11.

O   TRBC
●   TRP
△   TRBC Groundmass
▲   KGD
□   KGCH
✳   KGS
▼   KGCT
▽   Aplites
⬢   Pegmatites
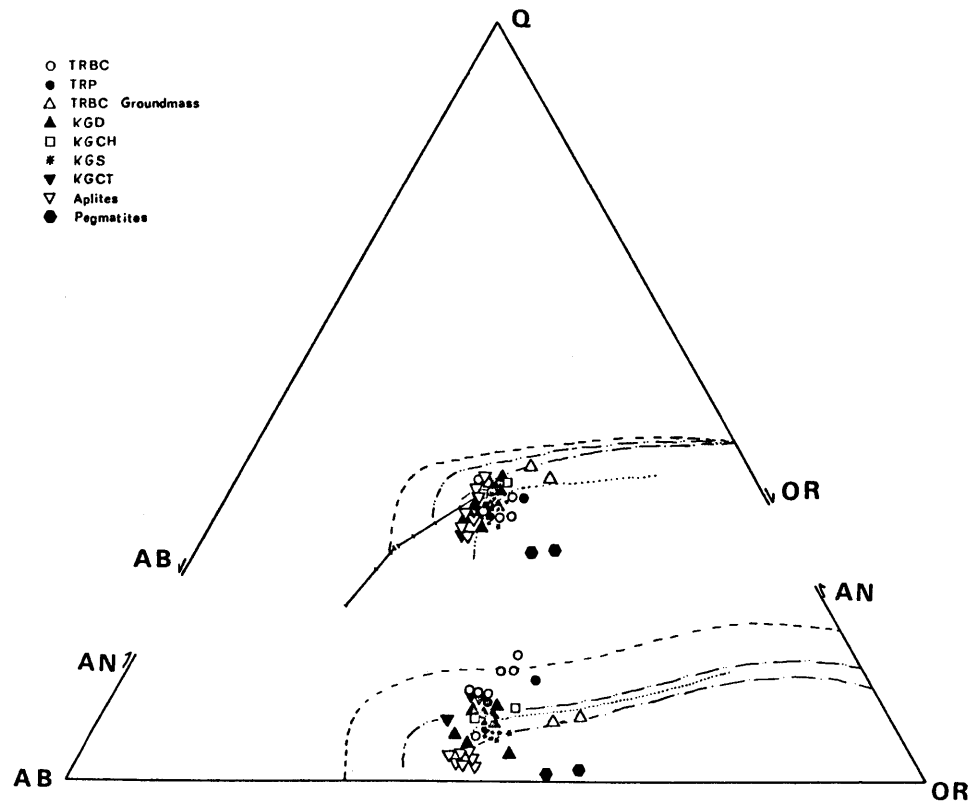
The altitude of the contact on the southern side is ap-
proximately 900 m and on the northern side of the plateau
600 m. The type locality for the Chimney facies is at
the base of the cliffs below the Chimneys. This facies
mainly occurs around the main mountain chain, on both
Turner Mountains, and around North Brother Mtn. The texture
of this facies is characterized by a granophyric intergrowth
and, toward the higher elevations, by the presence of quartz,
plagioclase, and alkali feldspar phenocrysts. Its color is
grey at lower elevations, but frequently pink or red at
higher elevations. Two analyzed samples of the Chimney
facies show strong chemical similarities to the Doubletop
facies (Figs. 18 and 19); the mineral composition of both
facies is identical.

    c.   Summit Facies

       The Summit facies of Katahdin Granite (KGS) is
recognized only at higher elevations in two out of the
three high elevation plateaus. These are (1) North Turner
and (2) Mt. Katahdin-Russel Mtn. The type exposures are on
Tableland (between Baxter Park and Hamlin Peak), where the
facies crops out as the more characteristic pinkish-white
variety. Near the vicinity of Mt. Katahdin and Hamlin Peak,
KGS is distinctly red colored as a result of extensive hydro-
thermal alteration.

       The granite of the Summit facies has a massive, sub-
porphyritic texture, composed of fine grained granophyric

intergrowths of alkali feldspar and quartz, radiating away from the 1-4 mm tablets of alkali feldspar and plagioclase phenocrysts. The groundmass becomes coarser and pinkish toward the abundant miarolitic cavities. The vugs are lined with euhedral projections of alkali feldspar and quartz and are partly or fully filled with epidote, tourmaline, and occasional fluorite. The size of these cavities ranges in diameter from 0.5-5.0 cm, rarely exceeding 2 cm. The frequency of cavities increases with higher elevations.

Major element data, plotted on granitic diagrams, show that KGS (Fig. 19) is similar to KGD (Fig. 18), except for lower An normative content in KGS. This difference may have been caused by hydrothermal alteration or by fractionation.

d. Other Facies of Katahdin Granite

Wassataquoik Facies:

The type exposures of Wassataquoik facies (KGW) are along the southern shore of Wassataquoik Lake. KGW is restricted to a zone, up to 0.5 km wide, between the Traveler Rhyolite and Debsconeag facies of Katahdin Granite. Near the contacts the facies have a panxenomorphic texture with occasional granophyric developments. As the distance from the contacts increases, the texture changes into subaplitic and subporphyritic.

South Brother Facies

The South Brother facies (KGSB) is a transitional

facies between KGD and KGCH, extending from South Brother

Mtn. to Wassataquoik Mtn. The type locality is on the up-

per part of a ledge unearthed by a recent landslide on the

western face of South Brother Mtn. The texture is porphyr-

itic to subporphyritic with rapakivi overgrowth around

alkali feldspar phenocrysts. As the elevation increases,

the groundmass becomes finer.

Cathedral Facies

Cathedral facies (KGCT) occurs only as thick, por-

phyritic dikes (30-200 m wide), usually at higher eleva-

tions. The type locality is on the southern face of OJI

Mtn. at an elevation of 695 m. KGCT is a porphyritic

granite with approximately 20-25% of alkali feldspar, plagio-

clase, quartz, and biotite phenocrysts. The matrix consists

of identical mineral composition. The dike contacts are

sharp, with fine grained, chilled margins; occasional aplit-

ic and pegmatitic dikes cross-cut or intrude along the con-

tacts. Therefore, KGCT is essentially of the same age as

KGD.

The tie-line between coexisting feldspars in the

goundmass (Fig. 5) indicates that the matrix crystallized

from a supercooled magma.

4. Estimates of Temperature, Total Pressure, Water Pressure and Oxygen Fugacity

The deuteric oxidation of magnetite-ulvospinel

solid solution, and the rarity of ilmenite prevented the

use of the ilmenite-magnetite geothermometer and geobarometer.
Temperatures may be estimated from coexisting alkali feldspar
and plagioclase; oxygen fugacity and water pressure can be
obtained from the stability of the biotite mica. Total pres-
sure can be independently estimated from the geologic evid-
ence; that is, the lithostatic pressure applied by the now
eroded sequence of overlying rocks.

a. <u>Alkali Feldspar - Plagioclase Pair</u>

Hon (1973) and Stormer (1974, 1975) independently
suggested a modification of Barth's geothermometer as a
means of estimating an equilibration temperature from co-
existing alkali feldspar and plagioclase. The thermometer
is based on the equilibrium requirement that the activity
of albite in alkali and plagioclase feldspars must be equal.
The activity of albite in alkali feldspar solid solution is
obtained from the numerical model of the excess-free energy
of mixing, as given by Waldbaum and Thompson (1969). A
similar model is not available for the plagioclase solid
solution. Although plagioclases are distinctly non-ideal at
lower temperatures (J. C. Smith, 1972; Crawford, 1966) and
at compositions above An50, Orville's (1972) ion exchange
experiments indicate that, at magmatic temperatures, the
ideal solution model is applicable for plagioclase composi-
tions between An0 and An50. A similar conclusion for a more
restricted range of compositions (An20 to An45) was deduced
from a thermodynamic analysis of experimentally determined
tie-lines between alkali feldspars and plagioclases (Saxena,

1971; Hon, 1972). We believe, therefore, that the ideal solution model is a sound assumption for a composition between An20 and An50 at or near magmatic temperatures. With this assumption and knowing the compositions of both feldspars (in terms of their albite mole fractions), the feldspar equilibration temperature may be estimated from the following expression (Hon, 1973):

$$T\ (^{o}K) = \frac{1970.61 + 0.02878*P - (587.93 + 0.0085*P)*(1.0-X)}{(\log(Y/X))/(1-X)^2 + 0.67332 + 0.33901 * (1.0-X)}$$

X = mole fraction of albite in alkali feldspar
Y = mole fraction of albite in plagioclase
P = assumed total pressure in bars

Coexisting feldspars of three selected samples of the Doubletop facies (Samples #29, 74, 150) and hand-picked phenocrystic feldspars from one sample of the Cathedral facies (Sample #121) were analyzed by electron microprobe (Fig. 5). To determine their exact bulk compositions, the perthitic alkali feldspars were analyzed as fused glasses. The compositions of these four feldspar pairs, and the computed equilibration temperature at three different pressures, are listed below.

Sample #	X(Ab in AF)	Y(Ab in PL)	Temperature ^{o}C		
			1.0 Kb	1.5 Kb	2.0 Kb
29	0.347	0.724	706	713	720
74	0.285	0.743	636	642	648
121	0.291	0.658	701	708	715
150	0.288	0.682	679	686	693

The calculated temperatures (except for Sample #74) are acceptable magmatic temperatures intersecting the granite minimum melting curve between 1200 and 1500 bars of $P(H_2O)$ (Fig. 21). The plagioclase of Sample #74 is noticeably lower in Ca and K, apparently as a result of deuteric reequilibrium demonstrated by saussuritization and sericitization of its plagioclase cores. The temperature estimate is consequently lowered by 60 degrees. The average temperature (excluding Sample #74) is 695°C at 1 Kb and 709°C at 2 Kb; the preferred estimate is 703°C at 1 Kb and 717°C at 2 Kb. As a consequence of water undersaturation, an increase in total pressure would tend to increase the temperature estimate by 1.4^{O}C per 100 bars. The granitic minimum melting curve is intercepted at a temperature of 700°C and $P(H_2O)$ of 1300 bars (Fig. 21).

b.   Biotite as an Indicator of Magmatic Environment

Wones and Eugster (1965) suggested a dehydration-oxidation reaction of biotite as a potential means of relating magmatic temperature, water fugacity, and oxygen fugacity. However, Wones (1972) modified the earlier numerical expression to the following:

$$\log f(H_2O) = 7409/T + 4.25 + 0.5 \log f(O_2) + 3 \log x \text{ (Ann)} - \log a(San) - \log a(Mt)$$

The above expression, given the compositions of all mineral phases, defines a unique surface in three-dimensional space with the temperature, $f(O_2)$ and $f(H_2O)$ as principal axes.

This surface can be projected on the $f(O_2)$-T plane as a
series of isobaric lines, each relating oxygen fugacity
and temperature at constant water fugacities. Such a
diagram, constructed for the mineral assemblage of the
Katahdin Granite, is shown in Fig. 21 using the following
input data:

1. The mole fraction of annite in the biotite solid
solution was determined from the structural formula as fol-
lows:

x(Ann)=(tot.Fe/sum of octahedral ions) - 0.05

The correction of five mole percent appears to be a differ-
ence between tot.Fe and Fe^{+2} at QFM buffer (Wones, Eugster,
1965, p. 1245). For the KGD biotite the corrected x(Ann)
is equal to 0.72.

2. The composition of partially exsolved magnetite-
ulvospinel solid solution was determined by electron micro-
probe using two different averaging techniques, both yield-
ing an essentially identical result: Mt75 Usp25. In the
first case, the composition was obtained by averaging 10 to
15 randomly analyzed points, and in the second case, by de-
focusing the beam to about 50 microns which is the approxim-
ate width of the grain. The activity of magnetite in the
above solid solution is considered to be equal to its mole
fraction a(mt) = 0.75.

3. The activity of sanidine is estimated from the analyzed alkali feldspars. For x(Or) = 0.70, T = 700°C and P = 1 Kb, a(San) = 0.74 (Waldbaum, Thompson, 1969). Variations due to pressure uncertainties are negligible and are, therefore, ignored.

4. Water fugacities are taken from tables of Burnham et. al. (1969).

Figure 21 is a plot of log $f(O_2)$ versus T at constant $p(H_2O)$'s for six assumed water pressures between 600 and 2600 bars. Also plotted on this diagram are the temperatures estimated from the coexisting feldspar pairs (three double lines) and two curves: one for the granitic minimum melting temperatures (as indicated by the isobaric lines) and another curve for minimum melting under constant total pressure (P_t = 2 Kb) but at a variable effective water pressure $P(H_2O)$ less than $P(T)$. Total pressure of 2 Kb was chosen as the maximum possible pressure under which the magma of the Katahdin Granite could have crystallized. This limit, probably grossly exaggerated, is estimated from both the grade of the regional metamorphism (chlorite zone to sub-chlorite zone) and from the thickness of the overlying volcanic sequence of the Traveler Rhyolite, presently assumed to be only one-half of the original thickness.

Fig. 21. Plot of Doubletop Facies Biotite Equilibrium Surface
(T^OC-log $f(O_2)$-$P(H_2O)$) Projected onto log $f(O_2)$-T^OC
Plane. Calculations Are Based on Numerical Values
of the Biotite Equilibrium Constant of Wones(1972):
X(Ann)=0.72, a(Mt)=0.75, a(San)=0.74.
See Text For Further Discussion and Significance of
Other Equilibria Curves.

log f(O₂) is rendered as $\log f(O_2)$

$\log f(O_2)$

-16

QFM*

USP 20   USP 25   USP 30

granitic minima
$P(T) = 2\,kb$

-17

granitic minima
$P(T) = P(H_2O)$

$P(H_2O)$

2.6

coexisting
feldspars

1.8

-18

1
kb

650   700   750   T °C
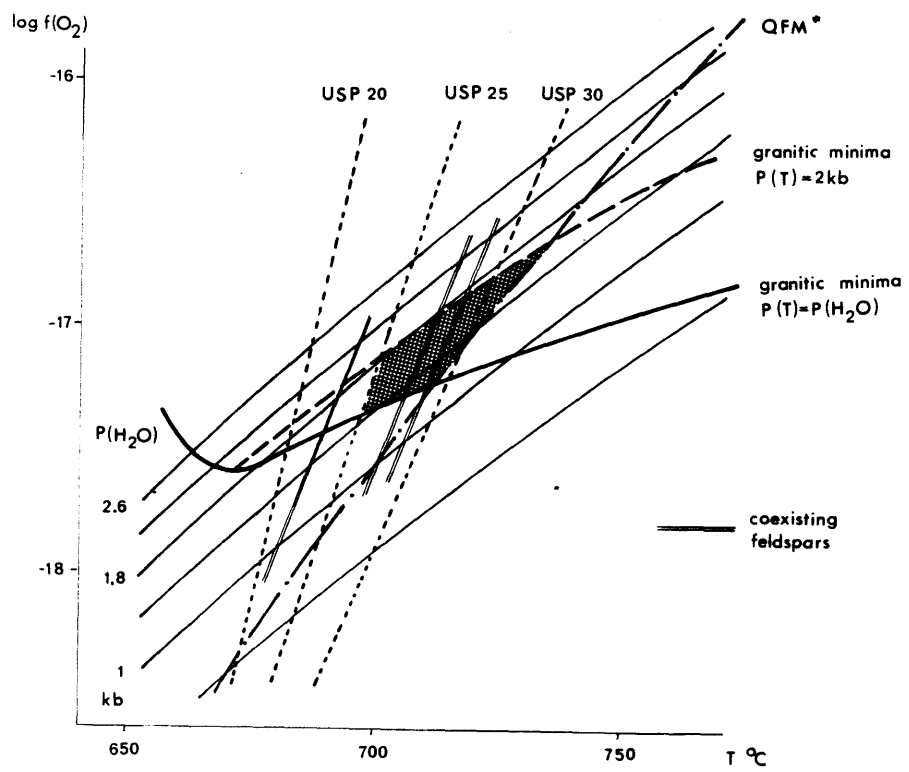
It is thus expected that the $f(O_2)$, T and $P(H_2O)$
for the Katahdin Granite (KG), as shown on Fig. 21, will be
anywhere between the granitic minimum and P_t = 2 Kb lines.
We can further narrow the possible range by constraining
$f(O_2)$ variations by information obtained from the coexisting
olivine and iron-titanium oxide. From the experimental data
on coexisting iron-titanium oxides by Buddington and Linds-
ley (1962), it appears that a spinel phase of the composi-
tion Mt75 Usp25, not coexisting with ilmenites, can be a
stable phase at higher T's or lower $f(O_2)$ away from the
curve where it would coexist with the ilmenites (see Fig. 21).
Furthermore, in one sample (Sample #29), ilmenites are vir-
tually absent, but a grain of a fayalitic olivine has been
identified nearly entirely enclosed within a larger grain of
plagioclase. Provided that the olivine was in equilibrium
at the time of its crystallization with quartz and magnetite,
and assuming that the melt could only be oxidized after the
olivine is formed, the possible range for the intensive
parameters of Fig. 21 is further limited (see Fig. 21)
between the QFM* curve and the line bearing numerals 25
(Usp25)[*]. The uncertainty range for temperatures is
between 697°C and 735°C for total pressure between 1200
and 2000 bars, water pressure between 1200 and 1800 bars,
and for log $f(O_2)$ between -16.65 and -17.35. It is quite

(*) The QFM* curve is calculated for a(Fa)=0.81, a(Q)=1.0
and a(Mt)=0.75.

reassuring that the temperature estimated from the coexist-
ing feldspars is in excellent agreement with this range.
The best estimate is taken at the intersection of the QFM*
line with the granitic minima and the coexisting feldspar
estimates. These are:

$$T = 710^{O}C, \log f(O_2) = -17.25 \text{ and } P_t = P(H_2O) = 1200 \text{ bars}.$$

The pressure estimate compares very well with the 1100 bars
estimated earlier for the Traveler Rhyolite, suggesting that
the KG represents essentially a solidifed magma chamber
underneath the volcano. Additional evidence for this con-
clusion is that both rhyolitic and granitic rocks register-
ed oxygen fugacities on the same $f(O_2)$ buffer curve, notably
QFM. An apparent discrepancy between the above estimated
pressure and pressure implied by the whole-rock chemical
composition ($P(H_2O) = 2$ Kb; Fig. 18) is best explained by the
chemical memory of the granitic rocks; that is, the whole-
rock chemistry is a weighed average of several crystalliza-
tion stages. The biotites of the Doubletop and Wassataquoik
facies have the same composition. However, the biotites of
the Summit facies are significantly lower in Ti and Fe and
noticeably higher in Mn. Petrographic study of the Summit
facies reveals that these biotites are phenocrysts within a
very fine graphic and granophyrically intergrown ground-
mass of quartz and feldspars. These biotites may have
crystallized at higher temperatures, which were subsequently
quenched as the magma was intruded into a colder environment.

Using the biotite reaction and assuming that the granitic melt was internally buffered with respect to $f(O_2)$ (on QFM buffer curve), the crystallization temperatures for these biotites may then be estimated as follows: 740^OC for Sample #183, and 727^OC for Sample KM6. The alternative explanation of constant T would invariably result in higher oxygen fugacity estimates. Biotite from the aplitic dike (Sample #145) also indicates an internally buffered $f(O_2)$ granitic melt with an estimated $f(O_2)$ just slightly below the QFM line. A temperature of 725^OC and a pressure of 1 Kb for the aplite were derived from the Q-OR-AB and AN-OR-AB diagrams.

The proposed existence of an internally $f(O_2)$ buffered natural melt is not without foundation. From $f(O_2)$-T plots of coexisting iron-titanium oxides for different suites of cogenetic rocks, it is apparent that there are definite $f(O_2)$-T trends parallel or subparallel with the QFM or the Ni-NiO buffer curves (Carmichael, 1967; Lipman, 1971; Hemming, Carmichael, 1972; Frisch, 1971). The results of these studies also suggest that internally $f(O_2)$ buffered magmatic environments are a rather common occurrence.

The internal buffer may be maintained by one or both of the following reactions:

1) through the Fe^{+2}/Fe^{+3} equilibria and precipitation of magnetite (Mueller, 1971); and

2) through the H_2/H_2O equilibria within the melt attributable to the ability of hydrogen to enter the silicate melts (Nakamura, 1974).

C.   Horserace Quartz Diorite

1.   Geology and Petrology

The Horserace Quartz Diorite (HQD) forms a
small elongated stock intruding the Doubletop facies of
Katahdin Granite (KG) in the western part of the Katahdin
Pluton (Fig. 14).   This body, first described by A. Griscom-
in prep.), was named after the Horserace, a series of rapids
in the West Branch Penobscot River.   The HQD is about 5.5 km
long, and at its maximum 2.0 km wide.   It forms a pronounced
topographic low on both sides of the Penobscot River between
Big Ambejackmockamus Falls and Nesowadnehunk Deadwater.

The Horserace intrusion parallels a prominent fault
system of the West Branch Penobscot River.   This same fault
system intersects the HQD and extends for a minimum of 30 km
from Chesuncook Lake along the West Branch River to the
center of the Katahdin Pluton, where its possible continua-
tion is obscured by thick glacial deposits.   A swarm of
lamprophyre-like dikes, which seem to parallel the fault
along its entire length, are considered part of the Horse-
race intrusion on the basis of geological, major and trace
element similarities.   Thus, it is evident that the ascent
of the quartz dioritic magma was tectonically controlled,
and that the fault remained active after the solidification
of the intrusion.

The shape of the Horserace stock on the vertical
plane was deduced from aeromagnetic data (Allingham, 1960).

The intrusion is symmetric; both, north and south contacts
dip outward at angles of about 55° to a depth of at least
3 km. The character of the contacts with the surrounding
Katahdin Granite is consistent with the model of a forceful,
tectonically controlled intrusion. Brecciation of the
granite and granitic inclusions within the quartz diorite
are commonly observed near the contacts.

In fresh hand-specimens the quartz diorite is a
bluish-grey rock; the varying intensities of grey depend on
the modal content of mafic minerals. On the weathered sur-
faces, however, the HQD turns light-grey and/or pinkish near
the joints or faults. The grain size varies from fine grain
near the contacts to medium grain in the interior. The
Horserace intrusion is concentrically zoned, with a composi-
tion of biotite-amphibole quartz diorite at the margins and
a composition of amphibole-bearing biotite granodiorite in
the interior. The content of the mafic minerals varies ac-
cordingly from about 25 modal percent to about 7 modal per-
cent. The principal mineral components of the stock are
plagioclase, quartz, alkali feldspar, amphibole and biotite;
the last two are often fully or partially chloritized. Com-
mon accessories are apatite, zircon, sphene, opaques, and
sulphides.

Modal analyses of two very fresh specimens collected
from the marginal zones are given in Table 6 . These two
(and additional modal analyses by A. Griscom) were plotted
on the IUGS recommended classification diagram (Fig. 22)

along with other plutonics of the Katahdin Pluton. From this
diagram there is no indication that the Horserace rocks and
the Katahdin granites may be related by either fractional
crystallization or fractional melting (see also discussion on
"Trace Element Geochemistry of the Traveler Rhyolite-Katahdin
Pluton Igneous Complex"). On the same diagram, several
hundred modal analyses from the Sierra Nevada Batholith
(Bateman, 1963) are shown for comparison.

A strong correlation between Horserace Quartz Diorite
and Debsconeag Granodiorite is suggested by the AFM diagram
(Fig. 23). Here, a unique and distinct trend is defined by
nearly colinear points of the Debsconeag, Harrington Lake,
and Horserace intrusions and by samples from the West Branch
dike swarm and the mafic dike on the east side of Doubletop
Mtn. This trend is not similar to that of the Traveler
Rhyolite-Katahdin Granite association. The HQD trend re-
quires removal of mafic silicates and substantial amounts of
magnetite. This implies a differentiation via fractional
crystallization under strongly oxidizing conditions (Mueller,
1971).

Numerous aplitic and pegmatitic dikes, found mainly
in the marginal zones, commonly contain albitic oligoclase,
alkali feldspar, quartz, and minor amounts of biotite along
with secondary chlorite and epidote. The marginal zone is
also noticeable because of a narrowly spaced network of thin
veinlets thought to be healed joints and fractures.

Table 6

Modal Analysis of Horserace Quartz Diorite

and

Debsconeag Granodiorite.

	Horserace Quartz Diorite		Debsconeag Granodiorite	
Sample #	235	238	13	166
Alkali Feldspar	4.7	5.1	23.4	19.4
Plagioclase	58.3	54.9	37.9	36.4
Quartz	8.8	13.0	29.3	33.8
Biotite	10.8	10.5	8.3	8.9
Amphibole	16.2	15.1	0.5	0.7
Others	1.2	1.4	0.6	0.8
Pl/(Pl+Af)	0.93	0.92	0.62	0.65
Amph/(Amph+Bi)	0.60	0.59	0.06	0.07

Fig. 22. Modal Abundances of the Katahdin Pluton Granitoids
          Plotted on the IUGS APQ Diagram (After Streckeisen,
          1973).

          Legend: KGD – Katahdin Granite: Doubletop Facies
                  DGD – Debsconeag Granodiorite
                  HQD – Horserace Quartz Diorite

          Labeled Fields: 1 – Granite
                          2 – Granodiorite
                          3 – Tonalite
                          4 – Quartz Syenite
                          5 – Quartz Monzonite
                          6 – Quartz Monzodiorite
                          7 – Quartz Diorite
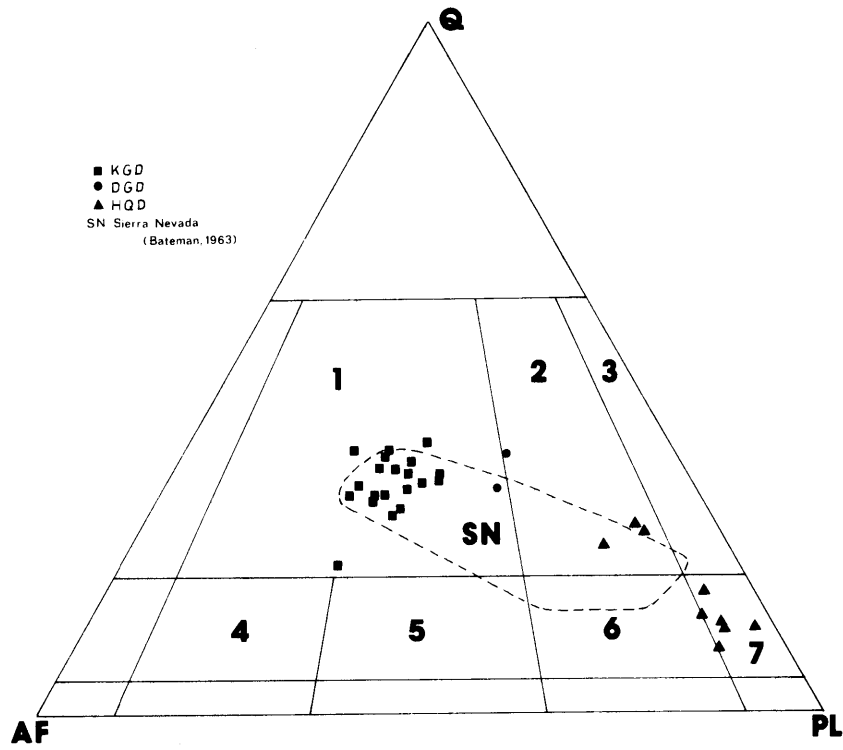
Fig. 23A. AFM Plot of the Katahdin Pluton Granitoids and
Harrington Lake Porphyry. The Lower California
Batholith Trend is After Larsen, 1948, and the
Skaergaard Trend After Chayes, 1970.

Legend: TR-KG – Traveler Rhyolite-Katahdin Gra-
nite Magmatic Sequence
DGD   – Debsconeag Granodiorite
HLP   – Harrington Lake Porphyry
HQD   – Horserace Quartz Diorite

122

- TR-KG
○ DGD
△ HLP
□ HQD
■ WEST BRANCH DIKE SWARM
◌ MAFIC DIKE, EAST SIDE OF
   DOUBLETOP MTN

SK Skaergaard Trend
LCB Lower California
    Batholith Trend
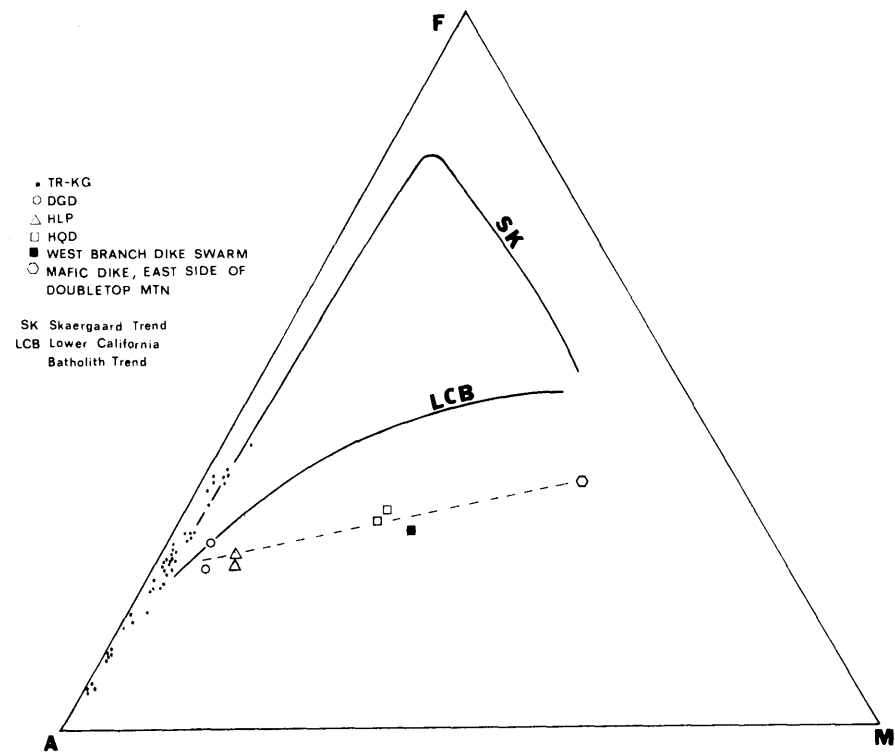
Fig. 23B. Plot of Normative (CIPW) Q-OR-AB Components of
the Katahdin Pluton Granitoids and Other Analy-
zed Granites of Northern New England. For Loca-
tions See Fig. 3.

Legend: Small Dots – Katahdin Granite
DGD   – Debsconeag Granodiorite
HLP   – Harrington Lake Porphyry
HQD   – Horserace Quartz Diorite

124
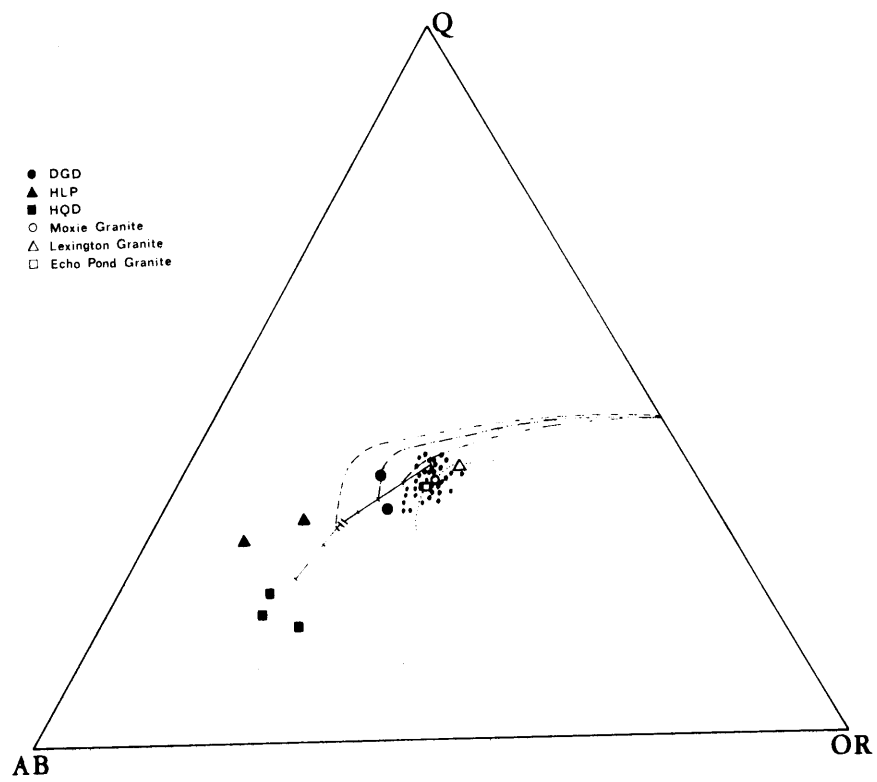
Fig. 23C.   Plot of Normative (CIPW) AN-AB-OR Components
of the Katahdin Pluton Granitoids and Other
Analyzed Granites of Northerh New England.
For Locations See Fig.3.

        Legend: Small Dots - Katahdin Granite
               DGD   - Debsconeag Granodiorite
               HQD   - Horserace Quartz Diorite
               HLP   - Harrington Lake Porphyry

AN

● DGD
▲ HLP
■ HQD
○ Moxie Granite
△ Lexington Granite
□ Echo Pond Granite

AB   OR
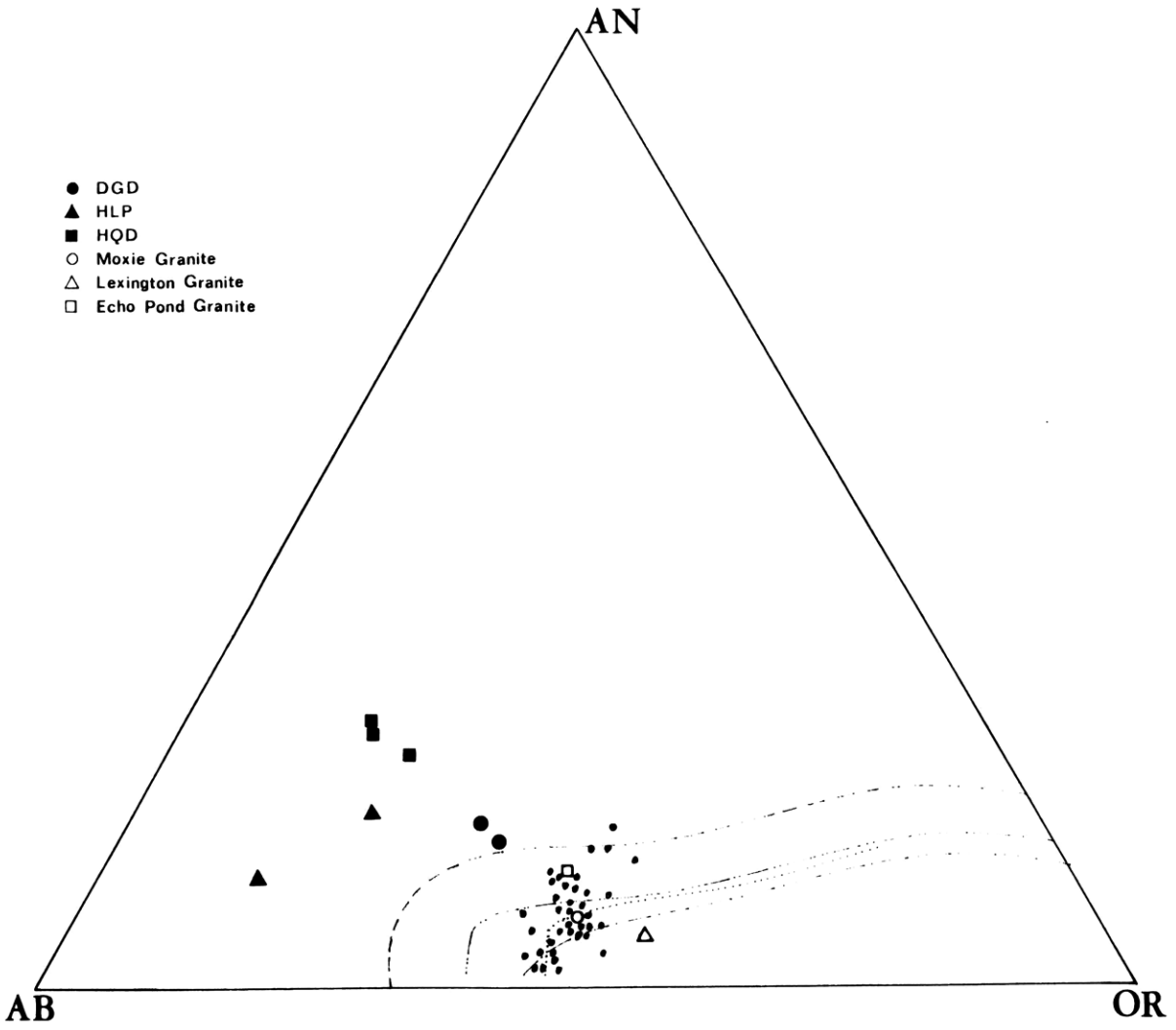
2. Mineralogy

The modal proportions in Horserace rocks varies appreciably from a rather mafic amphibole-rich quartz diorite to a relatively felsic biotite granodiorite. The modal variations of optically analyzed samples are graphically illustrated on Fig. 24. The diagram shows a convincing correlation between the abundances of amphibole, biotite and alkali feldspar, but shows a considerable scatter for the plagioclase and quartz contents. A similar variation diagram plotting the modal amphibole as a fraction of the total mafics against the modal plagioclase as a fraction of the total feldspars, suggests that the principal cause of differentiation was a simultaneous removal of plagioclase and amphibole (lower part of Fig. 24).

Plagioclase:

Euhedral to subhedral oscillatory-zoned, elongated crystals of plagioclase feldspars form a framework giving the rock a subophitic or subgabbroic textural character. The crystals are on average about 2 mm large, somewhat coarser in the center and finer at the margins of the intrusion . The composition varies from andesine to oligoclase with the mean composition around An25. alteration of plagioclase is scarce and limited to saussuritization of a basic core within the interior of the stock. Microprobe analysis of three different grains from Sample #235 yields an average composition of An24.

Fig. 24.   Mineral Variation Diagrams in the Horserace
           Quartz Diorite. Data From Griscom (in prep.)
           and This Work.

           Upper Diagram: Modal Variation of Biotite,
                Plagioclase, Alkali Feldspar and Quartz
                Plotted Against Modal Content of Amphibole.

           Lower Diagram: Variation of Modal Plagioclase
                as Fraction of Total Feldspars Against Mo-
                dal Amphibole as Fraction of Total Mafics.
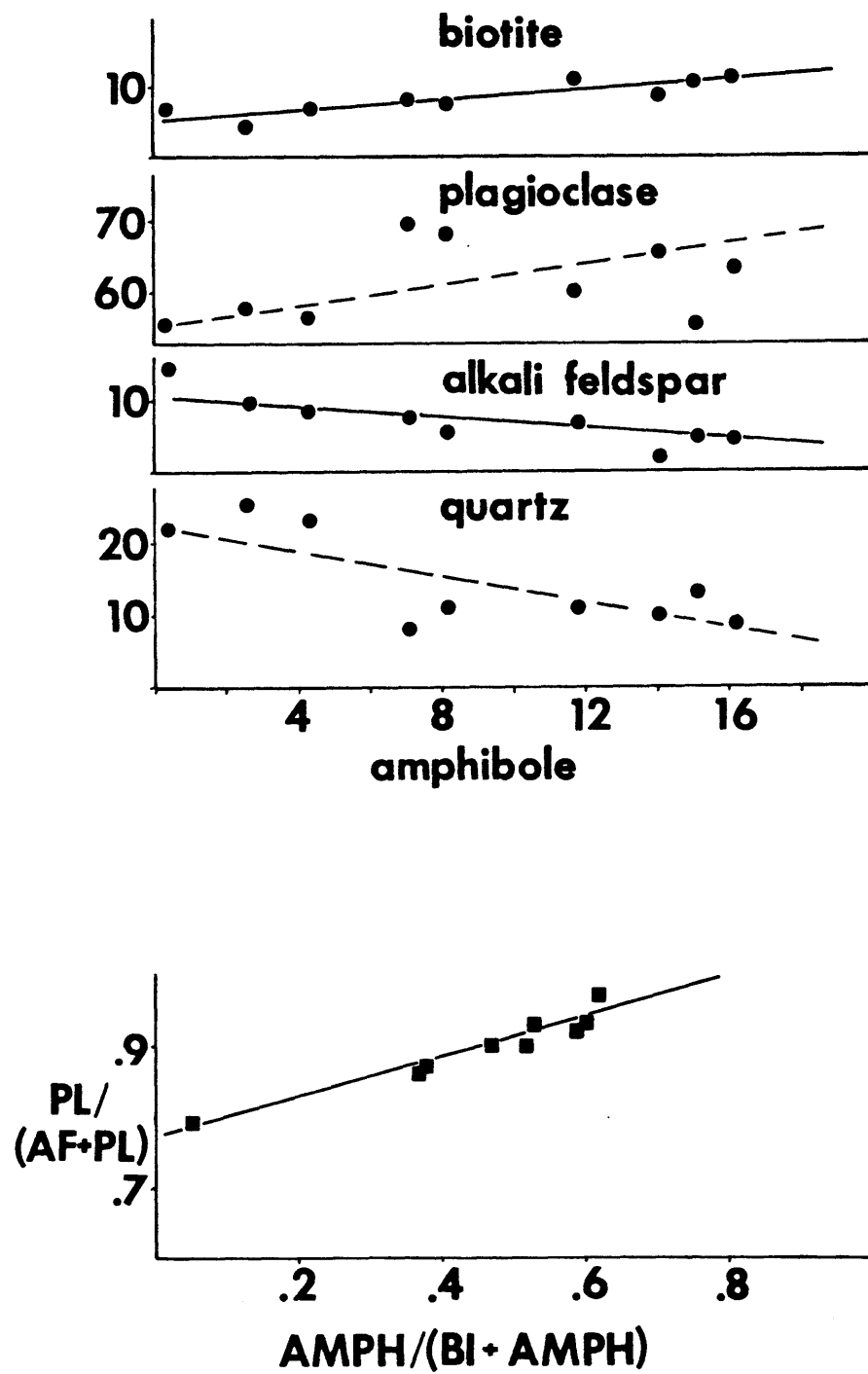
Alkali Feldspar:

Alkali feldspar is always present in the form of in-
terstitial grains, filling residual voids between euhedral
and subhedral plagioclases, amphiboles, and biotites. The
grains are fresh and homogeneous. An average of four micro-
probe analyses from two different grains corresponds to a
composition of Or87 Ab13.

Amphibole:

Amphibole is euhedral to subhedral within the marginal
zone of the intrusion but is more irregular toward the center.
The grains are up to 4 mm large with occasional resorption
remnants of clinopyroxenes in samples from near the contacts.
The pleochroism is strong from intense green to straw-yellow.
From indices of refraction, A. Griscom (in prep.) has shown
that the amphibole composition is constant throughout the
intrusion. The textural relationship with biotite indicates
that amphibole crystallization preceded biotite crystalliza-
tion. Amphiboles are conspicuous because of common, fine
sulphide grains in the interior of larger amphiboles. Chlor-
itization is commonly observed in the center of the stock.

Biotite:

Euhedral or subhedral grains, up to 2 mm in size, are
intensely pleochroic from dark brown to yellowish-tan. Bioti-
te occasionally encloses irregular grains of green amphibole.
Small grains of accessory zircon and apatites are frequent.
The biotite composition in the marginal zone, as determined

by electron microprobe, is distinctly different from the
biotite of the Katahdin Granite.

Fe*/sum (octahedral ions) = 0.38. This compares
with 0.77 of the Katahdin Granite. Assuming the same total
pressure for the Katahdin Granite and a water pressure of at
least one-half of P(tot), approximate calculations indicate
that the logarithm of oxygen fugacity for the Horserace in-
trusion was 1.7 to 2.3 units higher than for the Katahdin
Granite; i.e., near or above the Ni-NiO buffer. Biotites
from the interior are less ferrous, possibly by as much as
10 mole%, indicating therefore an oxidizing, magmatic
environment.

Minor Minerals:

Other common minerals are sulphides and iron-titanium
oxides. Sulphides occur as fine "droplets" almost exclusive-
ly in the cores of amphiboles. They are probably pyrrhotites
with minor chalcopyrites. A typical accessory mineral is
sphene; apatite and zircon are less frequent.

In conclusion, the chemistry and mineralogy of the
Horserace intrusion suggest that the quartz dioritic magma,
in contrast to the Katahdin Granite, crystallized under a
more oxidizing environment. The calculation based on bio-
tite composition shows that for the temperature range
between 700° and 800°C, the oxygen fugacity was above the
Ni-NiO buffer curve. This conclusion is supported by the
presence of sphene (Czamanske and Wones, 1973, p. 374) and
by the trend in the AFM diagram.

D.   Harrington Lake Porphyry

The porphyry is a light-grey, porphyritic rock, consisting of a fine-grained, subcrystalline matrix, with up to 15 modal% plagioclase phenocrysts, and fully chloritized mafic silicates--probably amphiboles.

All the samples studied are extensively hydrothermally altered to a mixture of sericite, chlorite, epidote, calcite, and other secondary minerals.

The Harrington Lake Porphyry is a semi-arcuate, sill-like intrusion, approximately 4.5 km long and 650 m wide, which crops out along the southern shore of Harrington Lake. A fault terminates the intrusion on the northwestern side; on the southeastern side it is ended by the Katahdin Pluton. The contact relationship with the Katahdin Pluton is uncertain due to the scarcity of exposures. A few crystalline inclusions, found within the interior of the intrusion, are mineralogically and texturally similar to the rocks of the Horserace Quartz Diorite stock. As a consequence, the Harrington Lake intrusion appears to be younger, possibly a differentiation product of the original Horserace magma. This possibility is further supported by the major elemental abundances; that is, low K/Na, intermediate Fe/(Fe+Mg), and by trends on the AFM, Q-OR-AB and OR-AB-AN diagrams (Figs. 22 and 23).

In 1968, Rankin considered this intrusion as part of a broader belt of granophyric bodies scattered between

Harrington Lake and Grand Lake Matagamon, describing them as
shallow igneous bodies, analogous to the Traveler Rhyolite.
However, a comparison of chemical compositions of Grand Lake
Matagamon granophyric sill with the analyses of the Harring-
ton Lake Porphyry and Traveler Rhyolites indicates, that
Rankin's interpretation may hold true only for some of these
bodies. The Harrington Lake Porphyry correlates with the
Horserace magmatic episode emplaced after the Katahdin
Granite. The magmatic association of the other "granophyric"
bodies is uncertain.

E. Debsconeag Granodiorite

Debsconeag Granodiorite (DGD) is a medium-grained
biotite-granodiorite, principally found in an 80-km^2 large,
V-shaped stock in the southeastern portion of the Katahdin
Pluton (KP). Another occurrence of DGD is mapped as a
separate, (1.5 km^2) small stock in the southern part of KP.
The type exposures are along the rapids in the West Branch
Penobscot River, namely at Abol Falls, Pockwockamus Falls,
and Debsconeag Falls.

DGD, the larger of the two stocks, is intruded by
the West Branch Penosbscot River dike swarm. Both stocks,
which are for the most part covered by extensive glacial
deposits, are entirely surrounded by Doubletop facies of
Katahdin Granite. Their contacts, however, were never
observed due to the absence of critical exposures. A study
of DGD float boulders near the vicinity of the contacts

indicates that DGD is finer-grained with increasing con-
centration of as much as 15% biotite and increasing
abundances of aplites and pegmatites.

Mineralogically and texturally, DGD shows consider-
able similarity to KGD. The noticeable differences include
a finer grain size of biotite and quartz, a lower modal
content of alkali feldspar, higher proportions of biotite
and plagioclase, along with subordinate amounts of horn-
blende which are present in all samples (Fig. 22). DGD
alkali feldspar tends to be more euhedral giving the DGD
rock a subporphyritic appearance. From a comparison of KGD
and DGD biotites, the latter are frequently euhedral with
distinctly lower Fe/sum (octahedral ions) = 0.59 vs. 0.77
for KGD. Plagioclase is continuously and cyclically zoned,
varying from An35 to An18 with occasional albitic rims.
Apatite, zircon, and allanite are frequent accessory minerals.

The deuteric alteration of DGD is much less extensive
than that of KGD. DGD specimens are light-grey and never
pink, even near joints. The only evidence of deuteric
changes is documented by partly chloritized biotites and by
infrequently saussuritized and sericitized plagioclase cores.

Two DGD analyses are plotted on Q-AB-OR (Fig.23B),
AN-AB-OR (Fig.23C), and on AFM (Fig.23A) diagrams. The major
element abundances are in support of the genetic relation-
ship of DGD with the younger HQD-HLP sequence. Based on
field relationships, the time of DGD emplacement is bracket-
ed by earlier KGD and younger HQD intrusions.

IV. TRACE ELEMENT GEOCHEMISTRY OF THE TRAVELER RHYOLITE-KATAHDIN PLUTON IGNEOUS COMPLEX

A. Introduction

Trace element abundances are a more sensitive indicator of igneous rock petrogenesis than are abundances of major elements. This is particularly true for acidic rocks where the bulk composition of the fractionating crystals is often very similar to the parent magma. For this reason, trace element (TE) abundances were determined in selected samples of the Traveler Rhyolite-Katahdin Pluton Igneous Complex.

As discussed in the preceding chapters, petrological and geological studies of igneous rocks from the Traveler Rhyolite-Katahdin Pluton Igneous Complex suggest two genetically independent magmatic episodes, each of a different igneous style. The earlier episode includes voluminous ignimbritic depositions of the Traveler Rhyolite (TR) and crystallization of six facies of the Katahdin Granite (KG) which underlies more than 95% of the 1330 km^2 large Katahdin Pluton. The younger igneous episode is comprised of three small intrusions of Horserace Quartz Diorite (HQD), Harrington Lake Porphyry (HLP), and Debsconeag Granodiorite (DGD), all of which intrude along the NW-SE West Branch Penobscot River fault system (Fig. 14).

Fifty-two (52) samples included in this study are represent-
ative of both episodes:

Traveler Rhyolite

      Pogy Member - Sample codes: 46, 51, 214, 215
                               and 216   5

      Black Cat Member - Sample codes: 217, 219, 220,
                         TR3, TR8, and TR10   6

Katahdin Granite

      Doubletop Facies - Sample codes: 29, 41, 74, 81,
                         134-1, 134-2, 150,
                         190F, 190W, 209 and
                         240   12

      Chimney Facies - Sample codes: 69 and KM9   2

      Summit Facies - Sample codes: 64, KM1 and KM6   3

      Wassataquoik Facies - Sample code: 43   1

      Cathedral Facies - Sample codes: 121, 198, and
                         KM2   3

      Horserace Quartz Diorite - Sample codes: 127A,
                         235 and 238   3

      Debsconeag Granodiorite - Sample code: 166   1

      Harrington Lake Porphyry - Sample code: 4   1

      Aplites - Sample codes: 134-3, 134-6, 134-7,
                         134-8, 145 and KM7   6

      Pegmatites - Sample codes: 134-4 and 134-5   2

                                       ———

        Total number of analyzed samples for
        TE from the TR-KP igneous complex   45
                                     ==

In addition, samples from similar magmatic complexes
of Northcentral Maine and Northern Vermont were also
analyzed (Fig. 3). The additional samples include:

Rhyolite of the Kineo Rhyolite (Piscataquis Volcanic
    Belt - Rankin, 1968): Sample code: 247   1 sample

Granite of the Lxington Pluton (Greenville Plutonic
    Belt): Sample code: NNP-2[*]   1 sample

Granite of the Moxie Pluton (Greenville Plutonic
    Belt): Sample code: 244   1 sample

Gabbros of the Pierce Pond Pluton (Greenville
    Plutonic Belt): Sample codes: PP1, PP235 and
                    PP379[**]   3 samples

Granite of Echo Pond Pluton (Northern Vermont):
    Sample Code: 6291[*]   1 sample

Postmagmatic changes, such as weathering, tectonic shear-
ing, hydrothermal and pneumatolytic alterations, may signifi-
cantly alter primary (magmatic) TE abundances (Rice, 1973);
Blaxland, 1974; Neiva, 1974) and, as such, could lead do
erroneous petrogenetic interpretations. In order to evalu-
ate the effects of postmagmatic alterations, several altered
granitic and rhyolitic samples were purposely analyzed to
study the possible extent of such changes. Also, the pos-
sible loss of TE due to vapor transport was studied by
analyzing aplites and pegmatites from a layered aplite-
pegmatite dike.

(*) Courtesy of R. S. Naylor
(**) Courtesy of P. Lyttle

B. Analytical Methods

TE abundances were determined by instrumental neutron
activation (INNA) analysis (Gordon et al., 1968) and by X-ray
fluorescence (XRF). The precision of the INNA technique, ex-
pressed as % fractional standard deviation (also known as
variation coefficient - VC), was obtained by multiple ana-
lyses of USGS Standard G-2. The precision (at ±1 sigma
level) is less than 5% for Cr, Co, Cs, Ce, Nd, Sm, Ho, Hf,
and Th; less than 10% for Sc, Rb, La, Eu, Gd and U; and 10-
12% for Yb, Lu and Ta. The lower precision for Yb and Lu is
attributed to low concentration of these elements in the
USGS G-2 standard. Cr abundances in the majority of the
analyzed rocks are below the detection limit. The Cr de-
tection limit, calculated at 3 sigma significance level,
is between 4 and 5 ppm. The XRF precision is probably
better than 20% (H. W. Fairbairn - personal communication).
The accuracy level of both techniques is comparable with
precision. In the XRF analyses, G-2 is used as a primary
standard.

C. Postmagmatic Changes of TE Abundances in Rhyolites
    and Granites

In order to evaluate the extent of deuteric changes
on TE abundances in rhyolitic and granitic rocks, the fol-
lowing two tests were carried out:
(1) The variation coefficients for individual elements of
seven, both fresh and altered, rhyolitic rocks were compared

with the variations caused by analytical imprecision
(samples analyzed by L. Lopez, 1972). These samples,
collected from a narrow stratigraphic zone of the Black
Cat Unit of the Traveler Rhyolite, were thought to rep-
resent an originally homogeneous section of rhyolitic rocks
with idential TE abundances. For this reason, the variation
beyond the limit of analytical imprecision is possibly due
to postdepositional changes (Figs. 25A, 25B). Both figures
also show variation coefficients (% standard deviation)
calculated for eleven (11) different samples from different
localities of Doubletop Facies of Katahdin Granite. These
variations represent a combination of analytical errors and
actual differences among the analyzed samples. The signif-
icance of these variations and their interpretation will
be discussed later in this study.

(2) Another evaluation of postmagmatic changes was obtained
by comparing trace element data of five (5) altered samples
at the KG Doubletop facies with the average trace element
abundances of unaltered Doubletop facies of the Katahdin
Granite (see Fig. 26). These altered samples are:

(a) Sample #81 - Tectonic mylonite: silicified fault gouge;

(b) Sample #190-W - Weathered crust around sample #190-F;

(c) Sample #240 - Hydrothermally altered zone near fault:
         deeply reddened Doubletop Facies granite;

(d) Samples #134-1 and 134-2 - From the contact with layered
         pegmatite-aplite. Sample #134-2 is direct-
         ly from the contact; Sample #134-1 is
         4 cm away from the contact and is unaffect-
         ed by the presence of the dike.

Fig. 25A, B.   Comparison of Analytical Precisions With Varia-
               tion Coefficients Obtained on 6 Different
               Samples of Black Cat Member of Traveler Rhyolite
               And on 8 Different Samples of Doubletop Facies
               of Katahdin Granite. Fig. 25A: Non Rare-Earth
               Elements; Fig. 25B: Rare Earth Elements.

VARIATION COEFFICIENTS

(A)
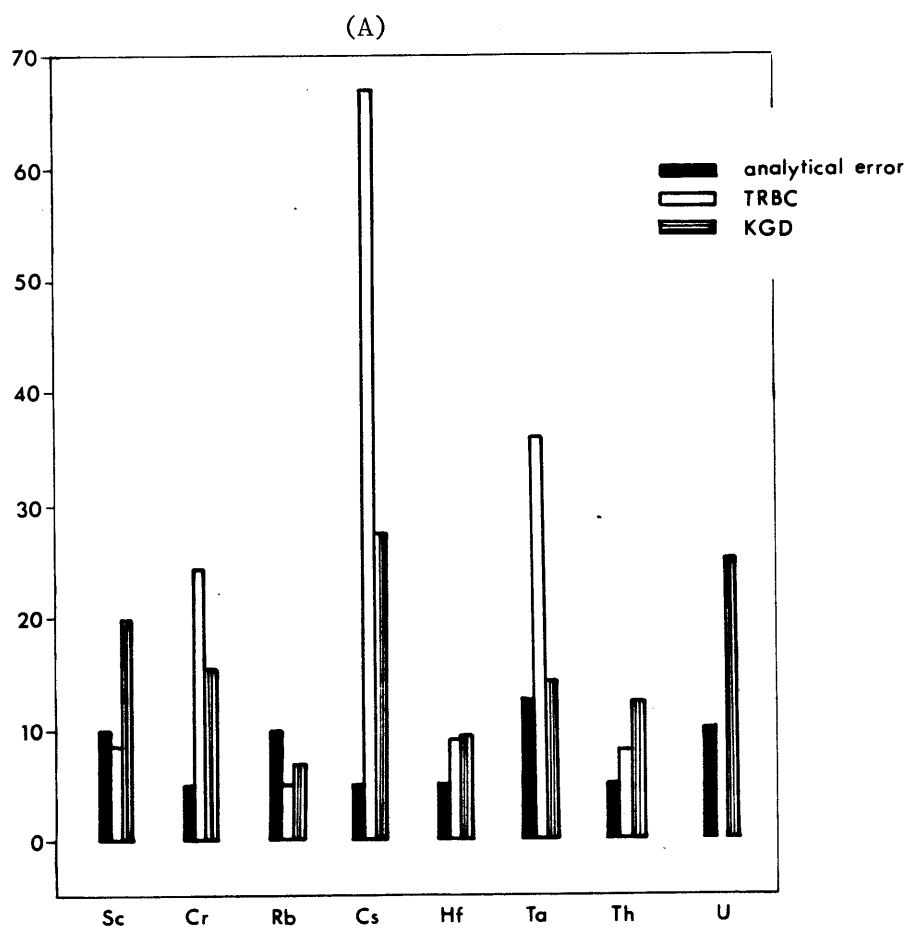
VARIATION COEFFICIENTS

(B)
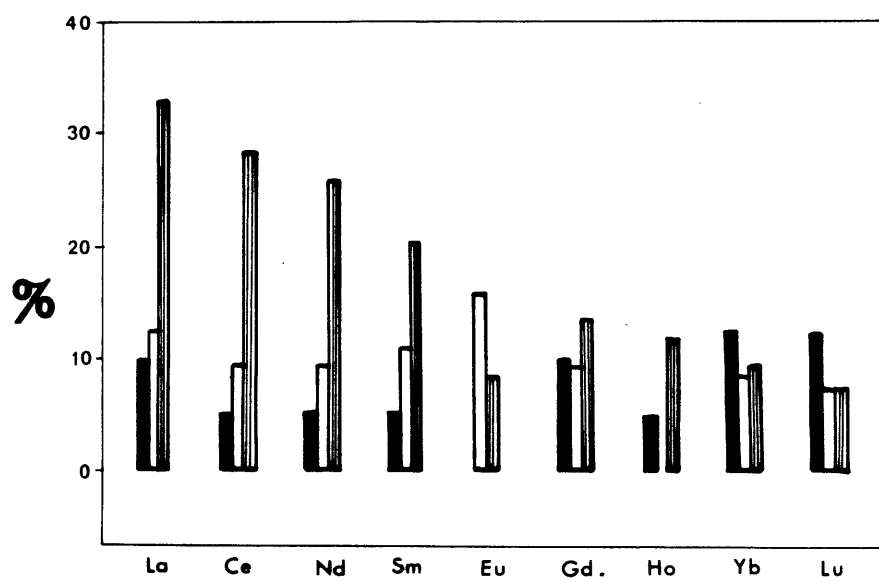
Rare Earth Elements (REE):

REE abundances in the Traveler Rhyolite are unaffected by deuteric changes, even in the few extensively altered specimens (see Fig. 25A). This is also true for the tectonically sheared granitic sample (Sample #81), and for the weathered crust sample (Sample #190-W). However, the sample of hydrothermally altered granite (#240) shows a depletion in HREE (Lu concentration is 0.6 of the average concentration in the Doubletop facies of Katahdin Granite), whereas the sample from the contact with the layered pegmatite-aplite (#134-2) shows a considerable enrichment in HREE (Lu is 2.4 times higher than the average content in the Katahdin Granite-Doubletop Facies). Since these postmagmatic changes are easily detectable in the field, I conclude that the REE abundance variations reflect variations imprinted by magmatic processes alone.

Scandium (Sc):

The Sc variation in the tested rhyolites and granites is within the limits of analytical precision, except for Sample #134-2 (contact with the aplite-pegmatite dike), which shows an enrichment of approximately 1.4 times the average Katahdin Granite-Doubletop Facies.

Cobalt (Co):

The variation coefficient of Co in rhyolites (24%) does not correlate with the degree of deuteric alteration; the dispersion is most likely a primary feature caused by a

144

Fig. 26. Plot of Rare-Earth Elemental Abundances of Variedly
Affected Samples of Doubletop Facies of Katahdin
Granite Normalized to an Average of 8 Fresh Samples
of Doubletop Facies of Katahdin Granite. See Text
For Further Discussion.

Legend: Sample 134-2 - From Contact With Layered
Aplite-Pegmatite Dike
Sample 240   - Strongly Reddened and Hydro-
thermaly Altered
Sample 190W - Weathered Rind From Around
a Fresh Sample 190F
Sample 81   - Sheared, Ground and Silici-
fied Sample From a Fault Zone
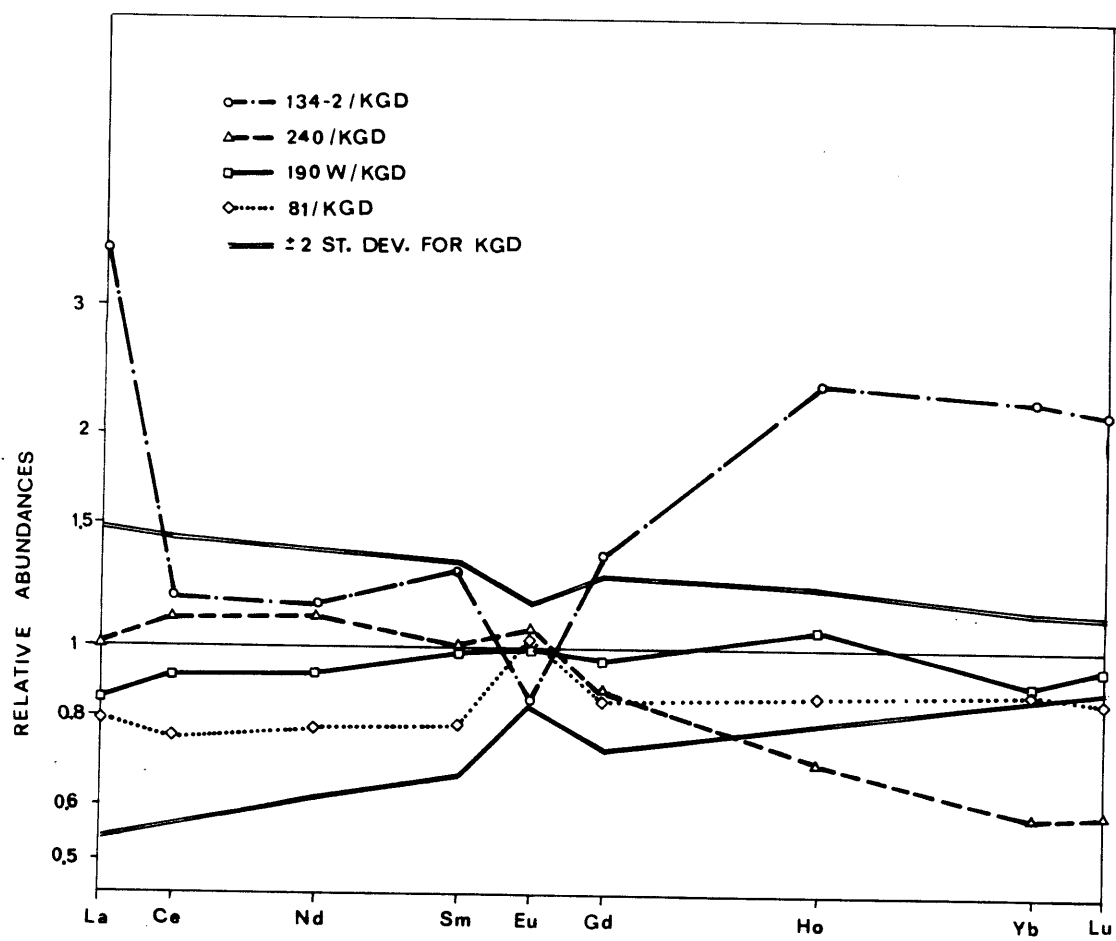
statistical variation in the modal content of clinopyroxene, opaques, and fayalite. The variation of Co in altered granitic rocks is within the limits of analytical precision, except for enrichment in Sample #240 (hydrothermally altered zone) of 1.4 times the average Katahdin Granite-Doubletop Facies (KGD).

Rubidium(Rb):

Rb abundances in granites and rhyolites are very uniform with a marked depletion found only in extremely altered samples, e.g., in hydrothermally recrystallized rhyolites (Sample #M-14)(L. Lopes, 1972). A significant depletion of 0.5 times the average Katahdin Granite-Doubletop Facies is also found in the tectonically sheared granite (Sample #81) and in the hydrothermally altered granite (Sample #240) (about 0.65 times the KGD).

Cesium (Cs):

Cs seems to be a very sensitive indicator of post-magmatic changes, as documented by large variation coefficients of 50 to 70% for the rhyolitic and granitic rocks. Cs is usually depleted in altered rocks but its abundance is enriched in the weathered crust sample (#190-W).

Hafnium (Hf):

All Hf variations are within the limits of analytical precision, except for the sample from the contact with the layered pegmatite-aplite, which shows an enrichment of

1.35 times above the average Katahdin Granite-Doubletop facies.

Tantalum (Ta):

Ta is next to Cs the most variable element. Its variation coefficient in rhyolites is about 35%. Although the variation coefficient in KGD is only about 15%, all altered samples show a significant depletion (about 20-50%) except for the weathered crust sample which is within normal limits. The large variation of Ta abundances may be due to the relative solubility of tantalum fluoride.

Thorium (Th):

Th variations in the rhyolites and granites are within the limits of analytical precision. Only two samples from near the contact with the pegmatite-aplite dike show an enrichment by about 42-50%.

Uranium (U):

It was difficult to assess the variation of U abundances, primarily because of the low analytical precision (about $\pm$ 20%). However, there is a strong indication that U abundances are sensitive to deuteric alterations; for example, the U content in the weathered crust sample #190-W) and in the sample from the contact with the pegmatite-aplite dike (#134-2) is twice as high as the average KGD facies.

These results show that the abundances of Cs, Ta and U
are strongly influenced by deuteric changes. For this reason
Cs, Ta and U variations cannot be used as indicators of frac-
tional crystallization. However, REE, Sc, Co, Rb, Hf and
Th abundances vary within the limits of analytical precision
and these elements are a reliable source of information on
magmatic processes.

On inspection of Figure 25B, there is a gradual increase
of variation coefficients from Lu to La for the granites of
Doubletop facies. I believe that this gradual increase of
uncertainty from Lu to La (except for Eu) is due to the
statistical variation between samples; e.g., unequal dis-
tribution of monazite or allanite in the analyzed samples.
Strong evidence for such apparent sample heterogeneity is
that the smallest and the coarsest samples yield the largest
deviations. From the known distribution of REE in these
accessory minerals, the difference between average and ex-
treme values (normalized to Lu) can be explained by the
weight variation of $\pm 1:6600$ for allanite or $\pm 1:17000$ for
monazite. These variation ranges are approximate, based on
estimated La partition coefficients of allanite and monazite
(3700 and 9500, respectively; Lee and Bastron, 1967;
Nagasawa, 1970; Lee et al., 1973).

D. Layered Pegmatite-Aplite

Upon fractionation of hydrous magmas, the continual-
ly evolving and escaping volatile-rich gaseous phase may

carry with it an unknown (but appreciable) amount of trace elements and may thus, during the late magmatic states, cause important changes in their abundances otherwise attributable to crystal fractionation processes. Further understanding of the effect of the exsolving hydrous phase on TE abundances is thought to be gained by a geochemical study of coexisting pegmatite and aplite within a layered pegmatite-aplite dike (Sample #134). As will be shown later, the aplite of this dike represents approximately 20% residual magma differentiated from the parental Debsconeag Granodiorite (DGD) melt. The associated pegmatite is a coarse crystalline rock, formed by a crystal growth from the hydrous vapor phase which was purged from the crystallizing magmas (Jahns, Tuttle, 1963; Luth, Tuttle, 1966; Jahns, Burnham, 1969).

Sample #134 comes from the upper part of a 0.5 m wide, layered aplite-pegmatite dike, exposed in the stream bed of the Katahdin Stream (elevation 395 m), approximately at the base of Mt. Owl and 0.5 km above the Katahdin Stream Campground. The dike intrudes the Doubletop Facies of Katahdin Granite.

A 2 cm thick and 30 cm long slab obtained from this sample was further divided into a sequence of the following eight blocks:

134-1   5 cm long block of Doubletop facies of Katahdin Granite - 4 cm away from the contact;

134-2   4 cm long block of Doubletop facies of Katahdin Granite - from the contact;

134-3   2 cm wide aplitic zone;

134-4   3.5 cm long block, half the thickness of the peg-
         matitic zone;

134-5   Ditto; and

134-6,7,8 4 cm long consecutive blocks of the main aplitic
         zone.
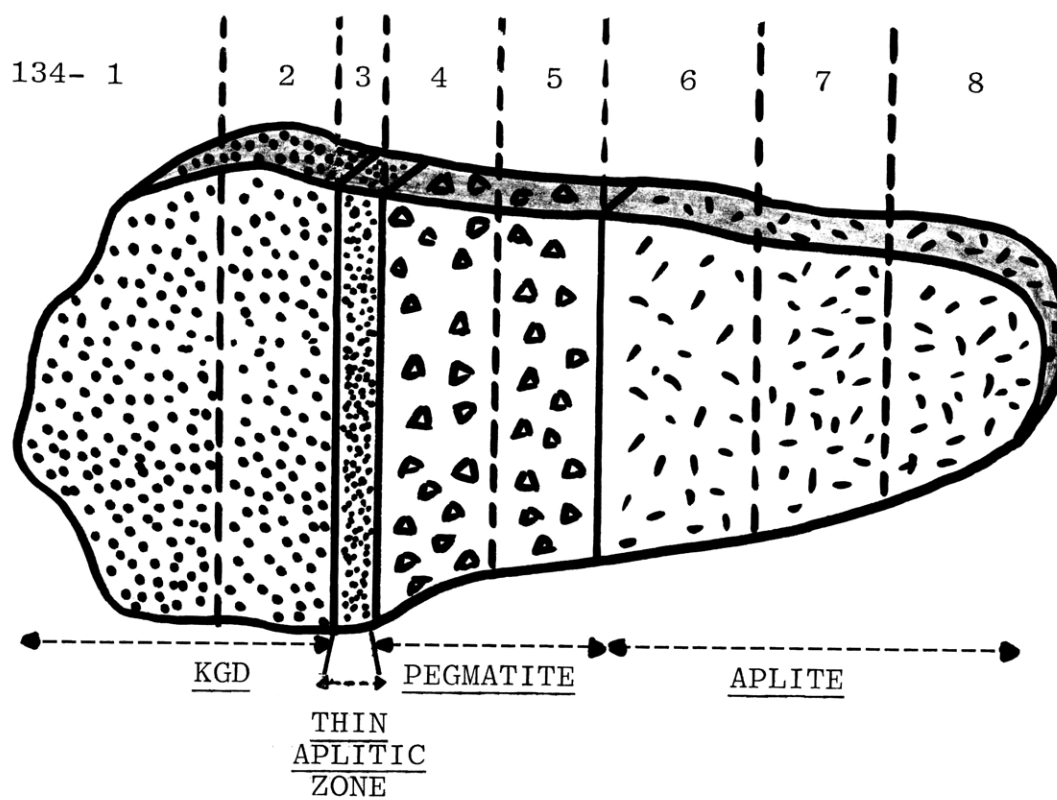
Trace element variations across Sample #134 are shown
on Figs. 27, 28, 29A, 29B, and 29C. The REE chrondrite
normalized distribution patterns are illustrated in Fig. 27.
Fig. 28 shows relative REE distributions of AP3 (average of
the four aplitic samples: #134-3, 134-6, 134-7 and 134-8,
and PEG3 (average of the two pegmatitic samples: 134-4 and
134-5) with respect to their parental DGD magma and the
relative distribution of PEG3 compared to AP3.

Fig. 27.   Chondrite-Normalized Rare Earth Element Abundances
in 6 Samples Taken From Across a Layered Pegmatite
Aplite Dike.
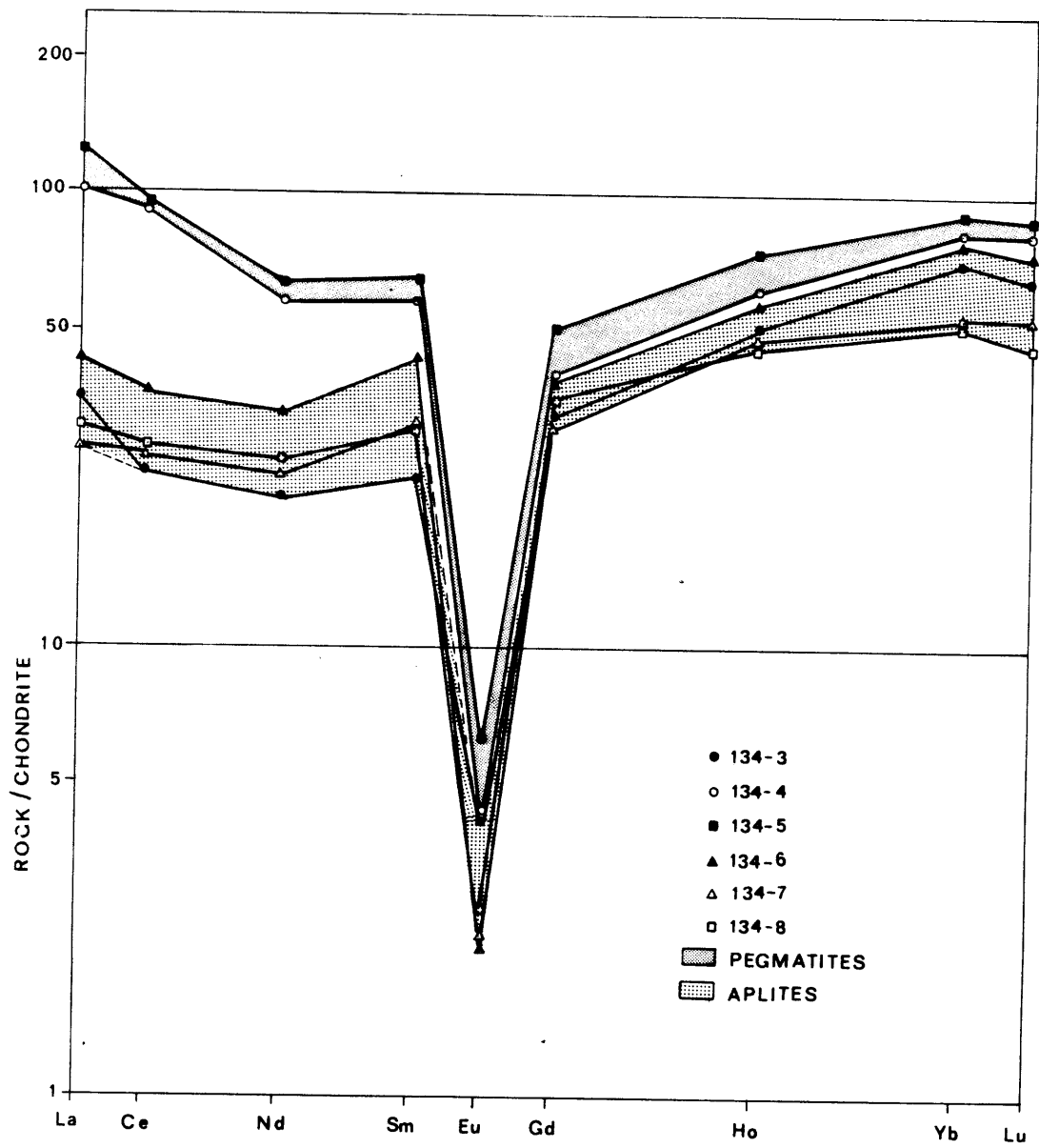
Fig. 28. Plot of Average Rare Earth Elemental Abundances in
          Aplites and Pegmatites Normalized to Debsconeag
          Granodiorite (Presumed Parental Magma) and Rare
          Earth Element Abundances of Pegmatite Normalized to
          Aplite.
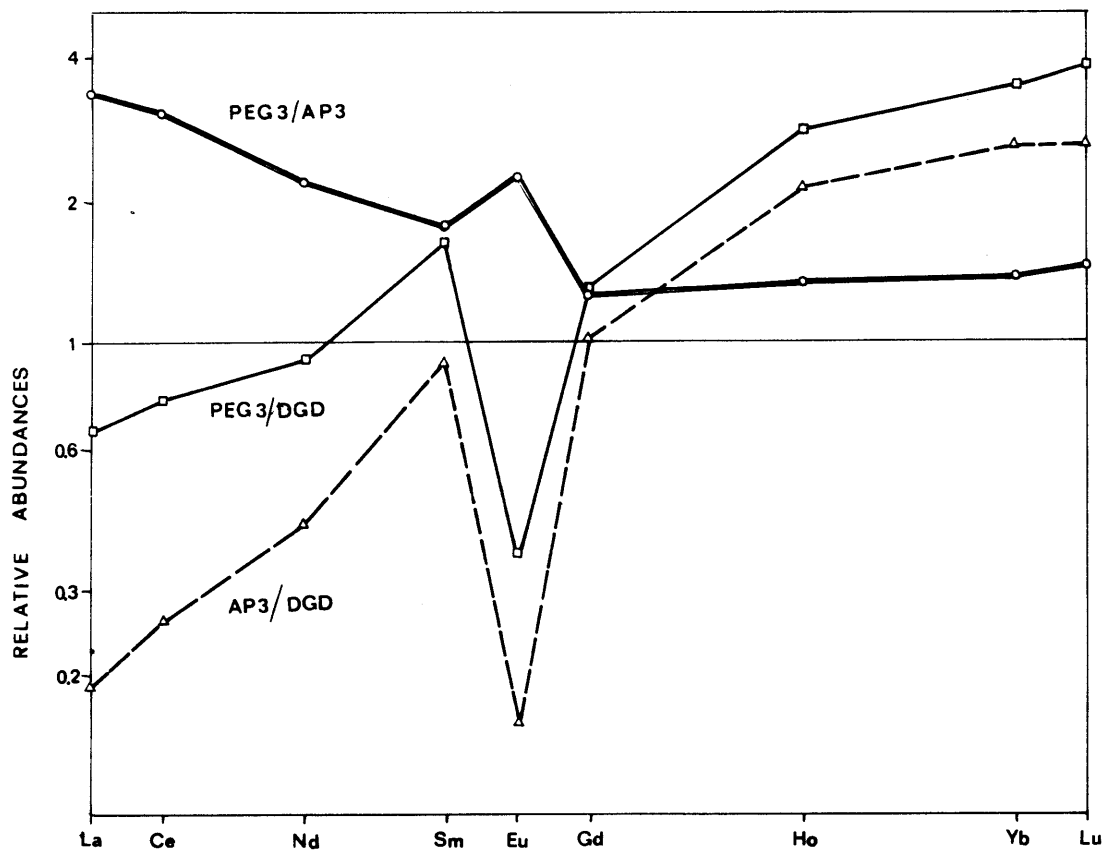
Concentration profiles of the individual trace elements across the analyzed portion of the layered dike are shown on Figs. 29A, 29B, and 29C. They are compared with average abundances in the Doubletop facies of KG with superimposed ± 3 standard deviations (99% confidence limit).

The diagrams are largely self-explanatory, but some general conclusions can be drawn:

1) REE are always more abundant in pegmatites than in coexisting aplites. Light RE(LRE) are two to three times more enriched in the pegmatitic phase than heavy Re(HRE) (Gd-Lu) which show only mild enrichment (1.35 times);

2) In Sample #134-1, 6 cm from the contact, only La, among the REE, shows marked enrichment relative to the average granite;

3) Near the vicinity of the contact, the granite (Sample #134-2) is strongly enriched in HRE (Ho-Lu: 2.2 times).

4) Except for Eu, Sc, and Co, there is a considerable enrichment of the other trace elements in the aplitic zone immediately adjacent to pegmatite;

5) Co abundances in both aplites and pegmatites are identical. There is no exchange of Co between the wall rock and the dike;

6) Sc, Th tend to be enriched in the wall rock; Th is relatively depleted in the pegmatites; Sc abundances in pegmatites and aplites are similar.

Fig. 29A,B,C.   Variation of Elemental Abundances Across Ana-
lyzed Portion of a Layered Aplite-Pegmatite
Dike. On Abscissa Are Plotted Average Double-
top Facies of Katahdin Granite and Individual
Segments of Sample # 134, e.g. 134-1 to 134-8.
Average Doubletop Facies of Katahdin Granite
is Plotted With ±3 Standard Deviations (99%
Confidence Interval).
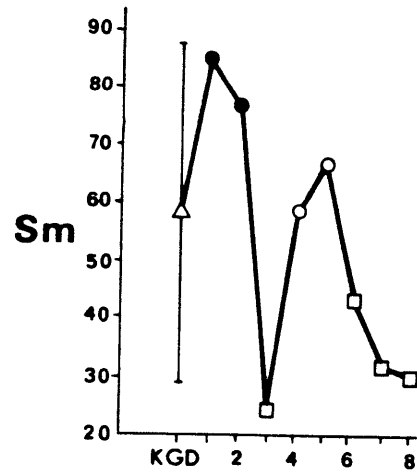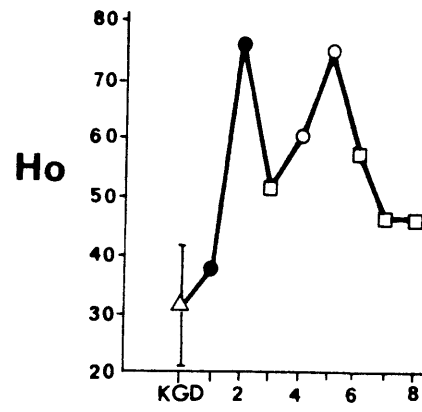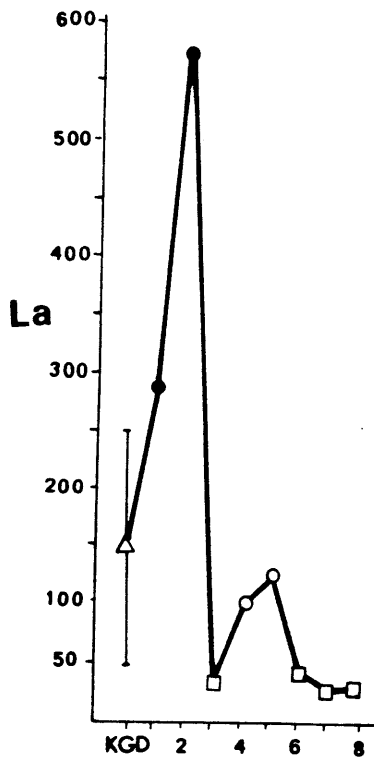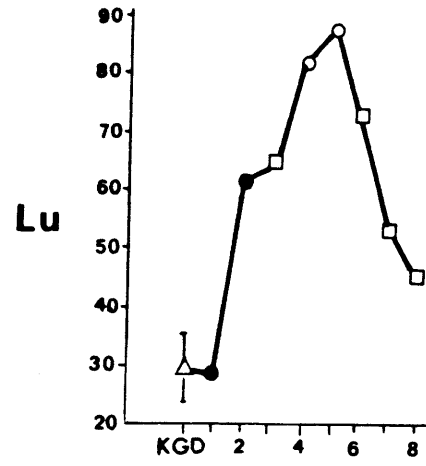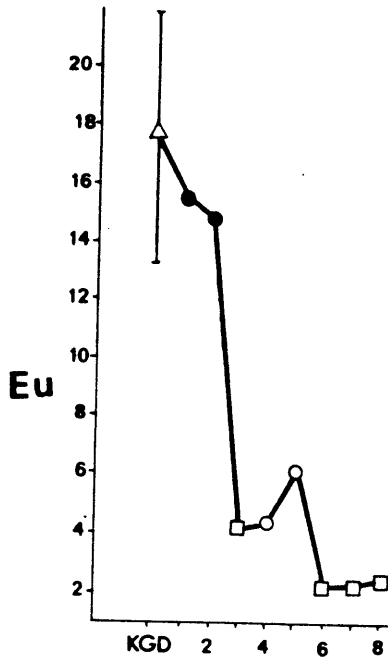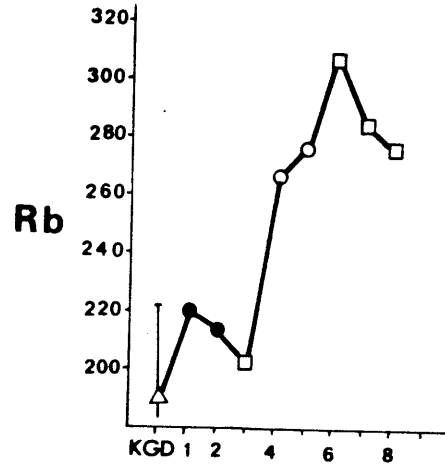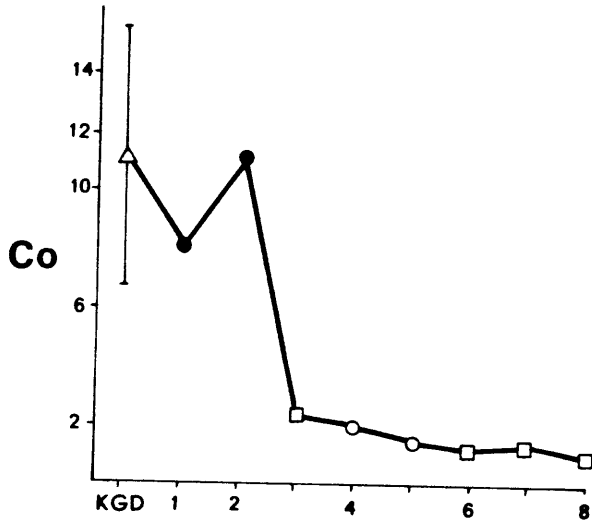
Legend:
- △ ∮KGD
- ● KGD
- ○ PEGMATITE
- □ APLITE
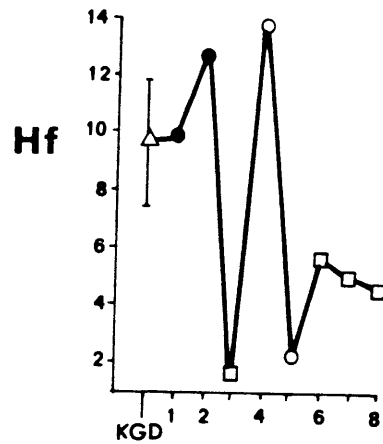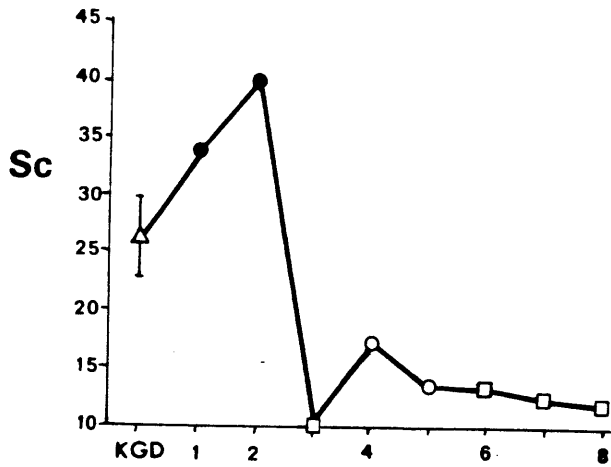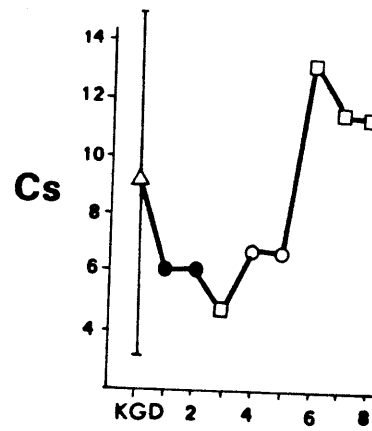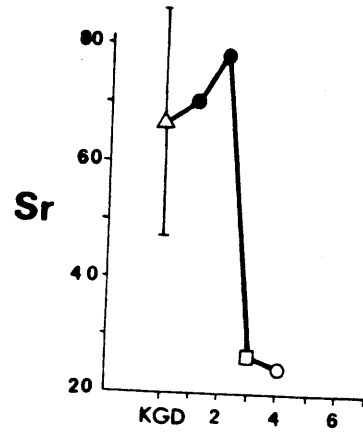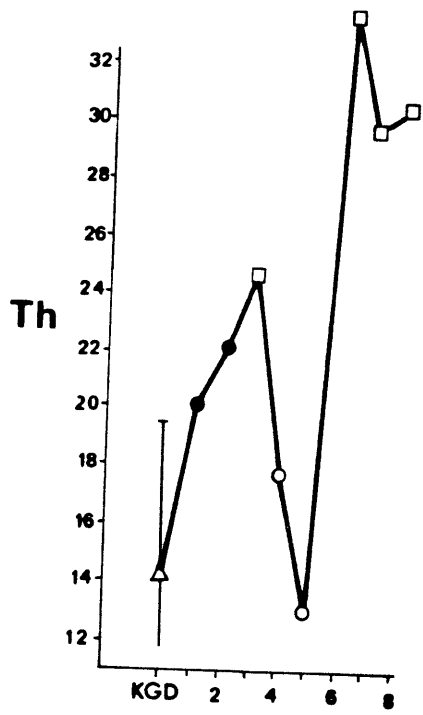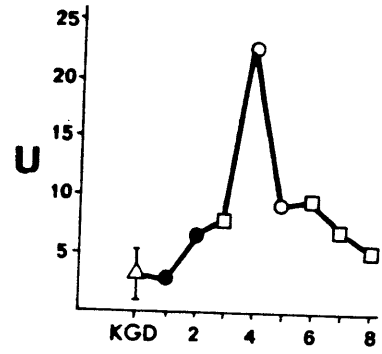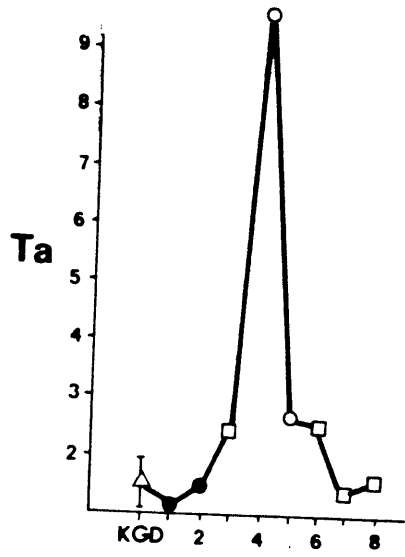
7)   Rb abundances in the main aplitic zone and in the
     pegmatitic zone are identical; original Rb abundances
     in the wall rock are unaffected.

The comparison of TE abundances in coexisting aplite and
pegmatite emphatically points to a diverse behavior of some
of the elements during the late stages of evolution of hydrous
granitic magmas. REE, Hf, Ta and U are preferentially incor-
porated in pegmatites whereas Cs and Th tend to be enriched
in aplites. The best indicators of fractionation during the
stages of vapor phase separation are the abundances of Rb,
Sr, Sc and Co; their excess relative pegmatite abundances
in percent of the average aplite (3%, -8%, 13% and 30%,
resp.) indicate their equal mobility in both the evolving
vapor phase and the magma. Abundances of Rb and Sc, and
possibly of Sr, are also valued for their passivity during
the postmagmatic alteration processes. The unique signifi-
cance of the Rb and Sr behavior will be reemphasized later
(see discussion on TR-KG sequence).

   E.   Results
      Trace elemental abundances of the studied samples
are given in Table 7 and the REE abundances normalized to a
chrondrite average (Haskin et al., 1968) are plotted in
Figs. 30, 31, 32 and 33. Based on petrography, it is pos-
sible to arrange all the rock samples into two groups, with
further subdivisions based on their Sc abundances:

Table 7. Trace Element Geochemistry. Samples Arranged in Ascending Numeric Order and Alphabetically.

Sample Symbol	4	29*	29*	41	43	46	51	64	69	74	81
Rock Unit	HLP	KGD	KGD	KGD	KGW	TRP	TRP	KGS	KGCH	KGD	KGD
Sc	5.68	27.68	27.24	25.27	26.01	22.19	32.43	27.71	24.60	26.98	21.38
Cr	BD	BD	BD	BD	BD	BD	BD	BD	BD	BD	BD
Co	5.98	1.27	1.19	0.93	0.51	0.28	2.11	0.67	0.71	1.08	1.07
Rb	68.80	189.7	NA	182.5	236.2	180.2	169.0	202.2	NA	212.5	87.42
Cs	2.23	10.47	9.19	7.58	9.33	8.09	8.73	8.46	9.73	8.87	1.09
Hf	3.91	10.55	10.12	9.87	6.35	9.86	11.42	10.74	8.04	8.83	8.73
Ta	0.37	1.37	1.58	1.62	1.60	1.32	1.38	1.12	2.32	1.33	0.93
Th	7.23	16.68	NA	14.54	14.72	15.20	14.16	16.07	NA	12.68	12.45
U	0.90	2.77	2.23	3.06	5.74	2.83	4.57	1.87	4.08	2.47	2.23
Sr	540	67	NA	63	26	45	NA	59	NA	68	NA
La	19.87	58.77	57.33	51.11	47.34	52.22	47.74	35.61	48.08	32.59	41.17
Ce	44.32	126.0	123.2	117.2	123.4	130.0	120.4	74.16	107.5	65.16	82.79
Nd	16.69	55.99	54.02	50.76	52.39	66.44	55.65	34.30	46.40	31.21	38.11
Sm	3.21	12.24	11.60	11.06	12.38	15.07	13.75	8.07	10.16	7.07	8.53
Eu	0.88	1.30	1.30	1.25	0.68	1.70	2.00	1.13	1.25	1.02	1.25
Gd	2.67	12.52	12.20	11.17	10.84	14.91	14.80	8.45	10.52	8.00	9.48
Ho	0.41	2.48	2.10	2.30	2.80	2.98	2.69	1.91	2.06	1.74	1.92
Yb	0.94	6.35	5.96	6.41	7.01	7.28	7.28	5.24	6.09	5.37	4.90
Lu	0.15	1.02	0.98	1.05	1.17	1.20	1.19	0.84	1.05	0.90	0.83

* Duplicate analyses.

NA Not analyzed.

BD Analyzed, but below detection limit. From counting statistics the detection limit for Cr is 4 ppm.

All data in ppm.

Table 7. Trace Element Geochemistry. (Cont.)

Sample Symbol :	115	121	127A	134-1	134-2	134-3	134-4	134-5	134-6	134-7	134-8
Rock Unit :	KGD	KGCT	HQD	KGD	KGD	AP3	PEG3	PEG3	AP3	AP3	AP3
Sc	24.92	15.93	12.23	33.68	39.70	9.65	17.28	13.66	13.40	12.56	11.86
Cr	BD	BD	167.7	BD	BD	BD	BD	BD	BD	BD	BD
Co	1.28	1.71	20.08	0.82	1.11	0.23	0.20	0.15	0.13	0.14	0.11
Rb	183.8	210.8	76.18	219.2	213.5	201.7	267.0	277.2	307.4	285.8	277.2
Cs	5.02	8.35	2.92	6.01	6.10	4.64	6.82	6.61	13.15	11.45	11.41
Hf	8.93	6.56	4.29	9.87	12.59	1.70	13.55	2.19	5.63	4.95	4.57
Ta	1.74	1.64	0.67	1.12	1.45	2.43	9.58	2.64	2.56	1.43	1.58
Th	15.94	16.67	7.97	20.24	22.15	24.66	17.69	13.23	33.79	29.73	30.58
U	4.07	6.02	2.26	2.66	6.54	7.89	22.71	9.28	9.60	7.32	5.36
Sr	79	NA	NA	70	78	26	24	NA	NA	NA	NA
La	46.35	41.61	34.63	94.62	190.0	11.69	33.30	41.87	14.24	9.26	10.12
Ce	97.58	92.93	66.55	183.1	130.9	21.53	79.88	83.45	33.02	23.19	24.25
Nd	42.55	41.11	27.34	79.24	57.02	12.70	34.72	38.34	19.88	14.49	15.58
Sm	9.74	8.74	4.32	15.42	14.13	4.32	10.59	12.02	7.95	5.76	5.42
Eu	1.08	0.94	1.18	1.08	1.02	0.29	0.30	0.43	0.15	0.16	0.17
Gd	10.95	9.21	4.28	12.46	15.15	8.06	9.74	12.74	9.89	7.91	8.85
Ho	2.19	1.92	0.50	2.67	5.36	3.58	4.24	5.26	4.07	3.31	3.34
Yb	6.31	5.37	1.01	6.55	13.27	14.43	16.62	18.45	15.75	12.36	10.44
Lu	1.06	0.89	0.17	0.99	2.11	2.22	2.81	3.01	5.21	1.84	1.58

NA Not analyzed.
BD Analyzed, but below detection limit. From counting statistics the detection limit for Cr is 4 ppm.

All data in ppm.

Table 7. Trace Element Geochemistry. (Cont.)

Sample Symbol	: 145	150	166	190F*	190W**	198	209	214	215	216	217
Rock Unit	: AP2	KGD	DGD	KGD	KGD	KGCT	KGD	TRP	TRP	TRP	TRBC
Sc	41.04	26.00	12.02	28.26	26.38	21.27	25.17	25.25	24.07	26.94	33.57
Cr	BD	BD	BD	BD	BD	BD	BD	BD	BD	BD	BD
Co	0.40	1.12	3.95	1.07	1.00	1.83	0.96	1.72	1.59	3.79	2.15
Rb	377.0	191.3	135.8	194.3	203.7	NA	179.6	160.5	200.0	143.2	189.8
Cs	7.16	9.36	7.62	10.96	13.10	8.38	11.15	8.17	10.71	2.50	11.72
Hf	7.84	9.27	6.77	8.61	7.96	9.82	10.76	9.32	9.47	15.12	14.53
Ta	4.23	1.35	1.27	1.51	1.47	2.19	1.59	1.30	1.24	1.39	1.70
Th	19.22	14.90	20.07	13.75	14.83	NA	10.89	12.50	15.70	12.90	15.33
U	15.07	2.65	3.32	4.58	6.13	3.03	2.51	6.23	5.58	3.98	4.21
Sr	8	60	186	62	NA	NA	66	74	51	84	78
La	15.35	65.10	57.53	44.38	44.75	41.71	36.06	57.83	53.35	52.69	54.24
Ce	29.45	133.8	104.3	101.8	102.0	96.15	84.94	131.7	134.5	121.1	127.9
Nd	16.39	57.92	40.04	45.93	45.40	43.94	41.41	57.70	58.99	56.34	55.70
Sm	5.09	12.40	6.85	11.55	10.76	9.09	9.48	13.13	13.77	13.29	12.96
Eu	0.08	1.27	1.03	1.27	1.21	1.57	1.24	1.53	1.44	2.16	1.88
Gd	5.39	12.32	8.57	12.31	10.81	9.23	9.97	14.67	13.57	14.19	12.55
Ho	2.09	2.48	1.69	2.38	2.40	1.76	2.14	2.94	2.88	2.55	2.81
Yb	8.51	6.48	4.92	5.60	5.24	4.95	5.57	7.49	7.02	6.91	7.97
Lu	1.44	1.05	0.75	1.00	0.91	0.80	0.90	1.25	1.12	1.14	1.30

NA Not analyzed.
BD Analyzed, but below detection limit. From counting statistics the detection limit for Cr is 4 ppm.
* Fresh sample
** Weathered crust

All data in ppm.

Table 7. Trace Element Geochemistry. (Cont.)

Sample Symbol :	219	220	235	238	240	244	247	6291	KM1	KM2	KM6
Rock Unit :	TRBC	TRBC	HQD	HQD	KGD	MG*	KR**	EPG***	KGS	KGCT	KGS
Sc	29.37	27.53	13.81	14.14	23.46	4.66	29.22	3.32	27.62	19.83	26.95
Cr	BD	BD	101.6	115.5	BD	BD	BD	BD	BD	BD	BD
Co	3.05	1.56	16.95	17.23	1.55	1.88	0.61	3.50	0.89	2.12	0.91
Rb	137.5	165.2	56.93	59.91	117.9	148.1	145.5	121.8	166.9	206.0	192.6
Cs	15.61	3.09	1.08	1.30	1.21	4.22	2.02	1.85	8.05	9.25	16.10
Hf	15.36	12.55	4.34	4.10	9.53	3.55	10.22	5.97	10.29	12.26	11.35
Ta	1.17	1.78	0.39	0.67	0.75	2.25	1.74	1.68	1.45	1.30	1.64
Th	12.86	14.68	6.29	6.13	16.35	19.55	15.66	12.76	17.08	15.57	16.24
U	7.50	4.11	1.22	1.68	2.99	5.77	4.26	1.88	4.94	6.75	5.49
Sr	88	63	883	NA	NA	77	50	424	NA	NA	NA
La	56.68	47.14	29.24	24.43	53.10	21.51	52.44	32.98	57.10	34.77	49.85
Ce	131.8	117.8	54.31	52.85	122.5	42.79	125.8	60.70	133.4	75.54	111.2
Nd	60.82	52.76	23.57	22.10	54.60	16.55	53.86	19.72	59.89	37.87	52.93
Sm	13.76	12.29	4.36	4.26	10.99	4.37	12.17	3.50	11.56	7.91	11.29
Eu	1.92	1.74	1.26	1.19	1.29	0.49	1.29	0.68	1.12	1.18	1.33
Gd	15.25	13.70	4.08	3.95	9.49	4.95	10.54	2.68	13.51	7.72	12.34
Ho	2.89	2.70	0.48	0.54	1.56	1.33	1.80	0.35	2.02	2.10	2.49
Yb	7.62	6.81	1.33	1.46	3.47	4.0	4.65	0.89	5.36	5.55	6.11
Lu	1.28	1.13	0.22	0.23	0.57	0.67	0.77	0.12	0.84	0.86	0.94

*   MG = Moxie Granite
** KR = Kineo Rhyolite
***EPG= Echo Pond Granite
 BD = Analyzed, but below detection limit. From counting statistics the detection limit for Cr is 4 ppm.
 NA = Not analyzed.

All data in ppm.

Table 7. Trace Element Geochemistry. (Cont.)

Sample Symbol :	KM7	KM9	NNP2	PP1	PP235	PP379	TR3[1]	TR8[1]	TR10[1]	G-2*	G-2*
Rock Unit :	AP1	KGCH	Lexington Granite	PPG[2]	PPG[2]	PPG[2]	TRBC	TRBC	TRBC	USGS-ST	USGS-ST
Sc	27.30	24.87	3.53	38.13	51.71	51.56	29.23	33.50	33.27	3.87	3.83
Cr	BD	BD	BD	222.8	227.6	75.8	NA	NA	.NA	8.25	NA
Co	0.26	1.30	1.63	54.50	46.20	45.73	2.16	2.26	2.00	4.66	4.62
Rb	290.5	176.0	290.4	BD	BD	BD	181.6	202.6	180.4	177.0	NA
Cs	8.06	13.59	17.69	0.33	0.79	0.88	2.98	12.97	18.14	1.34	1.33
Hf	5.75	9.76	2.80	0.75	0.76	1.78	12.10	14.44	15.02	8.81	8.41
Ta	2.01	1.47	2.25	0.04	1.03	0.32	1.28	2.70	2.35	1.01	1.07
Th	15.83	14.02	8.47	BD	1.90	0.59	14.37	14.99	14.22	23.52	NA
U	5.84	2.74	4.04	BD	0.65	0.33	NA	NA	NA	2.67	2.03
Sr	NA	NA	NA	NA	NA	NA	NA	NA	NA	NA	NA
La	28.03	38.89	18.62	0.64	19.28	5.83	57.64	65.31	58.68	81.54	81.48
Ce	80.71	86.96	40.23	1.00	41.65	14.19	114.8	129.5	113.0	163.7	161.3
Nd	35.42	41.08	14.95	0.62	20.58	8.75	55.78	64.25	57.44	49.16	47.80
Sm	9.84	10.49	4.21	0.22	4.76	2.66	14.02	15.26	13.91	7.18	6.99
Eu	0.17	1.24	0.52	0.60	1.96	1.13	1.84	2.15	1.90	1.27	1.29
Gd	14.28	9.73	3.17	0.63	5.27	3.04	12.69	14.20	12.28	4.10	4.08
Ho	3.21	2.76	0.44	0.15	1.01	0.70	NA	NA	NA	0.51	0.48
Yb	8.32	5.72	0.94	0.49	3.18	2.01	6.83	7.81	7.89	0.64	0.76
Lu	1.35	0.89	0.15	0.084	0.52	0.33	1.17	1.16	1.09	0.115	0.112

(1) According to L. Lopez, 1972.

(2) Pierce Pond Gabbro.

(*) Duplicate analyses.

NA Not analyzed.

BD Analyzed, but below detection limit. From counting statistics the detection limit for Cr is 4 ppm, for Rb 8 ppm, for Th 0.2 ppm and for U 0.1 ppm.

All data in ppm.

Fig. 30. Chondrite-Normalized Rare Earth Element Abundances
in Traveler Rhyolite - Katahdin Granite Magmatic
Sequence.

Legend: TRBC - Traveler Rhyolite: Black Cat Member
        TRP   - Traveler Rhyolite: Pogy Member
        KGD   - Katahdin Granite: Doubletop Facies
        KGW   - Katahdin Granite: Wassataquoik Facies
        KGS   - Katahdin Granite: Summit Facies
        KGCH - Katahdin Granite: Chimney Facies
        KGCT - Katahdin Granite: Cathedral Facies
        AP1   - Katahdin Granite: Aplite Dike # 1
        AP2   - Katahdin Granite: Aplite Dike # 2

TR-KG SEQUENCE

ROCK/CHONDRITE

○ TRBC
□ TRP
● KGD
✕ KGW
△ KGS
■ KGCH
▲ KGCT
◇ AP1
● AP2
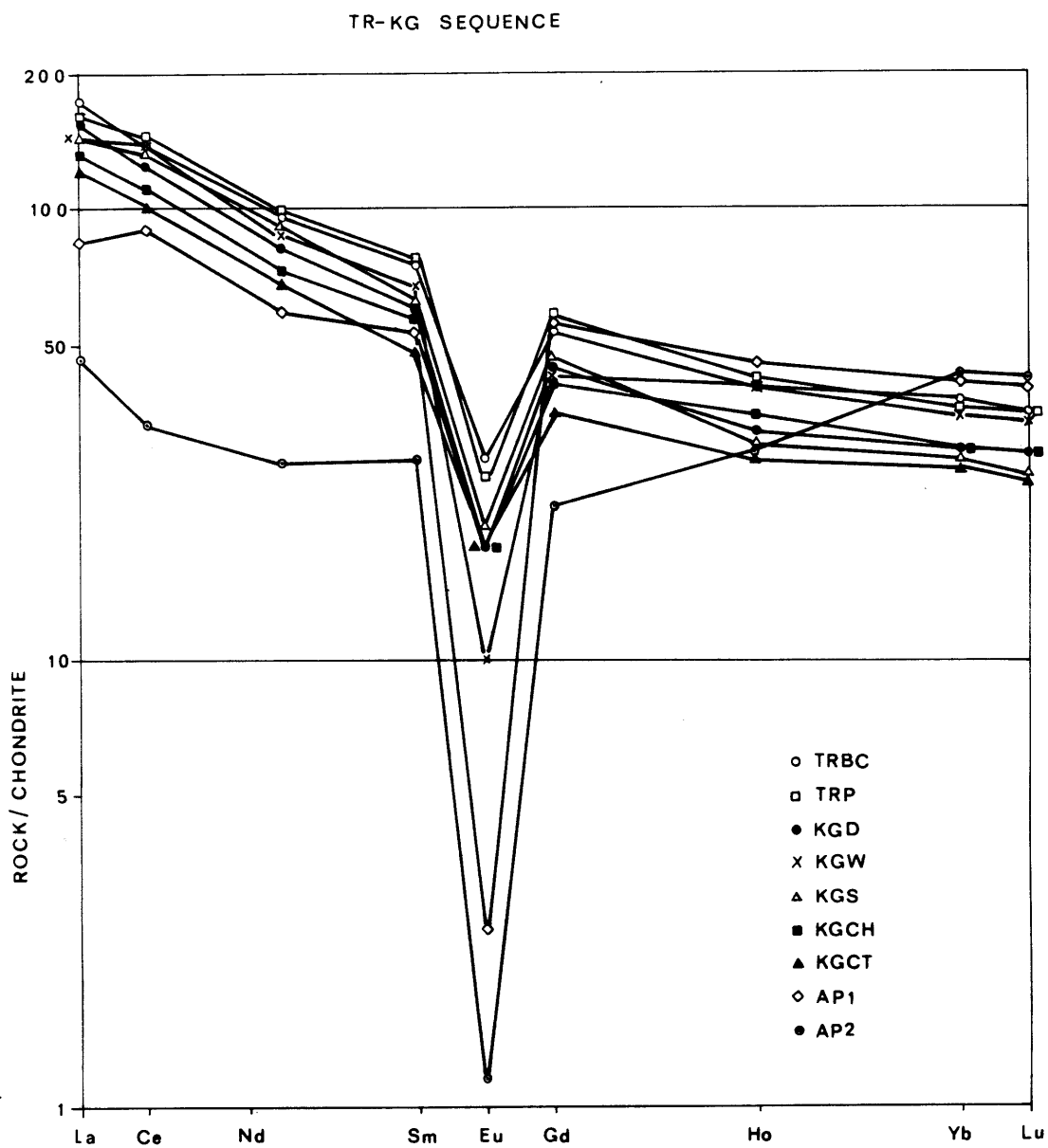
Fig. 31. Chondrite-Normalized Rare Earth Abundances For
          Horserace Quartz Diorite – Harrington Lake Porphyry
          Magma Sequence.

HQD—HLP   SEQUENCE
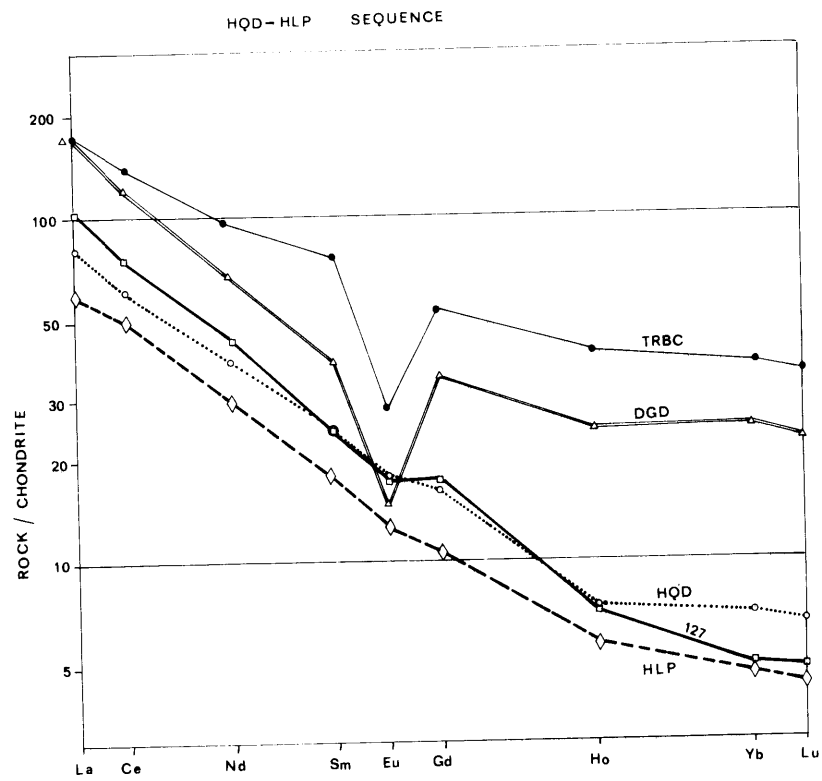
Fig. 32. Chondrite-Normalized Rare Earth Element Abundances
in Lexington Granite (NNP-2), Moxie Granite (244)
And Echo Pond Granite (6291).
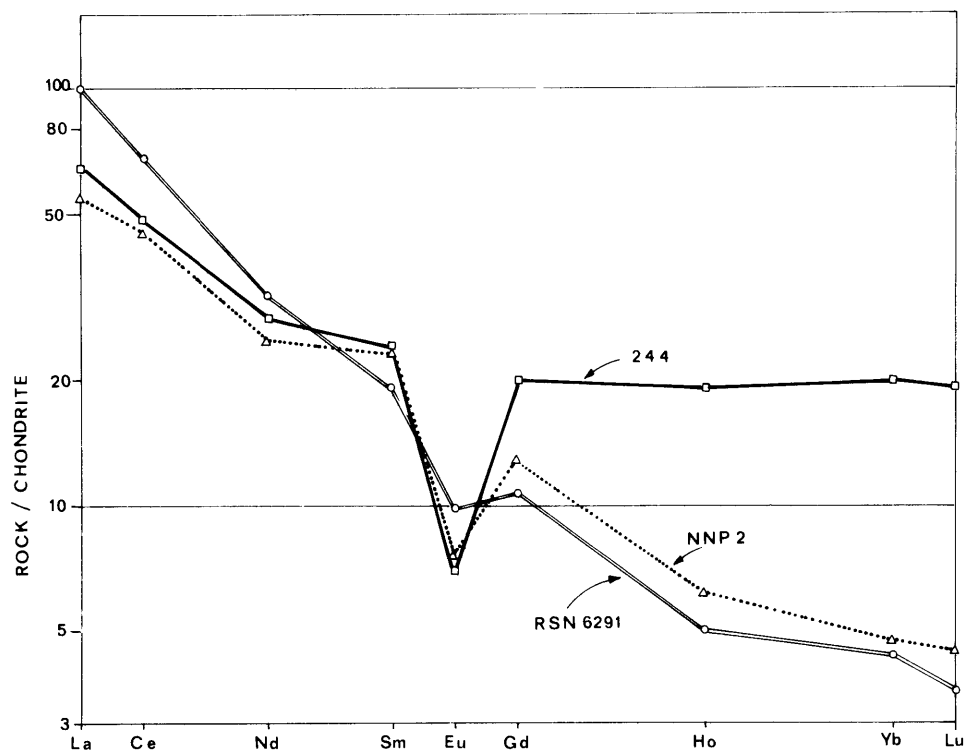
Fig. 33. Chondrite-Normalized Rare Earth Element Abundances
in Samples of Pierce Pond Gabbro.

PIERCE POND GABBRO
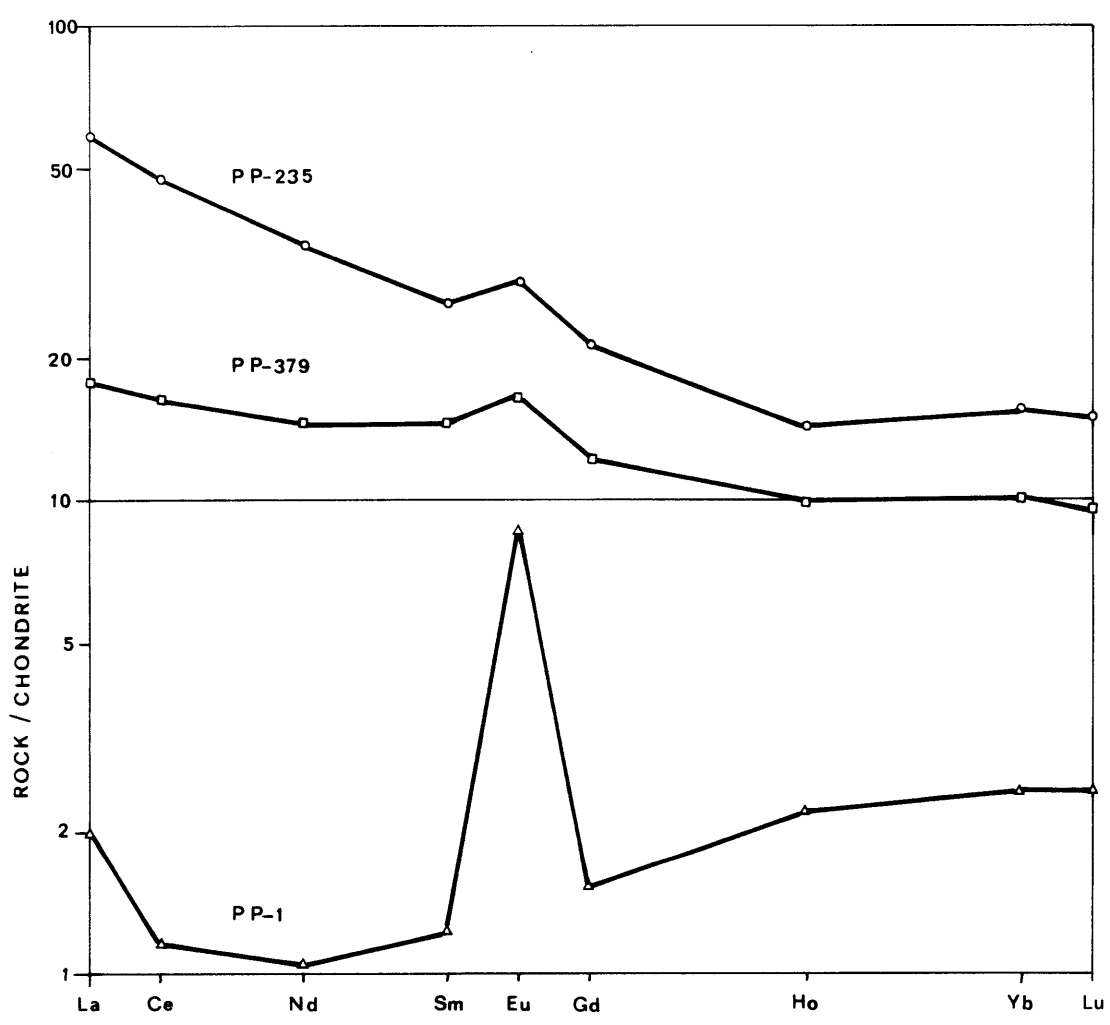
Acidic Rocks:

- High Sc Content (15-42 ppm)

  - Traveler Rhyolite (TR)
  - Katahdin Granite (KG)
  - Kineo Rhyolite (KR)

- Intermediate Sc Content (5-15 ppm)

  - Horserace Quartz Diorite (HQD)
  - Harrington Lake Porphyry (HLP)
  - Debsconeag Granodiorite (DGD)

- Low Sc Content (<5 ppm)

  - Granite from Moxie Pluton (MG)
  - Lexington Granite (LG)
  - Echo Pond Granite (EPG)

Basic Rocks:

- Pierce Pond Gabbro (PPG) (Sc = 38-52 ppm)

Scandium abundances are thus an important petrogenetic discriminator between rocks of distinct magmatic associations. The different Sc abundance levels appear to be of fundamental nature, allowing Sc to be used as a geochemical guide in identifying various igneous provinces in northcentral Maine.

1. High Scandium Rocks: TR-KG Sequence and Kineo Rhyolite

   a. General Statement

   To demonstrate the uniqueness of the Sc abundances in the TR-KG sequence, Table 8 lists Sc abundances in a variety of granitic rocks of different origin. From this table, it follows that the usual range of Sc abundances in acidic rocks is between 2 and 5 ppm, although it may reach up to 15 ppm. Hence, the unusually high Sc abundances

Table 8A

Scandium[*]

Table 21-E-2. *Content of Sc in igneous rocks*[a]

Rock type	Sc, ppm	Method	Reference
Granite G-1	2.7—2.8	NA	cf. FRYCKLUND and FLEISCHER (1962)
Granite G-1	2.4	NA	NORMAN and HASKINS (1968)
Granite G-1	2.83	NA	BRUNFELT and SLEINNES (1966)
Granite G-2	3.4	NA	BRUNFELT and SLEINNES (1966)
Granites (191, av.; 60—70% SiO_2)	10	NA	NORMAN and HASKINS (1968)
Granites (221, av.; >70% SiO_2)	2.8	NA	NORMAN and HASKINS (1968)
Granites (27, av.; Finland)	6.9	NA	NORMAN and HASKINS (1968)
Granites (~75)	1—9	S	BORISENKO (1959), BORISENKO and RODIONOV (1961), SAHAMA (1945), AHRENS (1954), TONGEREN (1938)
Granites, low Ca	7	S	TUREKIAN and WEDEPOHL (1961)
Granites, high Ca	14	S	TUREKIAN and WEDEPOHL (1961)
Granitoids, U.S.S.R., av.	2.7	S	VLASOV (1966a)
Rhyolites (24, av.)	5	S	FRYCKLUND and FLEISCHER (1962)
Rhyolites (av., 67% SiO_2)	9.2	NA	NORMAN and HASKINS (1968)
Obsidian	5.7	NA	NORMAN and HASKINS (1968)
Granodiorites (7)	2—8	S	BORISENKO and RODIONOV (1961)
Granodiorite GTM-1	5.6	NA	BRUNFELT and SLEINNES (1966)
Granodiorite	15.5	S	MEL'NICHENKO and MOGAROVSKY (1966)
Trachyte (2)	2.5—6.9	NA	NORMAN and HASKINS (1968)
Trachyandesite	7.7	NA	NORMAN and HASKINS (1968)
Syenites (8, av.)	1	S	BORISENKO and RODIONOV (1961)
Syenites, Lapland	2	S	SAHAMA (1945)
Rhyodacites (32, av.)	14	S	FRYCKLUND and FLEISCHER (1962)
Dacites (68, av.)	21	S	FRYCKLUND and FLEISCHER (1962)
Quartz latites (14, av.)	11	S	FRYCKLUND and FLEISCHER (1962)
Andesites (72, av.)	34	S	FRYCKLUND and FLEISCHER (1962)
Andesite AGV-1	11.5	NA	BRUNFELT and SLEINNES (1966)
Andesites	1—10	S	GOLDSCHMIDT (1934, 1954), VAN TONGEREN (1938)
Intermediate rocks (85, av., <60% SiO_2)	15	NA	NORMAN and HASKINS (1968)
Basalts (99, av.)	38	S	FRYCKLUND and FLEISCHER (1962)
Basalts, continental (282, av.)	30±1	NA	NORMAN and HASKINS (1968)
Tholeiitic basalts, oceanic (8)	35—50	NA	NORMAN and HASKINS (1968)
Basalts	23—92	S	NOCKOLDS and ALLEN (1959), GUNN (1966), PATTERSON and SWAINE (1958), TUREKIAN and WEDEPOHL (1961), ENGEL and ENGEL (1965), Cox and HORNUNG (1966)

[*]) From the Handbook of Geochemistry, ed. Wedepohl (1970)

S C A N D I U M   A B U N D A N C E S

:K TYPE	AVG. PPM	RANGE	# OF SAMPLES
.ER RHYOLITE - BLACK CAT UNIT	31	27 - 34	6
.ER RHYOLITE - POGY UNIT	26	22 - 32	5
)IN GRANITE	25	20 - 33	21
)IN GRANITE - APLITE	34	27 - 41	2
RHYOLITE	29		1
DIORITE	28	22 - 41	5
RACE QUARTZ DIORITE	13	12 - 14	3
: POND GABBRO	47	38 - 52	3
GRANITE	5		1
:TON GRANITE	4		1
'OND GRANITE	3		1
JGTON LAKE PORPHYRY	6		1

Table 8B

determined in the TR-KG rocks (15-42 ppm) strongly imply their genetic relationship and furthermore the special and unique conditions during the magma formation stage--mainly a subordinate role of minerals with high preference for Sc, i.e., mafic silicates.

The group of acidic rocks with high Sc content includes all rocks of the earlier voluminous episode, namely the Katahdin Granite (KG), and the two largest rhyolitic localities of the Piscataquis Volcanic Belt--the Traveler Rhyolite (TR) and the Kineo Rhyolite (KR). Based on the identical stratigraphic position and similar major trace elememt composition of other rhyolites contained in the Piscataquis Volcanic Belt, it is fair to say that the entire Piscataquis belt is part of the TR-KG sequence.

The main geological, petrological and mineralogical features of the TR-KG sequence are summarized below:

TR - Traveler Rhyolite (Fig. 4) is part of a caldera collapse structure which forms a 215 km^2 large, tectonically sunken block of rhyolitic ignimbrites occurring on the northern side of Katahdin Pluton. The emplacement of the volcanics preceded the KG intrusion as evidenced by the contact relationships. The TR consists of two units: the older, extensively hydrothermally altered Pogy Member (TRP), contains 20-25% phenocrysts, of which 60% are plagioclase, 30% quartz, 8% clinopyroxene and biotite, and 2% opaques. The overlying Black Cat Member (TRBC) is less altered and contains a lesser amount of phenocrysts (5 to 15%), of which 75% are plagioclase, 20% clinopyroxene, and 4% opaques.

KG - Katahdin Granite makes up about 95% of the Katahdin Pluton (Fig. 14) which extends over an area of approximately 1330 km^2. This granitic body is mineralogically and chemically homogeneous, consisting of 34% alkali feldspar, 35% quartz, 25% plagioclase, and 6% biotite. Six textural types--also called facies of KG--were identified: the main Doubletop facies (KGD) grades upward via Chimney facies (KGCH) into Summit facies (KGS) and laterally into South Brother facies (KGSB) and Wassataquoik facies (KGW); up to 50 m wide, rare porphyritic dikes of Cathedral facies (KGCT) cross-cut most of the other facies of KG. Thin, up to 1 m wide, aplitic dikes are frequent.

Since major element abundances of both rhyolites and granites of different facies are very similar (Table 4), no differentiation path is therefore indicated. From the AFM plot the only distinct unit is TRBC which is also the least differentiated. TE abundances are in accord with the major element variations, in that among the TR-KG group TRBC has the highest Sc, Co and Eu abundances and the lowest Rb abundance. Using TRBC as the parental magma, the fractionation model for other rhyolites and granites will be discussed in detail.

     b.   <u>Trace Element Evaluation of the Voluminous Magmatic Episode: Traveler Rhyolite-Katahdin Granite</u>

The similar distribution of TE in both TR and KG (Fig. 30) implies not only their cogenetic relationship, but also

their independent origin from the younger HQD-HLP episode
(Fig. 31). In order to demonstrate plausibility of the co-
genetic origin and in order to allow quantitative assessment
of the processes leading to the formation of the TR-KG se-
quence, it became apparent that evaluation of TE abundance
variations in terms of a fractional crystallization model
is necessary.

Table 9 gives average TE abundances of each of the nine
rock units that are to be considered for the fractionation
model, i.e., TRBC, TRP, KGS, KGCH, KGD, KGCT, KGW, AP1, and
AP2. In order to avoid undue propagation of analytical er-
rors and minimize the effect of postmagmatic changes, this
model will only use elements with the largest abundance var-
iations and the least susceptibility to deuteric alteration.
Based on the results of comparative studies of altered and
alteration-free samples (see section on "Postmagmatic
Changes") and on TE variations as given in Table 9, the
selected elements are Co, Rb, Hf, Sr, and Eu.

Using a surface equilibration model, the degree of
fractionation F (weight proportion of residual melt with
respect to the initial parental magma) and mean partition
coefficient (MPC: summation of fractional mineral/liquid
partition coefficients) are related as expressed by Rayleigh
distillation law (model B2 of Albarede, Bottinga, 1972):

(1) $\ln C/C_0 = (MPC-1) \ln F$

C and C_0 refer to trace element abundances in the daughter
and parental magma.

Table 9   180

	TRBC	TRP	KGS	KGD	KGCH	KGCT	KGW	AP-1	AP-2
Sc	31.07	26.18	27.26	26.44	24.74	19.01	26.01	27.30	41.04
Co	2.20	1.90	0.82	1.11	1.01	1.89	0.51	0.26	0.40
Rb	162.90	170.60	187.22	190.51	176.03	208.39	236.23	290.50	377.02
Cs	10.75	7.64	10.87	9.08	11.66	8.83	9.33	8.06	7.16
Hf	14.00	11.04	10.79	9.56	8.90	9.54	6.35	5.75	7.84
Ta	1.83	1.32	1.40	1.51	1.90	1.71	1.60	2.01	4.23
Th	14.41	14.09	16.46	14.20	14.02	16.12	14.72	15.83	19.22
U	5.27	4.64	4.10	3.04	3.41	5.27	5.74	5.84	15.07
Sr	76	64	59	66.4	N.A.	N.A.	26	N.A.	8
La	171.56	159.90	144.00	148.36	131.78	119.28	143.47	84.94	46.52
Ce	139.14	144.93	120.77	120.71	110.50	100.05	140.18	91.72	33.47
Nd	96.32	98.37	81.73	79.12	72.91	68.29	87.31	59.03	27.31
Sm	75.69	76.24	56.94	58.80	57.04	47.40	68.38	54.38	28.10
Eu	27.60	25.62	17.28	17.66	18.09	17.86	9.90	2.47	1.17
Gd	54.00	57.94	45.91	44.90	40.66	35.03	43.54	57.34	21.65
Ho	40.00	40.11	30.58	31.80	34.47	27.52	39.99	45.82	29.89
Yb	37.44	35.98	27.85	30.28	29.51	26.43	35.05	41.60	42.54
Lu	34.92	34.75	25.68	29.26	28.53	24.99	34.30	39.76	42.42
Number of Samples	6	5	3	8	2	3	1	1	1

Average Elemental Abundances in TR-KG Sequence

In the course of model calculations, the mean partition coefficient of each element is let to be a constant during the fractionation of the entire sequence. This corollary is substantiated by the fact that the major element composition of the melt, the crystallization temperature, as well as the relative proportion of minerals crystallizing from the magma, remain virtually unchanged during the crystallization process (see previous chapter).

However, the Rayleigh equations cannot be solved for F and MPC's simultaneously. The model calculation, therefore, requires two steps: in the _first_ step, an apparent solution satisfying the set of equations described below is obtained. For this purpose, the Rayleigh equation can be rewritten as follows:

(2)   ln C/Co = ((MPC-1)/Q)*(Q*ln F)

The constant Q relates relative (or apparent) and actual sets of values:

(3)   RMPC = ((MPC-1)/Q)+1

(4)   RF   = RF = F ** Q

In the _second_ step, the constant Q is evaluated through comparison of RMPC's and MPC's, which are estimated from published values of PC's (Table 12).

For the five selected elements (Co, Rb, Hf, Sr and Eu) and nine members of the fractionation sequence (TRBC, TRP, KGCH, KGD, KGCT, KGW, AP1 and AP2) there are thirty-seven

equations which interrelate twelve unknown parameters
(5 MPC's and 8 F's). This set of thirty-seven equations
is solved by an iterative numerical method by subsequent
approximations with assumed initial values of RMPC's equal
2 for all five elements.

From the solution which usually converges in three
iterations, the newly calculated daughter abundances are
compared with the actual (observed) TE abundances. If there
is more than a 20% difference between any calculated and
observed value, the data point with the largest deviation
is rejected and the computation cycle is repeated until all
the data points satisfy the 20% allowed deviation. A flow
chart showing how the final solution was obtained is shown
on Fig. 34.

The final solution, including the eight rejected data
points, are graphically illustrated in Figs. 35A, B, and C.
The initial unrestricted (no data points rejected), as well
as the final solutions are given in Table 10. The fast
convergence of the above methods indirectly proves the
validity of the initial corollary (constant MPC's). Other
solutions satisfying the initial set of thirty-seven equa-
tions can be obtained from equation (3). Table 11 lists
several such sets for different assumed values of Q which
are so chosen that they would yield apparent MPC's for Rb
as given at the top of Table 11.

Fig. 34.   Flowchart for the Iterative Method Used in Calcu-
           lating Mean Partition Coefficients And Degrees of
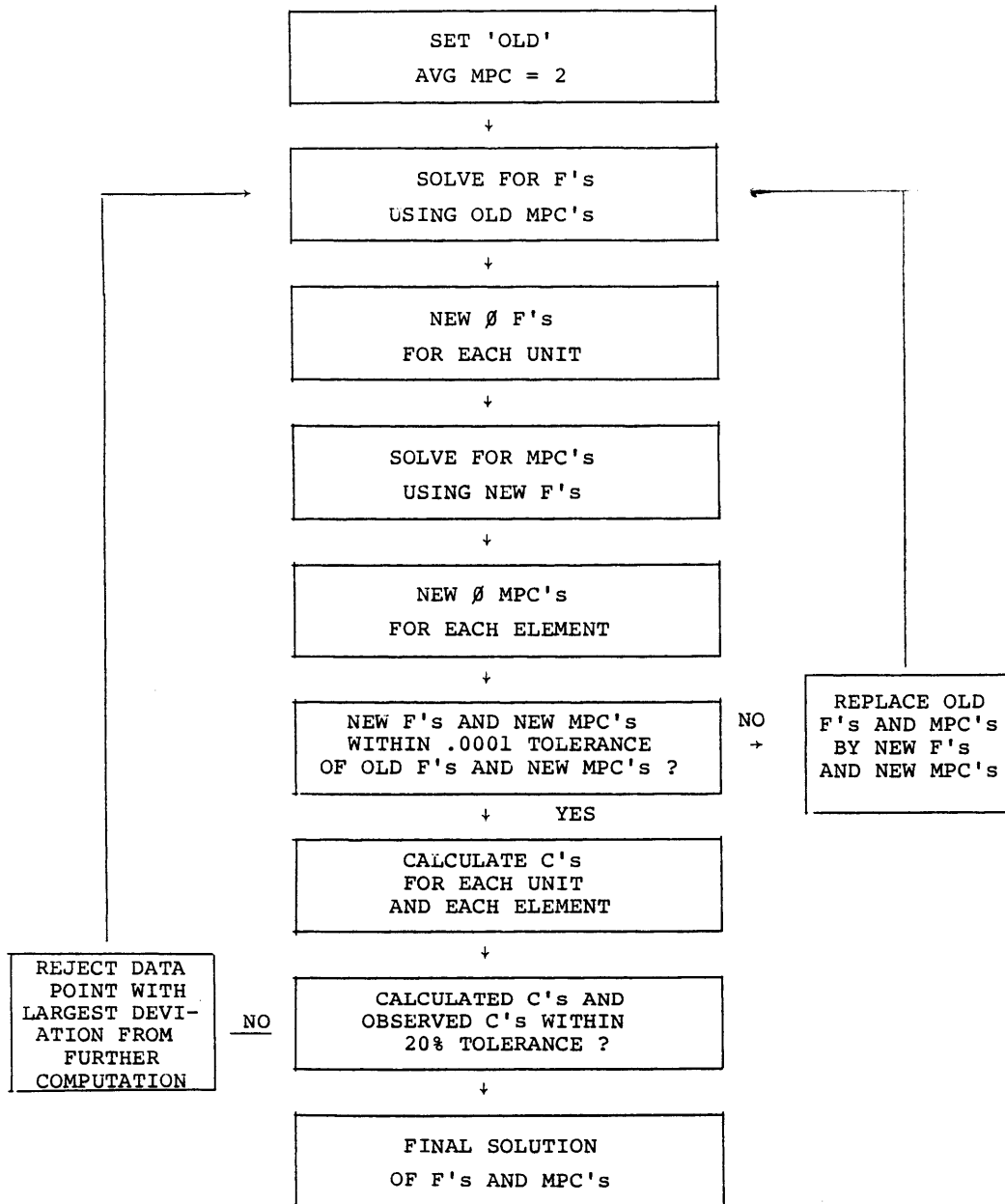   Fractionation. See Text For Further Explanation.

```
                    ┌─────────────────────────┐
                    │      SET 'OLD'          │
                    │     AVG MPC = 2         │
                    └─────────────────────────┘
                                 ↓
                    ┌─────────────────────────┐
        ──────────→ │     SOLVE FOR F's       │ ←──────────┐
                    │    USING OLD MPC's      │            │
                    └─────────────────────────┘            │
                                 ↓                         │
                    ┌─────────────────────────┐            │
                    │       NEW Ø F's         │            │
                    │     FOR EACH UNIT       │            │
                    └─────────────────────────┘            │
                                 ↓                         │
                    ┌─────────────────────────┐            │
                    │     SOLVE FOR MPC's     │            │
                    │     USING NEW F's       │            │
                    └─────────────────────────┘            │
                                 ↓                         │
                    ┌─────────────────────────┐            │
                    │      NEW Ø MPC's        │            │
                    │    FOR EACH ELEMENT     │            │
                    └─────────────────────────┘            │
                                 ↓                ┌───────────────────┐
                    ┌─────────────────────────┐   │  REPLACE OLD      │
                    │ NEW F's AND NEW MPC's   │NO │  F's AND MPC's    │
                    │ WITHIN .0001 TOLERANCE  │→  │   BY NEW F's      │
                    │ OF OLD F's AND NEW MPC's?│   │  AND NEW MPC's    │
                    └─────────────────────────┘   └───────────────────┘
                                 ↓   YES
                    ┌─────────────────────────┐
                    │     CALCULATE C's       │
                    │     FOR EACH UNIT       │
                    │    AND EACH ELEMENT     │
                    └─────────────────────────┘
  ┌──────────────┐               ↓
  │ REJECT DATA  │    ┌─────────────────────────┐
  │ POINT WITH   │    │   CALCULATED C's AND    │
  │ LARGEST DEVI-│ NO │   OBSERVED C's WITHIN   │
  │ ATION FROM   │────│      20% TOLERANCE ?    │
  │ FURTHER      │    └─────────────────────────┘
  │ COMPUTATION  │               ↓
  └──────────────┘    ┌─────────────────────────┐
                      │     FINAL SOLUTION      │
                      │    OF F's AND MPC's     │
                      └─────────────────────────┘
```

FIGURE 34

Table 10

Calculated Mean Partition Coefficients

	Co	Rb	Hf	Sr	Eu
Initial	2.905	0.480	2.183	2.187	1.566
Final	3.182	0.489	2.424	2.079	2.410

Calculated Wt. Fraction of Residual Liquid

	TRP	KGS	KGD	KGCH	KGCT	KGW	AP-1	AP-2
Initial	0.894	0.739	0.757	0.739	0.750	0.477	0.323	0.251
Final	0.899	0.775	0.766	0.754	0.703	0.512	0.348	0.155

Calculated apparent mean partition coefficients and apparent fractions of residual liquid for Traveler Rhyolite-Katahdin Granite fractionation sequence.

Fig. 35A,B,C.   Final Solution of Iterative Calculations For
                Traveler Rhyolite – Katahdin Granite Magmatic
                Sequence. Excluded Data Points Are Encircled.
                See Text And Table 34 For Further Explanation
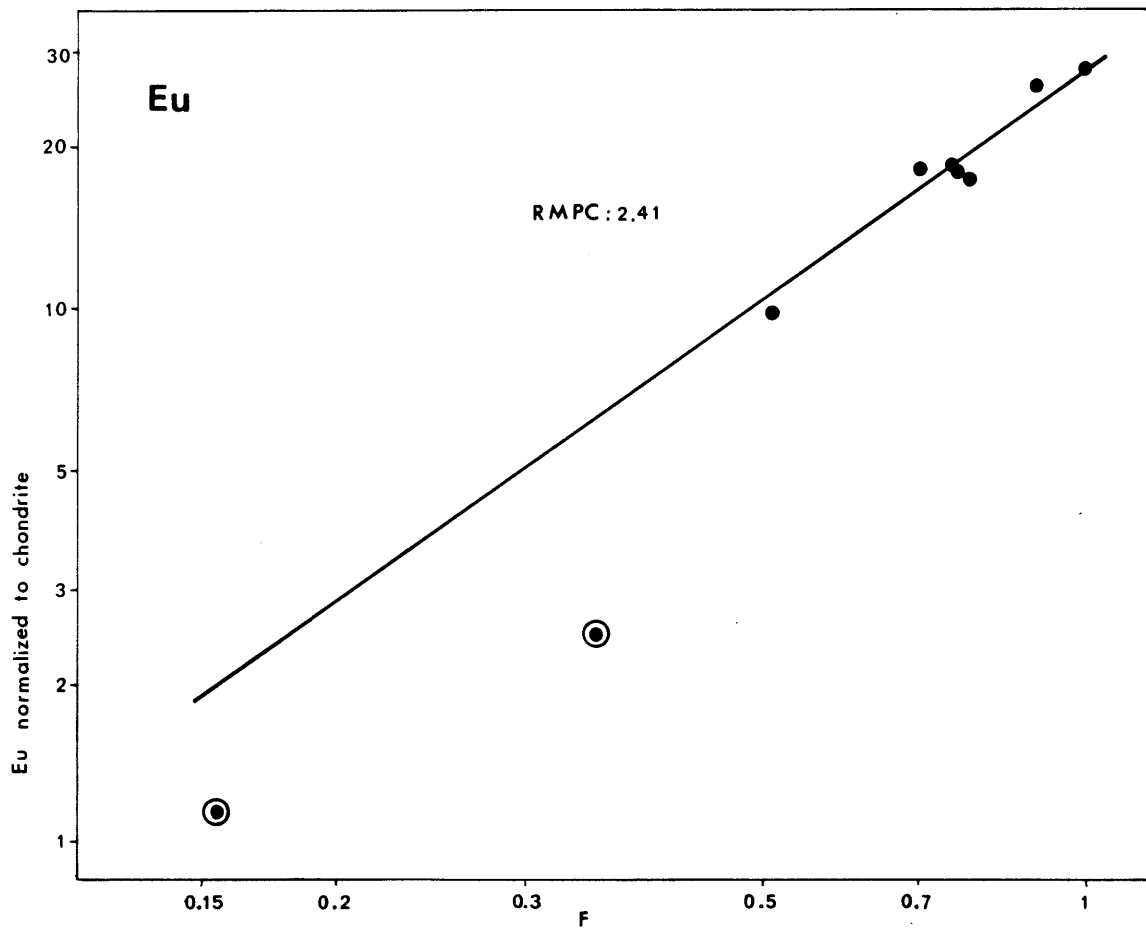   And Discussion.

187

(A)
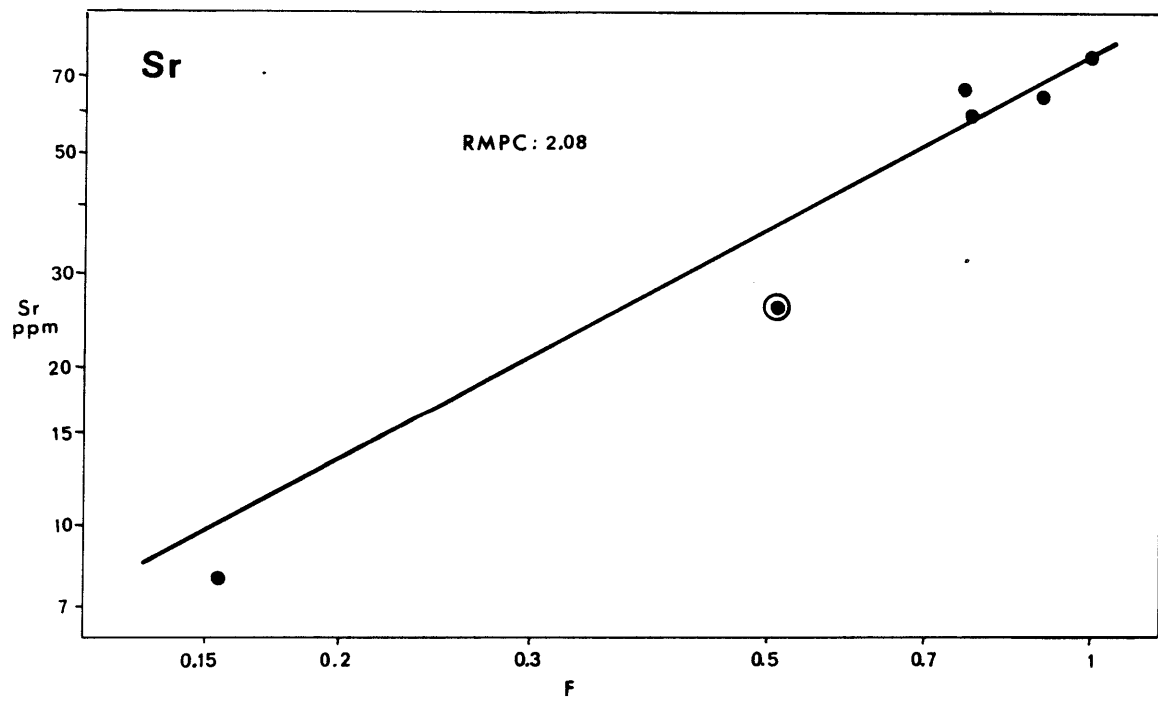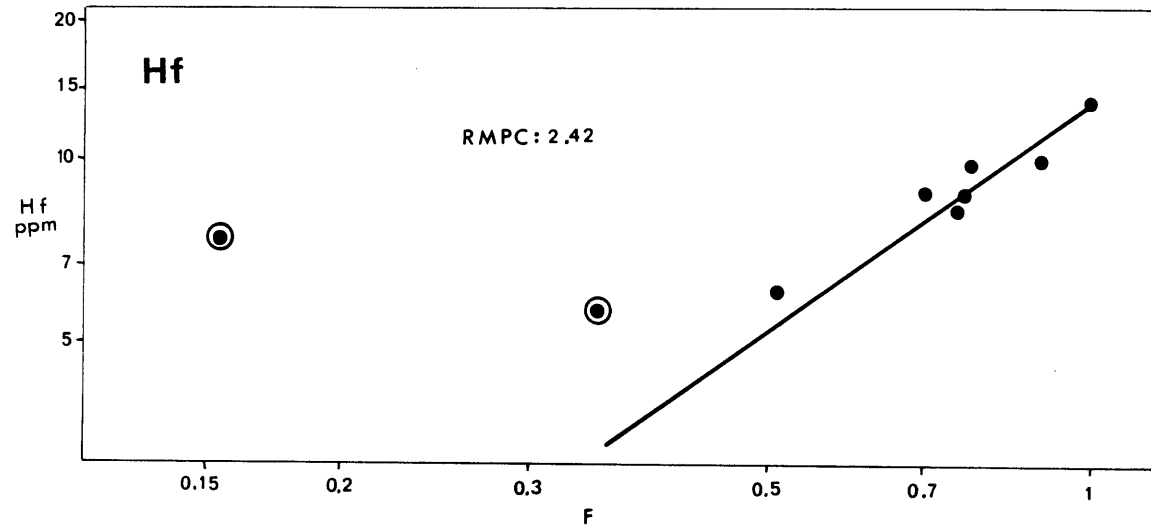
(B)
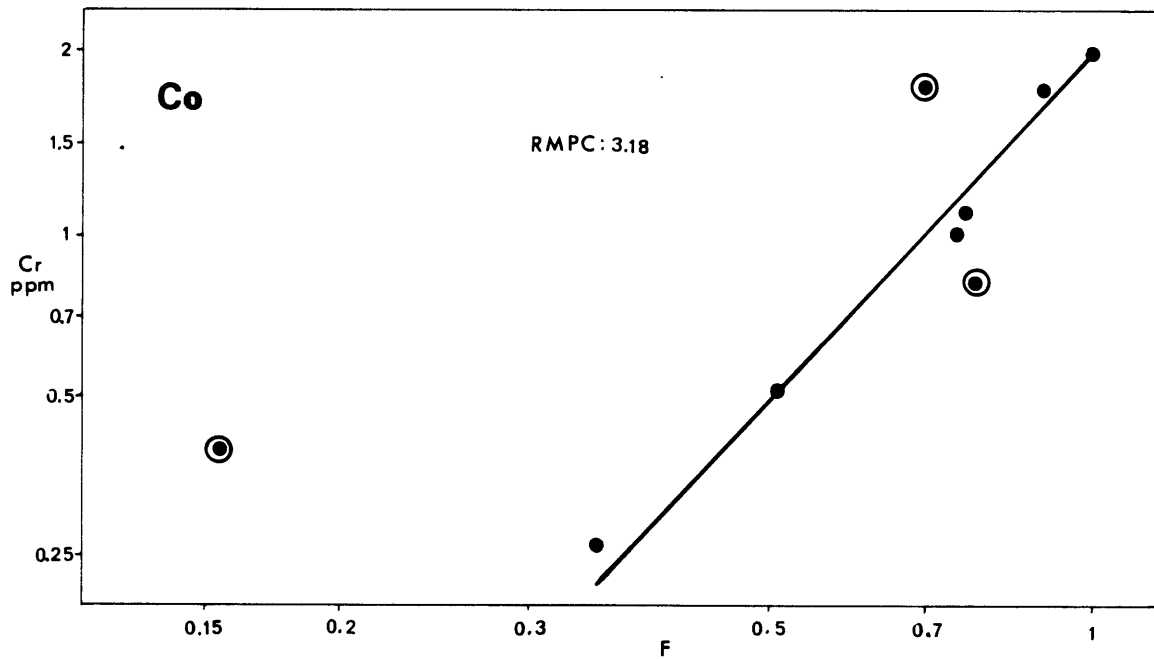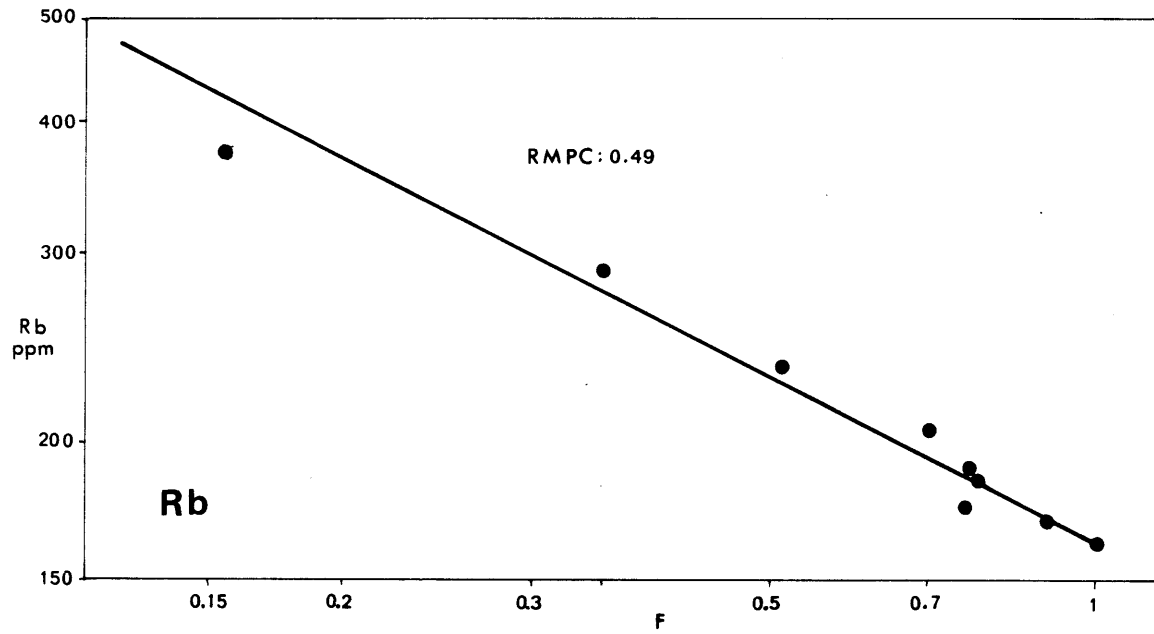
(C)

Table 11

Rb	0.000	0.100	0.200	0.300	0.400	0.500	0.600	0.700	0.800	0.900	0.49*
Sr	3.118	2.906	2.694	2.482	2.271	2.059	1.847	1.635	1.424	1.212	2.08
Co	5.275	4.847	4.420	3.992	3.565	3.137	2.710	2.282	1.855	1.428	3.18
Hf	3.784	3.506	3.227	2.949	2.671	2.392	2.114	1.835	1.557	1.278	2.42
Eu	3.765	3.488	3.212	2.935	2.659	2.382	2.106	1.829	1.553	1.276	2.41

* The last column gives solutions from Table 10.

Calculated apparent MPC's of Sr,
Co, Hf, and Eu corresponding to
different assumed apparent MPC (Rb).
(See text for further explanation).

During the second step, the actual MPC's for Rb, Sr, and Co are estimated for an average KGD assemblage (Table 12). Combining the results of Tables 11 and 12, the best set of MPC's is MPC(Rb) = 0.500 (Table 11); from this, the constant Q of equations (3) and (4) is equal to 0.98 or approx. to 1. The value of Q being equal approx. 1 is only coincidental and is the result of the "lucky" choice of 2 as the initial (seed) values of RMPC's. Therefore, the solutions obtained in Table 19 represent the best MPC's and F's.

The abundances of the TR-KG sequence support a model of fractionation from the TRBC-type parental magma in the following succession: TRBC-TRP-(KGS, KGD, KGCH)-KGCT-AP1-AP2. The TE abundances also indicate that KGS-KGD-KGCH crystallized from the same magma. Figures 36 and 37 show variations of REE and Sc, Cs, Ta, Th, and U as a function of the proportion of the residual liquid. For the discussion of these variations, see the section "Comparison of Aplites".

c. Kineo Rhyolite

Among other rhyolitic occurrences within the Piscataquis Volcanic Belt, Sample #247 of the Kineo volcanic center (Rankin, 1968) was studied as a comparison to the TR (Fig. 3, and Fig. 38). The TE data and REE chondrite normalized distribution of this Kineo sample are given in Table 7 and Fig. 39. The Kineo REE pattern is essentially identical with the pattern of KGD except for a significant depletion in HREE. If KGD is assumed as the parental magma, the only common

Table 12

Estimated MPC's of Rb, Sr, Co for TR-KG
Sequence

Mineral Proportions	PC(Rb)			PC(Sr)			PC(Co)	
wt %	low	high	pref.*	low	high	pref.*	low	high
Bi	8	2.2	4.4	3.1	0.1	1.0	0.2	12	30
Pl	25	0.1	0.2	0.15	5.0	7.0	7.0	0.05	0.50
Af	35	0.3	0.7	0.5	2.0	5.0	3.8	0.05	0.50
Mt	1	0.0	0.0	0.0	0.0	0.0	0.0	10	50
MPC		0.306	0.647	0.461	1.958	3.580	3.096	1.090	3.200

* Preferred Values

Sources:

	Rb	Sr	Co
Bi	1, 8, 13	1, 12, 13	8, 12
Pl	1, 4, 6, 8, 11, 13	1, 3, 4, 5, 6, 7, 8, 11, 13	4
Af	1, 2	1, 3	**)
Mt	*)	*)	7, 9, 10

1. Philpotts, Schnetzler, 1970
2. Noble, Hedge, 1970
3. Nagasawa, 1971
4. Dudas et al., 1971
5. Korringa, Noble, 1971
6. Ewart, Taylor, 1968
7. Ewart et al., 1973

8. Higuchi, Nagasawa, 1969
9. Duncan, Taylor, 1968
10. Paster et al., 1974
11. Nagasawa, Schnetzler, 1971
12. De Albuquerque, 1974, and Ewart, Taylor, 1968
13. Lyakhovich, 1972

*) PC assumed to be zero
**) PC assumed to be equal to PC of plagioclase

Fig. 36.   Chondrite-Normalized Abundances And Their Variation
          For Selected Rare Earth Elements in The Traveler
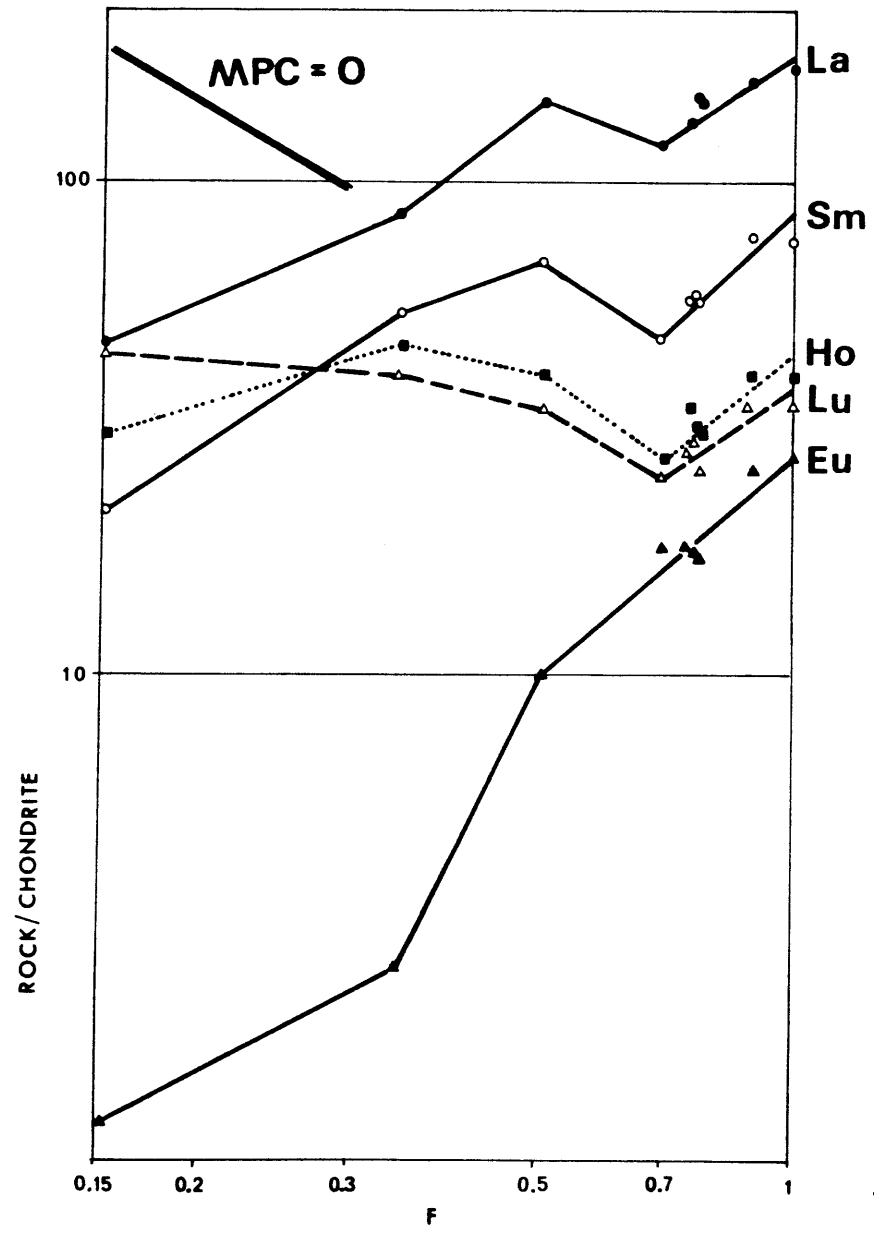   Rhyolite – Katahdin Granite Magmatic Sequence.

Fig. 37. Variation of Abundances of Th, Ta, Sc, U, and Cs
in The Traveler Rhyolite - Katahdin Granite
Magmatic Sequence.
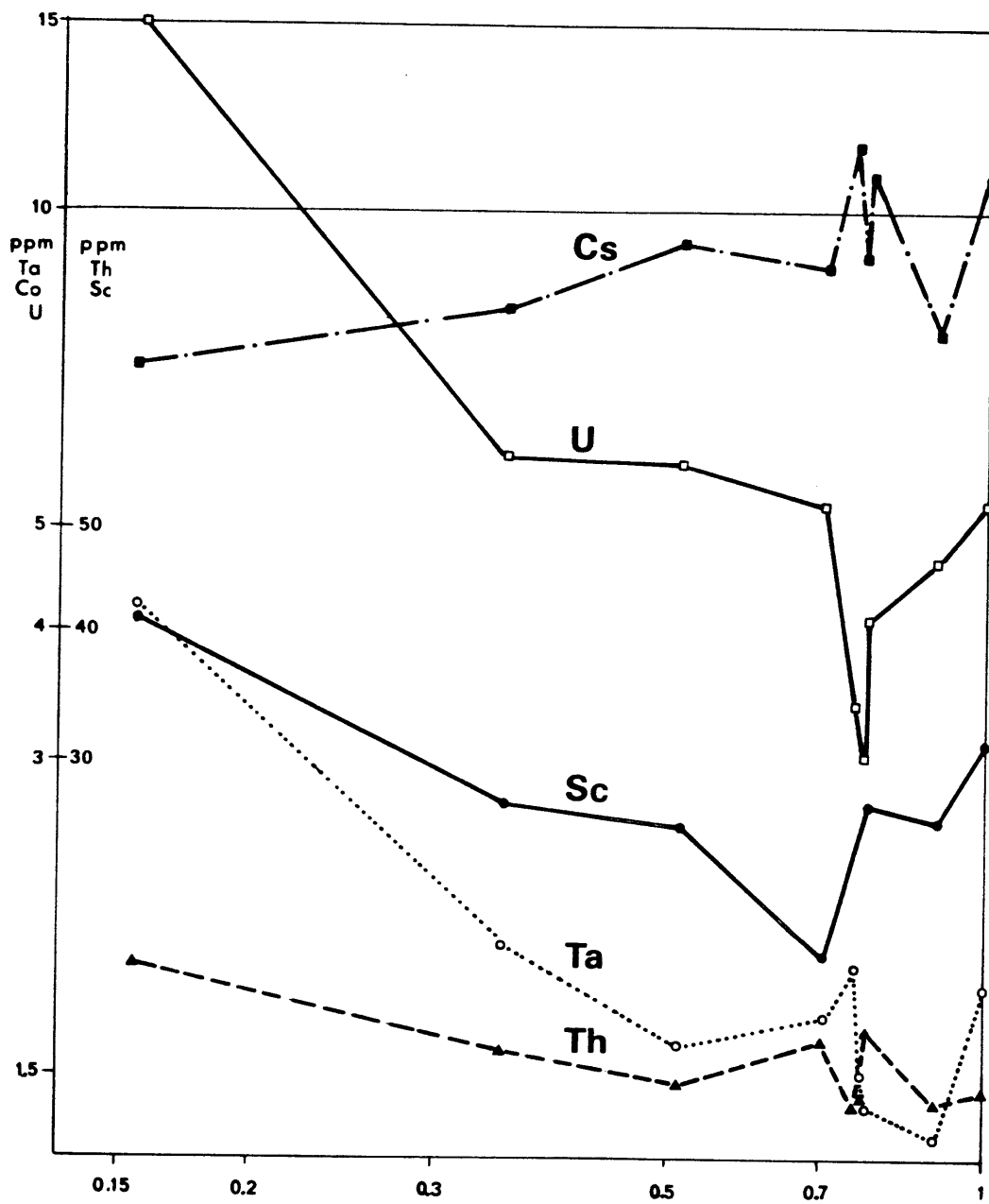
Fig. 38. Inferred Volcanic Centers in The Piscataquis
          Volcanic Belt (Fig. 27-1. of Rankin,1968).
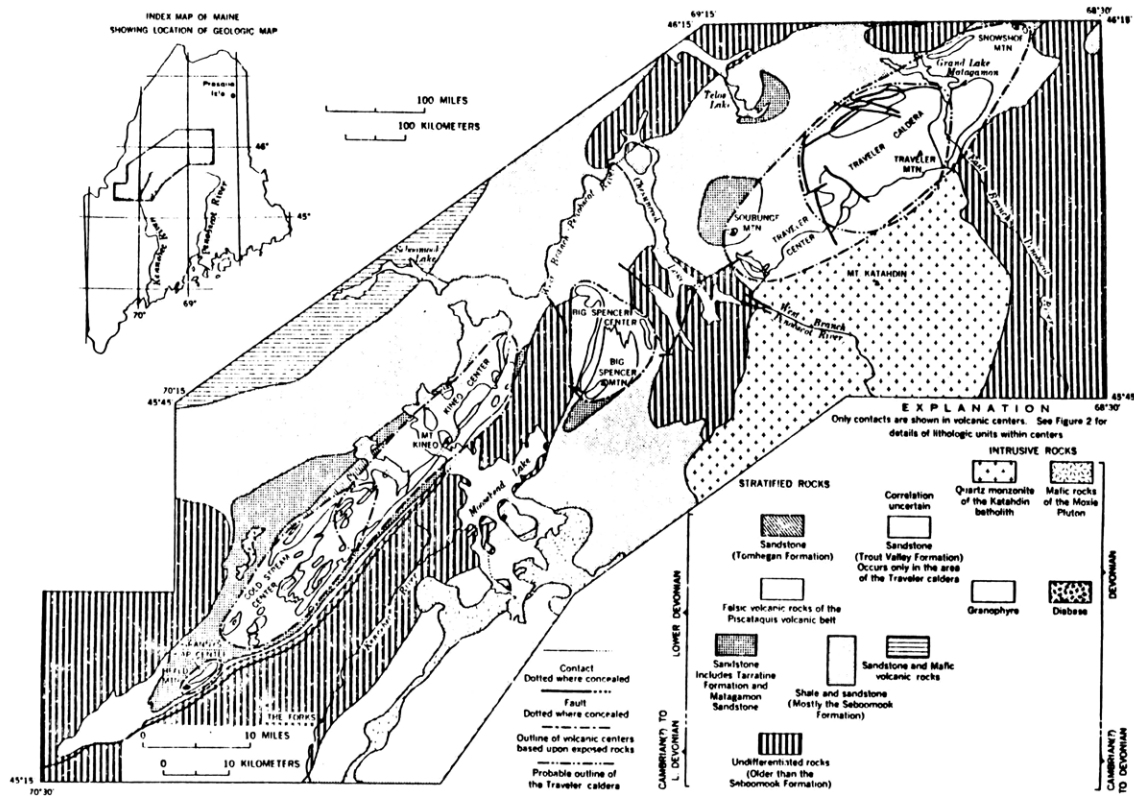
FIGURE 27-1. Generalized geologic map showing volcanic centers and geologic setting of the Piscataquis volcanic belt. Modified from Boucot (1961; written communication, 1966), Boucot and others (1964a), Doyle (1967), and Rankin (unpublished data).

(from Rankin, 1968)

Fig. 39. Chondrite-Normalized Rare Earth Element Abundances
          in Kineo Rhyolite.

          Legend: ∅TR – Average Abundances in Traveler
                          Rhyolite
                   KGD – Average of Katahdin Granite: Double-
                          top Facies
                   KR   – Kineo Rhyolite
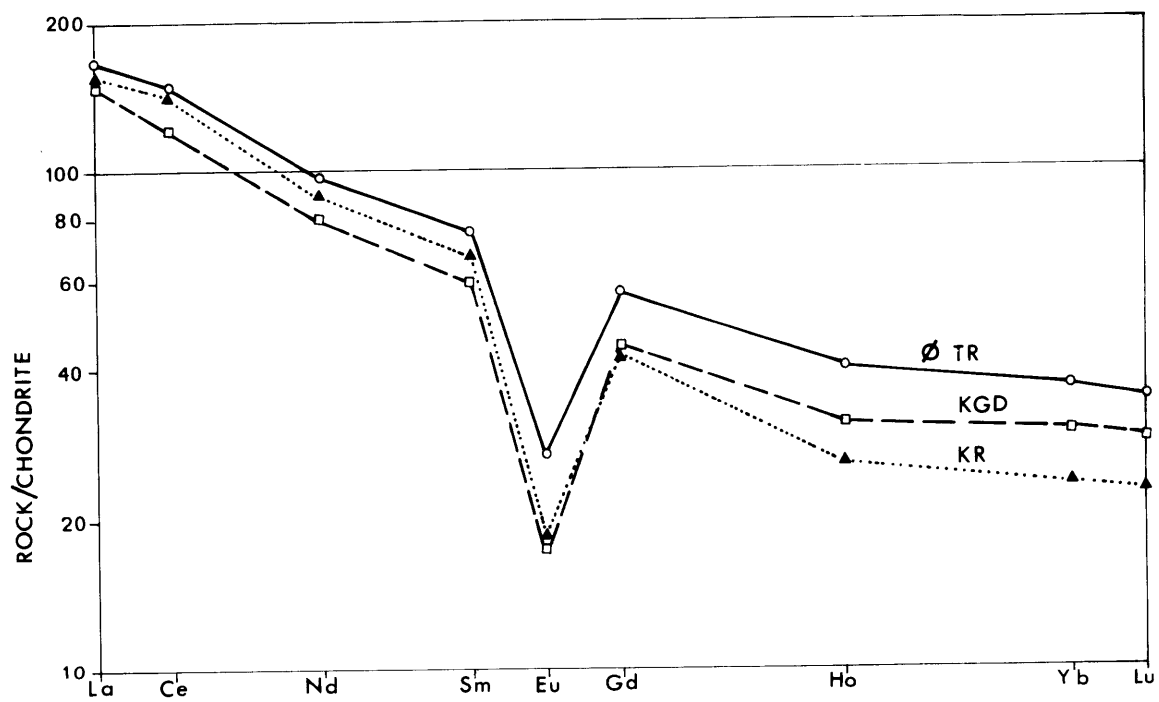
mineral which can cause such a depletion is garnet. Using

Rayleigh distribution law, it appears that a removal of 0.7%

garnet will reproduce the Kineo rhyolitic HREE abundances

(PC(Lu) = 30; PC(Yb) = 40; PC)Ho) = 35; Schnetzler, Philpotts,

1970). However, garnet does not occur in the Kineo center

but it is abundant in the nearby Cold Stream center and in

the Big Spencer center (Fig. 38; Rankin, 1968). Consequent-

ly, garnet may have been a fractionating mineral crystalliz-

ing in place of biotite. As both garnet and biotite have

strong preference for Sc, no change in Sc abundances is

observed.

Other TE's are not inconsistent with the proposed

derivation of Kineo Rhyolite from KGD magma. Although they

are within the limits of twice the TRBC variation coeffi-

cients (Fig. 25A), they show a considerable scatter. Rb

abundances--the best indicators of fractionation (see pre-

ceding section)--are also in favor of this model. The

average Rb abundances of TRBC and KGD (163 ppm and 191 ppm,

resp.) compare poorly with 146 ppm of Sample #247 but agree

well with the average value of 181 ppm obtained for Kineo

Rhyolite by Fullagar and Bottino, 1968.

Due to the large variation coefficients of some TE's

(Figs. 25A and B) and taking into account that only one

sample was analyzed, a detailed evaluation of Kineo Rhyolite

petrogenesis cannot, therefore, be formulated. Further geo-

chemical and petrological studies of other rhyolitic occur-

rences and mineral separates, namely that of garnet, are needed.

2. Intermediate Scandium Rocks: HQD-HLP Sequence

a. General Statement

Rock units of intermediate Sc abundances (5 to 15 ppm) are found only as minor igneous bodies emplaced near the West Branch Penobscot River fault system (Fig. 14). The close association of these bodies with the fault suggests tectonically controlled intrusions. This younger igneous episode consists of the Harrington Lake Porphyry (HLP), the Horserace Quartz Diorite (HQD), and the Debsconeag Grano-diorite (DGD) (Fig. 14). The main geological, petrological and mineralogical features of these bodies are summarized below:

HLP - Harrington Lake Porphyry: The semi-arcuate, sill-like intrusion of HLP (3.8 km^2) lies outside the main body of the Katahdin Pluton (KP) Although a direct contact with Katahdin Granite (KG) is presumed, the contact relationship remains unknown. The only geological link between HLP and other members of the younger episode is provided by rare in-clusions of hornblende quartz diorite found in HLP. These inclusions are believed to be identical with marginal facies of HQD. If this correlation is correct, HLP represents a younger phase of the HQD-HLP sequence. Mineralogically, the unit is composed of extremely altered, fine grained matrix with abundant plagioclase and subordinate hornblende pheno-crysts.

HQD-Horserace Quartz Diorite: HQD forms a small,
elongated stock (5.7 km^2) which is entirely enclosed within
the Doubletop facies of KG. This intrusion is accompanied by
a prominent, apophysical dike swarm, traceable on each side
of the stock for a distance of at least 10 to 15 km along
the West Branch Penobscot River fault system. The HQD body
is compositionally zoned, with gradational change from bio-
tite-bearing hornblende quartz diorite near the margins to
hornblende-bearing biotite granodiorite in the center.

DGD-Debsconeag Granodiorite: DGD is a medium grained,
hornblende-bearing biotite granodiorite which occurs in two
separate bodies within the Doubletop facies of KG (Griscom -
personal communication). Near the vicinity of the suspected
margins, the grain size of DGD tends to be finer and the
content of biotite increases to 15%.

The major element variation within the younger episode
implies the following fractionation sequence: HQD-HLP-DGD
(Fig. 23A, B, C). This differentiation sequence will be
further examined on the basis of trace element geochemistry.
Five samples from the younger episode were analyzed for trace
elements: two samples are from the marginal facies of HQD
(#235 and 238), one each from HLP (#4) and DGD (#166), and
one from the dike swarm (#127A). Their trace element
abundances are given in Table 7 and their chondrite normal-
ized REE distributions are plotted in Fig. 31.

b. Trace Element Evaluation of the Younger Magmatic
    Episode

On the basis of the most "primitive" TE and ME abundances (lowest Fe/Mg ratio, highest Cr and Co abundances), Sample #127A is considered to represent a parental magma from which the younger igneous episode might have evolved.

Although the TE abundances of the HQD marginal zone are similar to the assumed parental magma, they cannot be explained in terms of a simple fractionation model; for example, abundances of Co and Cr favor direct fractionation of HQD-margin from Sample #127A by the removal of mafic minerals, but the lower Rb and higher Sc abundances do not support this model. This seemingly contradictory behavior can best be reconciled if a partial cumulative nature of the marginal zone is assumed. Provided that Sample #127A represents the composition of the original magma and that the magma did not change during the crystallization of the settling crystals, the fraction of cumulus can be estimated from the following mass balance equation:

$$(HQD - margin) = (1-x)(127A) + (x)(MPC)(127A)$$

$$x = \text{fraction of cumulus}$$

The mean partition coefficients for Lu and Rb, calculated for a Cpx, Hb, Pl assemblage from PC's of Dudas et al., 1971; Philpotts, Schnetzler, 1970; Schnetzler, Philpotts, 1970; and Nagasawa, Schnetzler, 1971, are both equal to 0.2: PC(La-Cpx) PC(La-Hb) PC(La-Pl) 0.2; PC(Rb-Cpx) 0.02;

PC(Rb-Hb) 1.3; PC(Rb-Pl) = 0.05-0.15; e.g., MPC(Rb) = 0.02;
if plagioclase is dominant. The estimated fraction of
cumulus is 0.28 and 0.29, respectively. Based on the
average value (0.28), Table 13 lists calculated mean parti-
tions coefficients for other trace elements. This table
also shows literature values of PC for Cpx, Hb, Pl and zircon.
The calculated MPC's can be reconstituted from 95% Pl, 5%
Hb, and 0.4% zircon, or from 70% Pl, 30% Cpx and 0.4% zircon.
The actual mineral proportion is probably somewhere between
these two estimates, as both, Cpx and Hb, were identified in
HQD-margin rocks (Cpx forms frequent cores of Hb grains).
The observed differences of Cr, Cs, and U cannot be re-
conciled by this model. Cr was probably removed by opaques
and Cs and U were apparently lost during the late crystal-
lization stages if the model is to be valid. However, the
above model for the derivation of HQD is consistent with
petrological (Fig. 24) and field observations.

The REE distribution pattern of HLP compared with the
presumed parental magma is similar, but the absolute REE
abundances are approximately 30% lower. Since this deple-
tion indicates mainly a removal of accessory minerals (or
amphibole), REE can provide only qualitative evidence of
the genetic relationship of HLP-HQD. Also depleted in HLP
with respect to HQD are Cr, Cs, Co and Sr, which were pos-
sibly removed by mafic silicates, opaques and feldspars.
The depletion in Rb is most likely due to the extensive
hydrothermal alteration.

Table 13

Derivation of HQD-Margin from Sample #127A

	Parent #127A	HQD Margin $\emptyset$	Calcul- ated MPC's*	PC(Pl)**	PC(Cpx)**	PC(Hb)**	PC(Zr)**
Sc	12.23	13.98	1.51	--	6.2-17.0	2.7-260	--
Cr	167.66	108.51	(-0.26)	--	0.8-9.7	0.5-70	--
Co	20.08	17.09	0.47	--	2.3-8.0	3.9-12	--
Rb	76.18	58.42	0.17	0.06-0.46	0.03	0.4	--
Cs	2.92	1.19	(-1.12)	--	--	--	--
Hf	4.29	4.22	0.94	--	--	--	?
Ta	0.67	0.53	0.25	--	--	--	--
Th	7.97	6.21	0.21	--	--	--	?
U	2.26	1.45	(-0.28)	--	--	--	?
La	104.94	81.32	0.20	0.28-0.49	0.07-0.33	0.13-0.41	4
Nd	45.56	38.06	0.41	0.14-0.29	0.94-1.3	1.0-4.5	4
Eu	17.16	17.74	1.12	0.75-4.20	1.1-2.0	1.4-5.9	4
Gd	17.18	16.13	0.78	0.11-0.24	2.1-1.4	2.0-10.9	10
Ho	7.13	7.31	1.09	0.10-0.17	2.4-1.14	2.4-13.5	100
Lu	4.86	6.66	2.32	0.06-0.11	1.8-1.3	1.8-6.3	500

REE in chondrite normalized values, others in ppm.

* MPC's are calculated for 73% parent (#127A) and 27% cumulus
  (See text for explanation).

** PC for plagioclase are after Dudas et al., 1971.
   PC for Hb and Cpx: non-REE are for dacites after Ewart et al., 1972;
   Ewart, Taylor, 1968; and Philpotts, Schnetzler, 1970
   REE are for dacite after Schnetzler, Philpotts, 1970;
   and Nagasawa, Schnetzler, 1971.

Using the rate of REE depletion obtained from the fractionation of KG from TR, the REE abundances of HLP can be explained in terms of fractionation from HQD by the removal of 35 to 40% crystals. Sc, Cr and Co abundances also imply that HLP can be derived from Sample #127A by removing approximately 30 to 40% crystalline material. The calculated MPC's required by this model are: 2.5 (Sc), 3.37 (Co), 6.88 (Cr), and 2.10 (Sr). These MPC's can be reconstituted from 15 to 20% of mafic silicates, 80% plagioclase, and 3 to 4% opaques (compare with Table 13). The mineralogical composition of fractionating crystals is similar to the HQD marginal zone.

TE abundances in DGD differ considerably from TE abundances in either HLP or HQD. The REE are characterized by enrichment in HRE (4.5), LRE (1.7), and by a large negative Eu anomaly (Fig. 31). Also, in DGD the abundance of Rb is significantly higher (1.8 times) and Co and Sr are lower. The abundances of REE, Sc, Co and Rb preclude a fractionation model from the TR magma. The simplest model for the origin of the DGD magma is the mixing of HLP and TR-type magmas with subsequent surface equilibrium fractionation of Cpx and Pl. The model for the derivation of DGD magma is illustrated in Table 14. The first step of the proposed model is mixing 40% TRBC and 60% HLP designated as DGD-1. DGD-2 is derived from DGD-1 by removal of 28% crystals consisting of 80% Pl and 20% Cpx (typical TRBC assemblage). For most elements, the calculated (DGD-2) and observed

Table 14

Derivation of DGD from HLP

	DGD Observed	DGD-1 Calculated	CPX* PC	PL* PC	DGD-2 Calculated
Sc	12.02	15.84	10	--	11.40
Co	3.95	4.45	6	--	4.16
Rb	135.84	106.44	--	0.17	141.37
Cs	7.62	5.64	--	0.11	7.61
Hf	6.77	7.95	--	0.15	10.61
Ta	1.27	0.95	--	0.20	1.25
Th	20.07	10.10	--	0.05	13.84
U	3.32	2.65	--	0.20	3.49
Sr	186	354	0.50	3.50	190
La	174.33	104.76	0.2	0.3	132.71
Nd	66.74	55.22	1.0	0.2	68.14
Eu	14.86	16.67	1.7	1.3	14.71
Gd	34.43	28.04	2.0	0.1	33.26
Ho	24.08	19.52	1.8	0.1	23.46
Lu	22.18	16.61	1.5	0.09	20.42

For References See Table 13.

* Preferred Average Values.

abundances are in close agreement and therefore support the validity of the proposed model.

However, the discrepancies for Hf and Th remain unexplained. The poor agreement between calculated and observed values for La and Ce may be interpreted as an accidental concentration of accessory allanite (see end of "Postmagmatic Changes", subchapter).

c. Summary of the HLP-HQD Sequence

TE abundances support the hypothesis of cogenetic relationships of intrusive bodies of the younger igneous episode. The dike swarm represents the parental magma from which the HQD may have been derived. The marginal facies of HQD is formed by a combination of 73% parental magma and 27% cumulat crystals. HLP appears to be a product of the differentiation of HQD magma by fractional removal of 40% crystalline material. The model for the origin of DGD magma proposed mixing 40% TRBC and 60% HLP magmas with the subsequent removal of approximately 30% crystals. This model is consistent with the hypothesis that HQD-type magmatism--possibly of upper mantle origin--supplied the necessary heat to allow melting of sedimentary rocks and thereby generating TRBC.

During its rise to the Earth's surface, the HQD magma differentiated and in some regions the differentiated melt mixed with TRBC melt. The geological position of DGD in the center of Katahdin Pluton as well as its ME chemistry and

mineralogy conform with the proposed model.   HLP was probably extruded as the last magmatic event.

3.   Comparison of Aplites

TE abundances of aplitic samples of both HQD-HLP and TR-KG sequences, respectively, are derived from highly differentiated magmas. With respect to the parental KGD magma, Sample #145 (AP1) represents 20% residual melt and Sample KM-7 (AP2) approximately 45% of the same parental magma. The average of aplitic samples #134-3, 134-6, 134-7, and 134-8 (AP3) represents approximately 20% of the DGD parental magma.   If our fractionation estimates are correct, we may expect a reasonable agreement (within factor 2) between their mean partition coefficients.

Using observed TE abundances in aplites and in their assumed parental magmas and the above estimates of degree of fractionation, the mean partition coefficients are calculated from the Rayleigh distribution law:

$$MPC = (\ln C/C_o)/\ln F) + 1$$

The calculated mean partition coefficients (MPC's) presented in Table 15 and Fig. 40 are remarkably similar and provide additional support in favor of the employed models.

Discussion:

REE - Light REE are removed at a higher rate than heavy REE which tend to be enriched in the residual melts. Lyakhovich and Balanova (1971) have shown that REE are preferentially

Table 15

Calculated MPC's for Katahdin Pluton Aplites

	AP-1 from KGD	AP-2 from KGD	AP-2 from TRBC	AP-3 from DGD	TR-KG Sequence from Table 10	Baker**
	F=0.454	F=0.202	F=0.155	F=0.200		
Sc	0.96	0.73	0.85	0.97	0.91*	1.74
Co	2.84	0.64	1.91	3.12	3.18	2.30
Rb	0.47	0.57	0.55	0.52	0.49	0.40
Cs	1.15	0.85	1.21	0.72	--	--
Hf	1.64	1.12	1.31	1.18	2.42	0.52
Ta	0.64	0.36	0.55	0.76	0.57*	0.40
Th	0.86	0.81	0.85	0.72	0.89*	0.40
U	0.17	0.00	0.44	0.51	--	--
Sr	N.A.	2.32	2.21	2.22	2.08	--
La	1.71	1.73	1.70	2.02	--	--
Ce	1.35	1.80	1.76	1.84	--	--
Nd	1.37	1.67	1.68	1.55	--	--
Sm	1.10	1.46	1.53	1.08	--	--
Eu	3.49	2.70	2.70	2.15	2.41	0.86
Gd	0.69	1.46	1.49	0.98	--	--
Ho	0.54	1.04	1.16	0.33	--	--
Yb	0.60	0.79	0.93	0.40	--	--
Lu	0.61	0.77	0.90	0.40	--	--

* Average Values

** Personal Communication; Data Obtained for West African Rift Benmoreites

212

Fig. 40. Calculated Rare Earth Element Mean Partition
          Coefficients For AP1, AP2, and AP3.
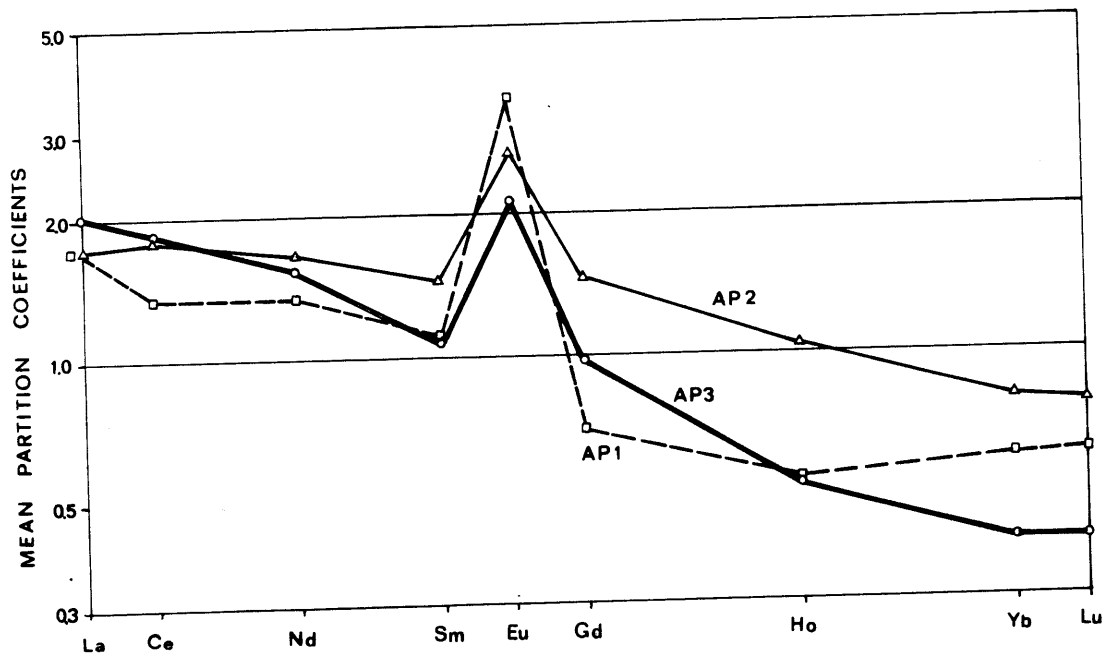
concentrated in accessory minerals: LREE in allanite and
monazite; the intermediate REE (Sm, Gd) in apatite and sphene;
and HREE in zircon and xenotime. The striking difference
between the mean partition coefficients of LREE and the
value of MPC of Lu being considerably less than 1 needs
further explanation. Xenotime is a rare mineral and its
role in controlling HREE is most likely minimal, because of
the preference of phophorous for apatite and the higher
level of HREE concentration needed for xenotime saturation.
The second possibility is that zircon crystallization is
suppressed because of Zr loss with the exsolving vapor phase.
The alternative explanation that the activity of Zr in the
melt is somehow lowered is regarded as unlikely. This
inferred possible Zr loss is further supported by observed
abundances of Hf; Hf abundances in the TR-KG sequence first
decrease logarithmically with fractionation and, as frac-
tionation reaches more than 40-50%, the trend reverses
indicating no further removal of zircons (Fig. 35B). HREE
follow a similar trend (Fig. 36). Because pegmatites are
more frequently associated with DGD, another source of in-
formation consistent with the proposed Zr vapor phase removal
is obtained from the lower values of calculated mean parti-
tion coefficients for HREE and Hf in DGD aplites due to
the higher loss of Zr in DGD.

The mean partition coefficient for Eu is dependent upon
oxygen fugacity; therefore, the reducing KGD magma has a
higher MPC (Eu) than the more oxidizing DGD magma (see

Fig. 41.   Abundances of Rare Earth Elements in Aplites Norma-
           lized to Their Respective Granitic Parents. Data on
           Susamyr Batholith Are From Balashov (1963). Data on
           Eagle Peak Pluton And Red Lake Pluton (Both of
           Sierra Nevada Batholith) Are From Noyes (1976).

217
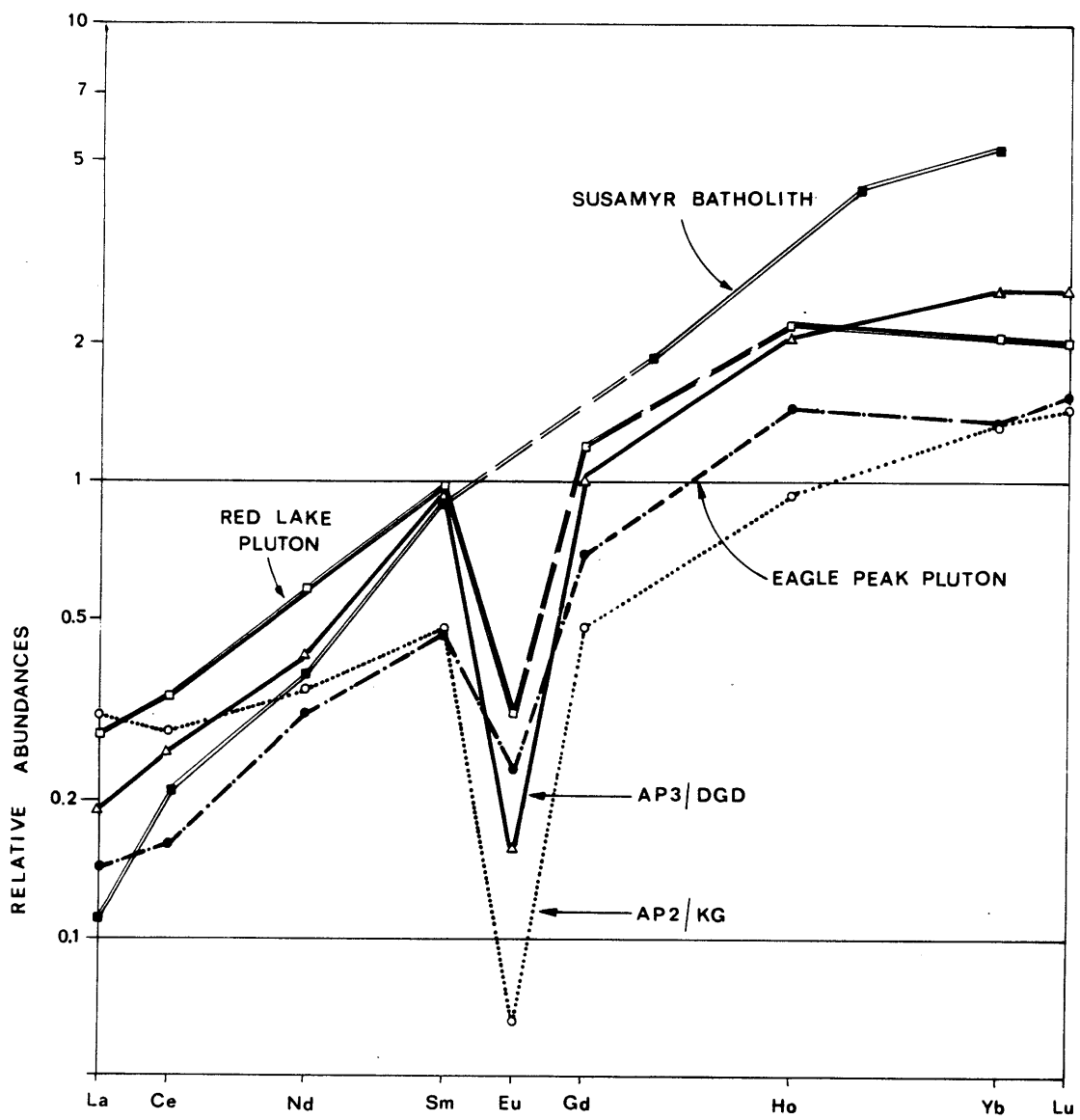
estimates of $f(O_2)$ in earlier chapters). Fig. 41 shows a relative distribution of REE in aplites normalized to their presumed parental rocks of different magmatic environments. This figure shows that the proposed model for REE during progressive differentiation is generally applicable. The tendency of HREE enrichment in late stage magmas is also supported by the comparison of sphene, monazite and apatite from both granites and granitic pegmatites (Fleischer, Altschuler, 1969).

Sc: The calculated mean partition coefficient of Sc, nearly equal to 1, is a consequence of the constant rate of 8 wt.% of biotite with PC equal to 10-15.

Co: The variable, estimated mean partition coefficient of DGD and KGD reflects a different oxidizing environment controlling the crystallization of magnetites. A higher removal rate is therefore observed for the more oxidizing DGD sequence.

Rb: The similar mean partition coefficients of all aplites, caused by constant fractional removal of alkali feldspar, plagioclase and biotite: 35% AF (PC=0.8); 25% PL (PC=0.2); and 8% Bi (PC=3).

Cs: The relative mobility of Cs during alteration is thought to be responsible for the large variations.

Hf: Removed by zircon during the early fractionation stages; in the late stages, Hf is concentrated in the melt.

Ta: Ta is always enriched in the residual magmas; perhaps slightly fractionating into vapor phase or lost via deuteric alteration.

Th: This is a good indicator of fractional crystal-lization with a constant mean partition coefficient equal to 0.8.

U: Uranium in aplites tends to be enriched in residual magmas.   The mean partition coefficient is always less than 0.5.

Sr: The constant rate of removal of Sr is a consequence of the constant fractional removal of feldspars: 35% of alkali feldspar (PC=3 to 4) and 25% plagioclase (PC=4 to 6) with a mean PC of 2.05 to 2.90.

In conclusion, the comparison of aplites shows that the mean partition coefficient may be employed as a useful indicator of fractionation for late-stage differentiation processes of granitic melts.

4.   Low Sc Acidic Rocks (<5 ppm Sc)

This group consists of granites from the Lexington Pluton, the Moxie Pluton, and the Echo Pond Pluton (Vermont) (see Fig. 3).   Their TE abundances are given in Table 7 and Fig. 32.

All three granitic bodies were analyzed in order to determine the areal extent of the TR-KG igneous complex. The low Sc abundances in the granites of this group (3-5 ppm),

as well as the dissimilar abundances of REE, Co, Rb, Hf,
Ta and Th (see Figs. 30, 32; Table 7), indicate distinct
differences between the TR-KG igneous complex and the other
Lower Devonian acidic plutonic rocks. Since these differ-
ences cannot be easily reconciled in terms of any simple
fractionation sequence, it is assumed that the TR-KG
igneous complex does not extend beyond the limits of the
Katahdin Pluton and the Piscataquis Volcanic Belt.

   5. Basic Rocks

   The close association of acidic and gabbroic bodies
in the Greenville Plutonic Belt (Fig. 2) may possibly
suggest that the granitic melts were derived by differen-
tiation from a parental basic magma. In order to evaluate
this possibility, gabbroic samples from Pierce Pond Pluton
were analyzed as representative gabbroic rocks of the pluton-
ic belt. The analytical data are given in Table 7 and their
chondrite normalized patterns are plotted on Fig. 33.

   For a detailed description of the geology, petrology
and mineralogy of the Pierce Pond Pluton, see P. Lyttle,
1975 . The TE abundances imply an adcumulitic origin of
Sample #PP-1 and the orthocumulitic nature of Samples #PP-
235 and PP-379. The TE abundances of the latter samples are
similar to the oceanic island tholeites or to the high alum-
ina basalts of active orogenic belts (Schilling, 1973; Lopez,
1974), which may indicate that the Greenville Plutonic Belt
was formed near a plate margin. Until further work is done,

however, this conclusion must be regarded as tentative.

The possible derivation of granitic melts from the gabbroic magma can be demonstrated only for the granite of Moxie Pluton. Here, the similar REE distribution, except for a strong Eu anomaly, in Samples #244 (Moxie Granite) and PP-235 (Pierce Pond Gabbro) suggests the possibility of a cogenetic relationship. From the observed abundances of Rb, Ta, Th and U in granite of the Moxie Pluton, the degree of fractionation needed for the granite can be calculated by assuming that these elements are totally concentrated in the residual melt. The calculated degree of fractionation, expressed in terms of the removal of crystals, is: Rb-96%, Ta-86%, Th-97%, and U-94%, which is consistent with the strong Eu anomaly (removal of plagio-clases) as well as with the depletion of Co, Cr and Sc (re-moval of mafic silicates). Such a large gabbro/granite volume ratio is supported by field observation (Espenshade, 1969). The large volume of the TR-KG igneous complex, as well as its distinct TE abundances, makes a derivation of the TR-KG sequence from a parental gabbroic magma unlikely.

F. Origin of TR-KG

The petrologic evidence outlined in the previous chapters suggests that the TR-KG complex was formed by the partial melting (approximately 20%) of sedimentary rocks at a depth of 25-30 km. Since the low regional metamorphic grade (a chlorite zone) precludes exposure of the parental rocks,

the REE content of the parental rocks may, instead, be
deduced from data obtained by Cullers et al. (1974) for
meta-sedimentary Silurian strata of the Rangeley and
Perry Mountain Formations. According to Moench (1974),
the Rangeley formation represents massive, graded conglom-
erates, sandstones and shales, whereas the overlying Perry
Mtn. formation consists of reworked shales and siltstones.
Provided that most of the geosynclinal sediments in north-
western and northcentral Maine were originated from a
lithologically similar source (Naylor-personal communication),
the sedimentary rocks parental to the TR-KG sequence may
have similar REE abundances.

Fig. 42 shows REE patterns of the average REE contents
of the Rangeley and Perry Mt. Formations (Cullers et al.,
1974) as well as the 1:1 mixture of these two averages and
the average Black Cat unit of the Traveler Rhyolite.

Based on a general resemblance of REE patterns, it is
conceivable that TRBC magma could have been derived by a
partial melting of sediments. In order to illustrate this
possibility further, in the table below, calculated mean
partition coefficients are given for individual REE's on
the assumption that TRBC represents a 20% melt formed in
equilibrium with a residue derived from either the Rangeley
Formation or the 1:1 mixture of the Rangeley and Perry Mt.
Formations. These mean partition coefficients were obtained
from the equation:

Fig. 42. Average Abundances of Rare Earth Elements in Range-
          ley, Perry Mountain And 1:1 Mixture of Rangeley And
          Perry Mountain Formations. Data From Cullers and
          Others, 1974.
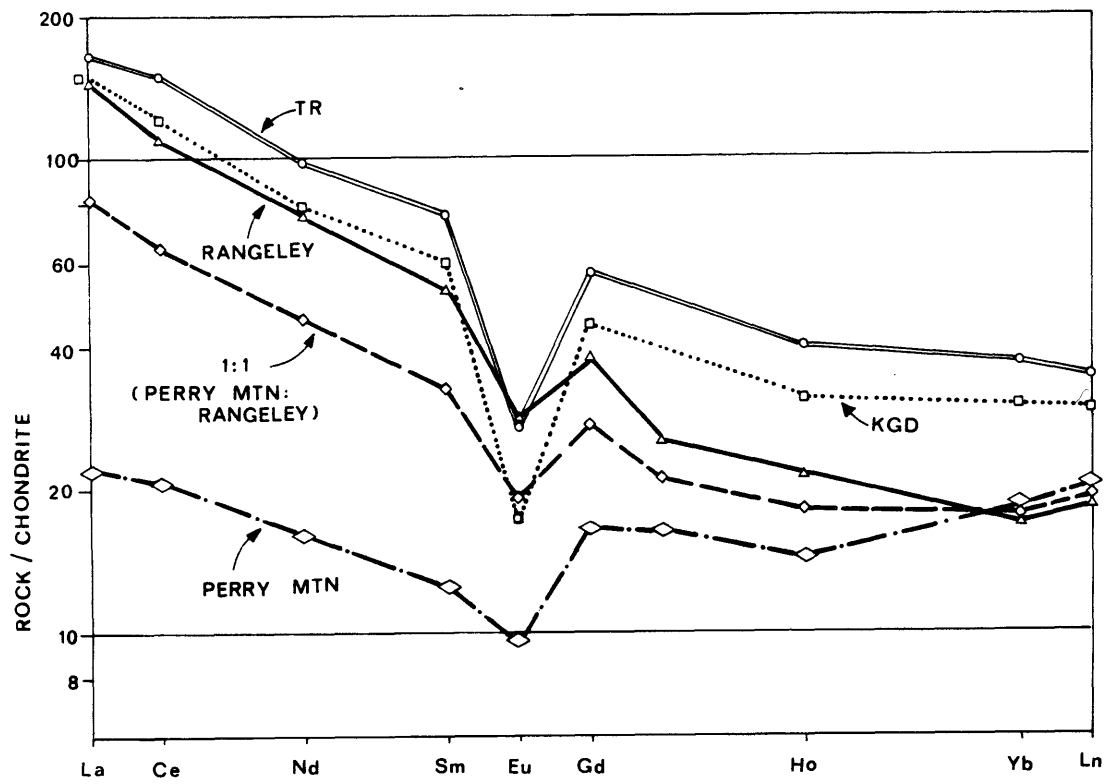
$$MPC = 1.25 \text{ x (Sediment} - 20\% \text{ TRBC}) / \text{ TRBC}$$

<u>Mean Partition Coefficients for TRBC and Its Residue</u>
<u>for Two Different Parent Sources</u>

	<u>Rangeley</u>	1:1 (Rangeley/Perry Mt.)
La	.79	.35
Ce	.74	.34
Sm	.62	.29
Eu	1.04	.62
Gd	.64	.39
Ho	.43	.32
Yb	.32	.34
Lu	.43	.45

The validity of either model requires that the calculated mean partition coefficients can be reconstituted from the known partition coefficients of minerals which may be present in the residue. From experimental studies of Winkler (1957), Winkler and v. Platten (1958, 1959, 1960), such a residue in equilibrium with the anatectic melt is likely to contain plagioclase, alkali feldspar, quartz, biotite, sillimanite or kyanite, cordierite, opaques and undisclosed amounts of accessory minerals (monazite, apatite or zircon, etc.). From published data by Dudas et al., 1971; Nagasawa and Schnetzler, 1971; Higuchi and Nagasawa, 1969, the REE partition coefficients of plagioclase (except for Eu), alkali feldspar and biotite, have nearly uniform values (0.1-0.3). REE content in quartz, kyanite and opaques is essentially negligible and can, for all purposes, be ignored.

Assuming that octahedrally coordinated Mg or Fe
have similar preference for REE, the REE partition co-
efficients of cordierite can then be estimated from REE
partition coefficients of orthopyroxene. Since OPX has
50% octahedral sites and cordierite only 18%, we may
expect that REE partition coefficients of cordierite have
a similar relative distribution but with absolute values
approximately 2.75 times lower than PC's of orthopyroxene,
e.g., PC(La) 0.05, PC(Sm) 0.09, PC(Dy) 0.15, PC(Lu) 0.33
(Nagasawa and Schnetzler, 1971).

Taking into account the uncertainty due to the
relative content of the residual minerals (typically quartz
30%, plagioclase 35%, alkali feldspar 10%, biotite 10%,
cordierite 15%), then, the MPC's calculated above for 1:1
(Rangeley/Perry Mt.) represent values well within the
range of feasibility and, consequently, provide a convincing
qualitative evidence for the genetic relationship of TRBC
magma and the geosynclinal sediments of northcentral Maine.

V. SUMMARY

The geological setting, major and trace element geo-
chemistry, as well as the intensive parameters deduced from
the coexisting mineral assemblages, show that the Traveler
Rhyolite-Katahdin Pluton igneous complex consists of two
penecontemporaneous but genetically independent igneous
episodes. The earlier voluminous episode includes thick
ignimbrite deposits of Traveler Rhyolite and six textural
facies of Katahdin Granite. The younger sequence con-
sists of several minor bodies of Horserace Quartz Diorite,
Harrington Lake Porphyry and Debsconeag Granodiorite.

The unusually high Sc abundances (15-42 ppm) of both
members of the earlier magmatic episode demonstrate their
close genetic relationship and contrast sharply with the
lower Sc content (5-15 ppm) of the younger series. Model-
ing of Co, Rb, Hf, Sr and Eu abundances provides a strong
evidence that the Katahdin Granite is derived from the
Traveler Rhyolite magma by a fractional removal of 25% of
alkali feldspar (35 wt.%), plagioclase (25 wt.%), quartz
(31 wt.%), biotite (8 wt.%), and magnetite (1 wt.%), with
the following estimated mean (bulk) partition coefficients:
3.18, 2.42, 2.08 and 2.41, respectively. The estimated
temperature, water pressure and logarithm of oxygen
fugacity for Traveler Rhyolite ($800^{\circ}C$, 1100 bars and 15.00)
and for Katahdin Granite ($710^{\circ}C$, 1200 bars and 17.25) are

consistent with the model, that the Katahdin Granite represents a solidifed magma chamber underneath the Traveler volcano. Both oxygen fugacity estimates lie slightly below the QFM buffer curve which is in agreement with relative values of Eu and Sr mean partition coefficients.

The magma source of the earlier episode is best explained by a partial fusion of Appalachian eugeosynclinal sediments, a model which is consistent with several lines of evidence as discussed below:

1. A conspicuous absence of mafic or intermediate rocks associated with the earlier episode, as well as homogeneous major element composition and relatively constant petrology throughout the Traveler Rhyolite and Katahdin Granite, imply a steady state melting process as the only possible mechanism to generate such large quantities of acidic magma.

2. Based on major element geochemistry, it is deduced that at the time of its formation the Traveler Rhyolite magma was under 8 Kb total pressure (depth of 25-30 km), 4 Kb water pressure, a temperature of $810^{\circ}C$, and in equilibrium with two feldspars and quartz.

3. Oxygen fugacity of the magma was maintained through equilibrium with graphite which is common in Appalachian eugeosynclinal sediments.

4. High Sc abundances imply special conditions during
the formation of the Traveler Rhyolite magma, namely the
subordinate role of minerals with high preference for Sc,
such as mafic silicates. The range of Sc abundances in
the Traveler Rhyolite and Katahdin Granite is typical of
basalts and basaltic andesites, but not of granites.

5. The REE abundances of the Traveler Rhyolite magma
are consistent with the postulated anatectic origin of the
TR magma from the Appalachian eugeosynclinal sediments.

6. The strontium isotope initial ratio of 0.7100
(Fullagar, Bottino, 1968) is also consistent with the
partial fusion of preexisting sediments.

The petrology, mineralogy and crystallization path
of the younger magmatic episode, i.e., HQD, HLP and DGD,
is much more varied even though it underlies only approxim-
ately 5% of the Katahdin Pluton. In contrast with the
earlier TR-KG magmatic episode, the evolution of the
younger sequence was controlled by an oxidizing environment.
Trace element abundances show that both, the Horserace
Quartz Diorite and the Harrington Lake Porphyry, are
genetically unrelated to the earlier episode, and that the
Debsconeag Granodiorite is best explained by mixing of
40% Traveler magma and 60% Harrington Lake Porphyry.
The presented data do not provide sufficient constraint
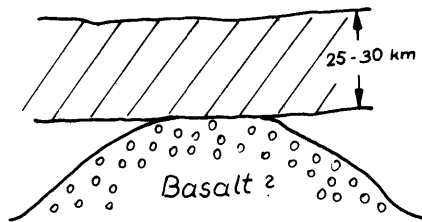about the origin of the magma of the younger episode.

However, the major and trace element abundances are consistent with calc-alkaline associations of continental margins. If this inference is correct, then the younger episode may represent magma derived from a subducting oceanic crust.

In conclusion, Fig. 34 illustrates schematically the possible time sequence for the origin of the Traveler Rhyolite-Katahdin Pluton igneous complex. Mafic magma of mantle origin (possibly derived along a subducting plate) raises the temperature near the base of the crust causing its partial fusion. The resulting melt of rhyolitic composition is then pushed up into shallow levels within the crust. From there it is rapidly moved to the surface through violent ash flow eruptions. The residual melt fractionates and, on crystallization, forms the Katahdin Granite which is in turn intruded by smaller intrusions of quartz diorite (HQD) and granodiorite (DGD).
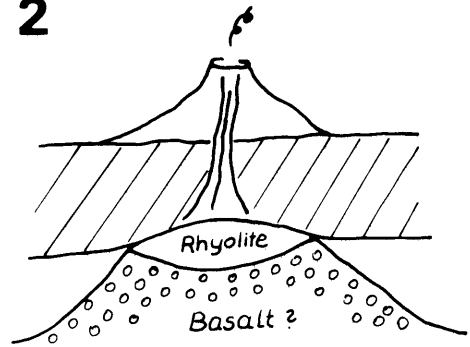
Fig. 43. Schematic Illustration of The Evolution of The Tra-
veler Rhyolite - Katahdin Pluton Igneous Complex.

             Legend: TR   - Traveler Rhyolite
                      TRBC- Traveler Rhyolite: Black Cat Member
                      TRP - Traveler Rhyolite: Pogy Member
                      KG   - Katahdin Granite
                      KGD - Katahdin Granite: Doubletop Facies
                      KGS - Katahdin Granite: Summit Facies
                      HQD - Horserace Quartz Diorite
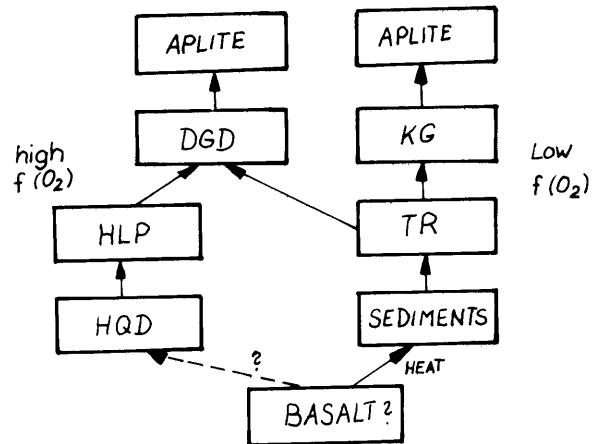   HLP - Harrington Lake Porphyry
                      DGD - Debsconeag Granodiorite

1

25 - 30 km

Basalt ?

2

Rhyolite

Basalt ?

3

TR

KG

Basalt ?

4

HQD

HLP

DGD

KG

Basalt ?
Gabbro

5

KGS

TRBC

KGD

TRP

HLP

HQD

DGD

APLITE

APLITE

high f(O_2)

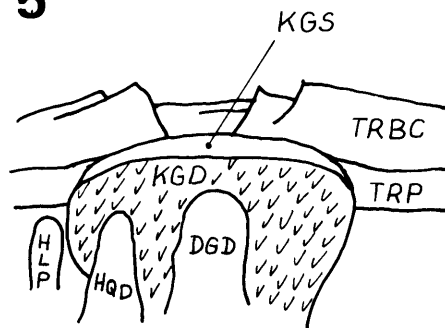DGD

KG

Low f(O_2)

HLP

TR

HQD

SEDIMENTS

?

HEAT

BASALT ?
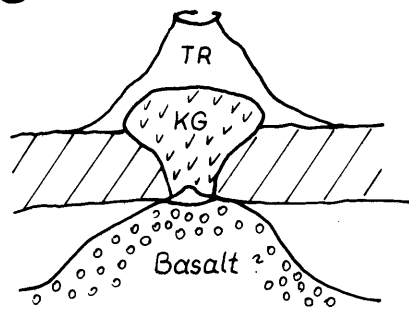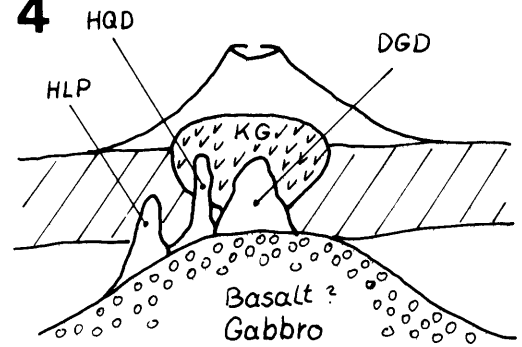
Albarede, F., Bottinga, Y., 1972, Kinetic disequilibrium in trace element partitioning between phenocrysts and host lava: GCA, v. 36, p. 141.

DeAlbuquerque, C.A.R., 1974, Geochemistry of actinolitic hornblendes from tonalitic rocks, Northern Portugal: GCA, v. 38, p. 789.

Allingham, J.W., 1960, Use of aeromagnetic data to determine geologic structure in Northern Maine: USGS Prof. Paper 400-B, p. B117.

Althaus, E., Karotbe, E., Nitsch, K.H., Winkler, H.G.F., 1970, An experimental re-examination of the upper stability of muscovite plus quartz: N. Jb. Min. Mon., v. 7, p. 325.

Anderson, A.T., 1968, Oxidation of the LaBlache Lake titanoferrous magnetite deposit, Quebec: J. Geol., v. 76, p. 528.

Andrews, H.N., Kasper, A.E., 1970, Plant Fossils of the Trout Valley formation: Bulletin No. 23 of Maine Geological Survey, p.3.

Anfilogov, V.N., Glyuk, D.S., Trufanova, 1973, Phase relations in interaction between granite and sodium fluoride at water vapor pressure of 1000 kg/cm^2: Geochemistry International, v. 10, p. 30.

Balashov, Yu. A., 1963, Regularities in the distribution of the rare earths in the earth's crust: Geochemistry, No. 2, p. 107.

Blaxland, A., 1974, Geochemistry and geochronology of chemical weathering, Butler Hill granite, Missouri: GCA, v. 38, p. 843.

Boucot, A.J., 1969, Geology of the Moose River and Roach River synclinoria, Northwestern Maine: Bulletin No. 21 of Maine Geological Survey.

Boucot, A.J., Griscom, A., Allingham, J.W., 1964, Geologic and aeromagnetic map of Northern Maine: Map GP-312.

Brown, G.C., 1970, A comment on the role of water in the partial fusion of crystal rocks: EPSL, v. 9, p. 355.

Brown, G.C., Fyfe, W.S., 1970, The production of granitic melts during ultrametamorphism: Contr. Min. Petr., v. 28, p. 310.

Buddington, A.F., Lindsley, D.H., 1964, Iron-titanium oxide minerals and synthetic equivalents: J. Petrology, v. 5, p. 310.

Burnham, C.W., 1967, Hydrothermal fluids at the magmatic stage: in Geochemistry of hydrothermal ore deposits, edit. H.L. Barnes, p. 34.

Burnham, C.W., Holloway, J.R., Davis, N.F., 1969, Thermodynamic properties of water to 1000°C and 10000 bars: GSA, Spec. Papers 132.

Burnham, C.W., Jahns, R.H., 1962, A method for determining the solubility of water in silicate melts: AJS, v. 260, p. 721.

Caldwell, D.W., 1966, Pleistocene geology of Mt. Katahdin: in New England Intercollegiate Geological Conference Guidebook, ed. Caldwell, p. 51.

Cann, J.R., 1970, Upward movement of granitic magma: Geol. Mag., v. 107, p. 335.

Carmichael, I.S.E., 1960, The pyroxenes and olivines from some tertiary acid glasses, J. Petr., v. 1, p. 309.

Carmichael, I.S.E., 1967, The iron-titanium oxides of salic volcanic rocks and their associated ferromagnesian silicates: Contr. Min. Petr., v. 14, p. 36.

Carmichael, I.S.E., Nicholls, J., Smith, A.L., 1970, Silica activity in igneous rocks: Am. Miner., v. 55, p. 246.

Crawford, M.L., 1966, Composition of plagioclase and associated minerals in some schists from Vermont, USA, and South Westland, New Zealand, with inferences about the peristerite solvus: Contr. Min. Petr., v. 13, p. 269.

Cullers, R.L., Yeh, L.T., Chaudhuri, S., Guidotti, C.V., 1974, Ree in Silurian pelitic schists: GCA, v. 38, p. 389.

Czamanske, G.K., Wones, D.R., 1973, Oxidation during magmatic differentiation, Finmarka complex, Oslo area, Norway: Part 2, The mafic silicates: J. Petr., v. 14, p. 349.

Dewey, J.F., Kidd, W.S.F., 1974, Continental Collisions in the Appalachian - Caledonian Orogenic Belt: Variations Related to Complete and incomplete suturing: Geology, v. 2, p. 543.

Dudas, M.J., Schmitt, R.A., Harward, M.E., 1971, Trace element partitioning between volcanic plagioclase and dacitic pyroclastic matrix: EPSL, v. 11, p. 440.

Duncan, A.R., Taylor, S.R., 1968, Trace element analysis of magnetites from andesitic and dacitic lavas from Bay of Plenty, New Zealand: Contr. Min. Petr., v. 20, p. 30.

Espenshade, G.H., 1972, Geology of the Moxie Pluton in the Moosehead Lake - Jo-Mary Mountain area, Piscataquis County, Maine: GS Bulletin 1340.

Ewart, A., Bryan, W.B., Gill, J.B., 1973, Mineralogy and geochemistry of the younger volcanic islands of Tonga, S.W. Pacific: J. Petr., v. 14, p. 429.

Ewart, A., Taylor, S.R., 1969, Trace element geochemistry of the rhyolitic volcanic rocks, Central North Island, New Zealand. Phenocryst data: Contr. Min. Petr., v. 22, p. 127.

Fleischer, M., Altschuler, Z.S., 1969, The relationship of the rare earth composition of minerals to geological environment: GCA, v. 33, p. 725.

French, B.M., 1966, Some geological implications of equilibrium between graphite and a C-H-O gas phase at high temperatures and pressures: Reviews of Geophysics, v. 4, p. 223.

Fullagar, P.D., Bottino, M.L., 1968, Geochronology of Silurian and Devonian age volcanic rocks from northeastern North America: in 23rd International Geological Congress, v. 6, p. 17, Prague.

Glyuk, D.S., Anfilogov, V.N., 1973, Phase equilibria in the system granite-H_2O-HF at a pressure of 1000 kg/cm^2: Geochemistry International, v. 10, p. 321.

Goranson, R.W., 1931, The solubility of water in granitic magmas: AJS, v. 22, p. 481.

Goranson, R.W., 1938, Silicate-water systems: phase equilibria in the $NaAlSi_3O_8$-H_2O and $KAlSi_3O_8$-H_2O systems at high temperatures and pressures: AJS, 35A, p. 71.

Gordon, G.E., Randle, K., Goles, G., Corliss, J., Beeson, M., Oxley, S., 1968, Instrumental activation analysis of standard rocks with high resolution gamma ray detectors: GCA, v. 32, p. 369.

Haskin, L.A., Frey, F.A., Wildeman, T.R., 1968, Relative and absolute terrestrial abundances of the rare earths: in Origin and distribution of the elements, Int. Ser. Monographs Earth Sci., ed. L.H. Ahrens, v. 30, p. 889.

Heming, R.F., Carmichael, I.S.E., 1973, High-temperature pumice flows from the Rabaul caldera Papua, New Guinea: Contr. Min. Petr., v. 38, p. 1.

Higuchi, H., Nagasawa, H., 1969, Partition of trace elements between rock-forming minerals and the host volcanic rocks: EPSL, v. 7, p. 281.

Hitchcock, C.H., 1861, General report upon the geology of Maine: Maine Board Agriculture, 6th Ann. Report.

Hon, R., 1973, Barth's geothermometer and thermochemical properties of plagioclase feldspars (Abstr.): Transactions, Am. Geoph. Union, v. 54, p. 483.

IUGS subcommission on the systematics of igneous rocks, 1973, Classification and nomenclature of plutonic rocks. Recommendation: N. Jb. Miner. Mh. Min., v. 1973, p. 149.

Jackson, C.T., 1838, Second report on the geology of the state of Maine: Augusta, Maine, Luther Severance.

Jahns, R.H., Burnham, C.W., 1958, Experimental studies of pegmatite genesis: Melting and crystallization of granite and pegmatite: GSA Bull., v. 69, p. 1592.

Jahns, H.J., Burnham, C.W., 1969, Experimental studies of pegmatite genesis: I. A model for the derivation and crystallization of granitic pegmatites: Economic Geology, v. 64, p. 843.

Jahns, R.H., Tuttle, O.F., 1963, Layered pegmatite-aplite intrusives: in Min. Soc. Am. Spec. Paper 1, p. 78.

James, R.S., Hamilton, D.L., 1969, Phase relations in the system $NaAlSi_3O_8$-$KAlSi_3O_8$-$CaAl_2Si_2O_8$-SiO_2 at 1 kb water vapor pressure: Contr. Min. Petr., v. 21, p. 111.

Kerrick, D.M., 1972, Experimental determination of muscovite + quartz stability with $P(H_2O) < P(total)$: AJS, v. 272, p. 946.

Korringa, M.K., Noble, D.C., 1971, Distribution of Sr and Ba between natural feldspar and igneous melt: EPSL, v. 11, p. 147.

Kudo, A.M., Weill, D.F., 1970, An igneous plagioclase thermometer: Contr. Min. Petr., v. 25, p. 52.

Lee, D.E., Bastron, H., 1967, Fractionation of REE in allanite and monazite as related to geology of the Mt. Wheeler mine area, Nevada: GCA, v. 31, p. 339.

Lee, D.E., van Loenen, R.E., Mays, R.E., 1973, Accessory apatite from hybrid granitoid rocks of the southern Snake range, Nevada: Jour. Research USGS, v. 1, p. 89.

Lipman, P.W., 1971, Iron-titanium oxide phenocrysts in compositionally zoned ash-flow sheets from southern Nevada: J. Geol., v. 79, p. 438.

Lopez, L.E., 1972, Appalachian rhyolites: Geochemical data concerning their origin: M.Sc. Thesis - M.I.T.

Lopez, L.E., 1974, Plutonic and Volcanic rocks from Central Chile ($33°$-$42°S$): Geochemical evidence regarding eheir petrogenesis: Ph.D. Thesis - M.I.T.

Luth, W.C., 1969, The systems $NaAlSi_3O_8$-SiO_2 and $KAlSi_3O_8$-SiO_2 to 20 kb and the relationships between H_2O content, P(water), and P(total) in granitic magma: AJS, v. 267A, p. 325.

Luth, W.C., Jahns, R.H., Tuttle, O.F., 1964, The granite system at pressures of 4 to 10 kilobars: JGR, v. 69, p. 759.

Luth, W.C., Tuttle, O.F., 1966, The hydrous vapor phase in equilibrium with granite and granite magmas: in Memoir 115, The Geological Society of America, p. 513.

Lyakhovich, V.V., 1967, Distribution of rare earth among the accessory minerals of granites: Geochem. Int., v. 4, p. 691.

Lyakhovich, V.V., 1972, Partition of rarer elements between porphyritic phenocrysts and vitreous groundmass in a vitroandesite: Geochemistry International, v. 9, p. 793.

Lyakhovich, V.V., Balanova, T.T., 1971, On average contents and composition of rare-earth elements in accessory minerals of graniloids: Geokhimiya, No. 2, p. 131, (in Russian).

McKerror, W.S., Ziegler, A.M., 1971, The Lower Silurian paleogeography of New Brunswick and adjacent areas: Jour. Geology, v. 79, p. 635.

Moench, R.H., Boudette, E.L., 1970, Stratigraphy of the northwest limb of the Merrimack synclinorium in the Kennebago Lake, Rangeley, and Phillips quadrangles, western Maine: in NEIGC Guidebook, ed. G. Boone, part A-1, p. 1.

Mueller, R.F., 1971, Oxidative capacity of magmatic components: AJS, v. 270, p. 236.

Nagasawa, H., 1970, Rare earth concentrations in zircons and apatites and their host dacites and granites: EPSL, v. 9, p. 359.

Nagasawa, H., 1971, Partitioning of Eu and Sr between co-existing plagioclase and K-feldspar: EPSL, v. 13, p. 139.

Nagasawa, H., Schnetzler, C.C., 1971, Partitioning of rare earth, alkali and alkaline earth elements between phenocrysts and acidic igneous magma: GCA, v. 35, p. 953.

Nakamura, Y., 1974, The system $SiO_2-H_2O-H_2$ at 15 kbar: in Annual Report of the Director, Geophysical Laboratory, p. 259.

Neiva, A.M.R., 1974, Greiseintization of a muscovite-biotite albite granite of northern Portugal: Chem. Geol., v. 13, p. 295.

Nicholls, J., Carmichael, I.S.E., Stormer, J.C., Jr., 1971, Silica activity and P(total) in igneous rocks: Contr. Min. Petr., v. 33, p. 1.

Noble, D.C., Hedge, C.E., 1970, Distribution of Rb between sodic sanidine and natural silicic liquid: Contr. Min. Petr., v. 29, p. 234.

Noble, D.C., Korringa, M.K., Hafft, J., 1971, Distribution of Ca between alkali feldspar and glass in some highly differentiated silicic volcanic rocks: Am. Miner., v. 56, p. 2088.

Orville, P.M., 1963, Alkali ion exchange between vapor and feldspar phases: AJS, v. 261, p. 201.

Orville, P.M., 1972, Plagioclase cation exchange equilibria with aqueous chloride solution at 700°C and 2000 bars in the presence of quartz: AJS, v. 272, p. 234.

Paster, T.P., Schauwecker, D.S., Haskin, L.A., 1974, The behavior of some trace elements during solidification of the Skaergaard layered series: GCA, v. 38, p. 1549.

Philpotts, J.A., Schnetzler, C.C., 1970, Phenocrysts matrix partition coefficients for K, Rb, Sr, and Ba, with applications to anorthosite and basalt genesis: GCA, v. 34, p. 307.

v. Platten, H., 1965, Kristallisation granitischer Schmelzen: Beit. Min. Pet., v. 11, p. 334.

Rankin, D.W., 1968, Volcanism related to tectonism in the Piscataquis Volcanic Belt, an island arc of Early Devonian Age in North-Central Maine: in Studies of Appalachian Geology: Northern and Maritime, p. 355.

Rice, C.M., 1973, Chemical weathering on the Carnmenellis granite: Min. Mag., v. 39, p. 429.

Roeder, P.L., 1974, Activity of iron and olivine solubility in basaltic liquids: EPSL, v. 23, p. 397.

Roeder, P.L., Emslie, R.F., 1970, Olivine-liquid equilibrium: Contr. Min. Petr., v. 29, p. 275.

Saxena, S.K., Ribbe, P.H., 1972, Activity-composition relations in feldspars: Contr. Min. Petr., v. 37, p. 131.

Schilling, J.-G., 1973, Iceland mantle plume: Geochemical evidence along Reykjanes ridge: Nature, v. 242, p. 565.

Schnetzler, C.C., Philpotts, J.A., 1970, Partition coefficients of REE between igneous matrix material and rock-forming minerals - II: GCA, v. 34, p. 331.

Seck, H.A., 1971, Koexistierende Alkalifeldspäte und Plagioclase im System $NaAlSi_3O_8$-$KAlSi_3O_8$-$CaAl_2Si_2O_8$-H_2O bei Temperaturen von 650° bis 900°C: N. Jb. Min. Abh., v. 115, p. 315.

Smith, E.S.C., 1930, Contributions to the geology of Maine, Number 4. The geology of the Katahdin area. Part I, a new rhyolite from the state of Maine: AJS, v. 19, p. 6.

Smith, E.S.C., 1933, Contributions to the geology of Maine, Number 5. An occurrence of garnet in rhyolite: AJS, v. 25, p. 225.

Smith, J.V., 1972, Critical review of synthesis and occurrence of plagioclase feldspars and a possible phase diagram: Journal of Geology, v. 80, p. 505.

Smith, R.L., 1960a, Ash flows: a review: GSA Bull., v. 71, p. 795.

Smith, R.L., 1960b, Zones and zonal variations in welded ash flows: USGS Prof. Paper 354-F, p. F149.

Sprunt, E.S., 1973, Scanning electron microscope study of cracks and pores in crystalline rocks: M.Sc. Thesis - M.I.T.

Steiner, J.C., Jahns, H.J., Luth, W.C., 1975, Crystallization of alkali feldspar and quartz in the haplogranite system $NaAlSi_3O_8-KAlSi_3O_8-SiO_2-H_2O$ at 4 kb: GSA Bull., v. 86, p. 83.

Stormer, J.C., Jr., 1974, Retooling Barth's two feldspar geothermometer using recent thermodynamic data (Abstr.): Transactions, Am. Geoph. Union, v. 55, p. 482.

Stormer, J.C., 1975, A practical two feldspar geothermometer: Am. Miner., v. 60, p. 667.

Thompson, J.B., Robinson, P., Clifford, T.N., Trask, N.J., 1968, Nappes and gneiss domes in west-central New England: in Studies of Appalachian Geology: Northern and Maritime, p. 203.

Tuttle, O.F., Bowen, N.L., 1958, Origin of granite in the light of experimental studies in the system, $NaAlSi_3O_8-KAlSi_3O_8-SiO_2-H_2O$: Geol. Soc. Am. Mem. 74.

Waldbaum, D.R., Thompson, J.B., Jr., 1969, Mixing properties of sanidine crystalline solutions: IV. Phase diagrams from equation of state: Am. Miner., v. 54, p. 1274.

Whitney, J.A., 1975, The effects of pressure, temperature and $x(H_2O)$ on phase assemblages in four synthetic rock compositions: J. Geol., v. 83, p. 1.

Winkler, H.G.F., 1957, Experimentelle Gesteinsmetamorphose - I. Hydrothermale Metamorphose karbonatfreier Tone: GCA, v. 13, p. 42.

Winkler, H.G.F., Ghose, N.C., 1973, Further data on the eutectics in the system Qz-Or-An-H_2O: N. Jb. Min. Mh., v. 1973, p. 481.

Winkler, H.G.F., Lindemann, W., 1972, The system Qz-Or-An-H_2O within the granitic system Qz-Or-Ab-An-H_2O. Application to granitic magma formation: N. Jb. Min. Mh., v. 1972, p. 49.

Winkler, H.G.F., v. Platten, H., 1958, Experimentelle Gesteinsmeta-
    morphose - II. Bildung von anatektischen Schmelzen bei der
    Metamorphose von NaCl-führenden kalkfreien Tonen: GCA, v. 15, p.91.

Winkler, H.G.F., v. Platten, H., 1961, Experimentelle Gesteinsmeta-
    morphose - IV. Bildung anatektischer Schmelzen aus metamorpho-
    sierten Grauwacken: GCA, v. 24, p. 48.

Wones, D.R., 1972, Stability of biotite: a reply: Am. Miner., v. 57,
    p. 316.

Wones, D.R., Engster, H.P., 1965, Stability of biotite: experiment,
    theory, and application: Am. Mineralogist, v. 50, p. 1228.

Wones, D.R., Gilbert, M.C., 1969, The fayalite-magnetite-quartz
    assemblage between $600^{\circ}C$ and $800^{\circ}C$: Am. Mineralogist, v. 50,
    p. 1228.

Wyllie, P.J., Tuttle, O.F., 1961, Experimental investigation of
    silicate systems containing two volatile components. II. The
    effects of NH_3 and HF, in addition to H_2O, on the melting
    temperatures of albite and granite: AJS, v. 259, p. 128.

Wyllie, P.J., Tuttle, O.F., 1964, Experimental investigation of
    silicate systems containing two volatile components. Part III.
    The effects of SO_3, P_2O_5, HCl and Li_2O, in addition to H_2O,
    on the melting temperatures of albite and granite: AJS, v. 262,
    p. 930.